The Role of Ultrasound in Sports Medicine

5

Gina A. Ciavarra and Ronald S. Adler

Abstract

The use of ultrasound in musculoskeletal imaging and, in particular, sports medicine has dramatically increased with the technical advances of the last 20 years. These improvements allow detailed evaluation of the structures of the musculoskeletal system including tendons, ligaments, muscles, nerves, joints, cartilage, and bursae. In addition to its wide availability, portability, and lower cost, the greatest advantages of ultrasound, particularly in the musculoskeletal system, are the ability to perform dynamic imaging as well as the opportunity to interact with the patient and correlate symptoms with sonographic findings. The real-time nature of ultrasound provides a unique evaluation of structures in their dynamic state, thereby identifying pathology that may be demonstrated only when the patient performs certain motions.

5.1 Introduction

With advances in ultrasound technology over the last 20 years, the utilization of ultrasound in musculoskeletal imaging and, in particular, sports medicine has dramatically increased. The development of high-frequency transducers has allowed for improved in-plane resolution that is equivalent to and in some cases may exceed that of magnetic resonance imaging (MRI) (Erickson 1997; Jacobson 2002). These improvements have allowed for the more detailed evaluation of the structures of the musculoskeletal system including tendons, ligaments, muscles, nerves, joints, cartilage, and bursae. Both MRI and ultrasound have been shown to have similar efficacy in the assessment of tendon pathology (Bryant et al. 2002; Chang et al. 2002; Davies et al. 1991; Teefey et al. 2000a, b, c, 2004) and other structures in the musculoskeletal system; however, each modality has certain advantages over the other, and they are best used as complementary tools to better serve the needs of the patient (Adler and Finzel 2005; Jacobson 1999). For example, MRI provides a broader assessment of

G.A. Ciavarra, MD (✉) • R.S. Adler, MD
Department of Radiology,
NYU Langone Medical Center,
New York, NY, USA
e-mail: Gina.Ciavarra@nyumc.org;
Ronald.Adler@nyumc.org

A. Guermazi et al. (eds.), *Imaging in Sports-Specific Musculoskeletal Injuries*,
DOI 10.1007/978-3-319-14307-1_5

a joint and is particularly useful when the clinical picture may be uncertain. It also allows for the evaluation of structures that cannot be assessed by ultrasound due to inability of the ultrasound beam to penetrate past bone. This is true for the assessment of the bone (beyond the cortical surface) and certain intra-articular structures such as cartilage, fibrocartilage, or ligaments (e.g., the anterior cruciate ligament in the knee). Please refer to the chapter on the use of MRI in sports medicine for further discussion of MRI and its utility in evaluating pathology in the musculoskeletal system.

On the other hand, ultrasound is especially useful when a targeted assessment of a particular structure is requested. Ultrasound has certain distinct advantages over MRI. In addition to its wide availability, portability, and lower cost, the greatest advantages of ultrasound, particularly in the musculoskeletal system, are the ability to perform dynamic imaging as well as the opportunity to interact with the patient and correlate symptoms with the findings at examination. Because MRI is a static examination, some pathology may be missed as routine MRI examinations are performed with the patient in a specific position. Ultrasound allows for dynamic evaluation of structures and can identify pathology that may be demonstrated only when the patient performs certain motions. For example, ulnar nerve subluxation is produced with the elbow joint in flexion; however, standard MRI examinations are performed with the arm in extension, thus limiting the ability of the radiologist to identify the condition. A dynamic ultrasound examination that assesses the nerve through the dynamic range of flexion and extension can identify nerve subluxation.

Some of the pathology identified during the course of imaging may not be associated with patient symptoms. By interacting with the patient, it is possible to determine whether the identified pain is the cause of the patient's pain or simply an incidental finding.

5.2 Ultrasound of Normal Structures in the Musculoskeletal System

Virtually the entire spectrum of structures within the musculoskeletal system are visible with ultrasound imaging, although some structures may be more readily assessed, and assessed in their entirety, than others. The normal sonographic appearance of tendons is hyperechoic with a fibrillar pattern (Fig. 5.1) which is due to the visualization of the individual tendon fibers that comprise the tendon (Martinoli et al. 1993). This normal appearance is generated when the ultrasound beam is perpendicular to the ultrasound beam. If the beam is positioned at an angle of less than or greater than 90°, the tendon will appear artifactually hypoechoic, mimicking pathology. This characteristic of tendons is known as anisot-

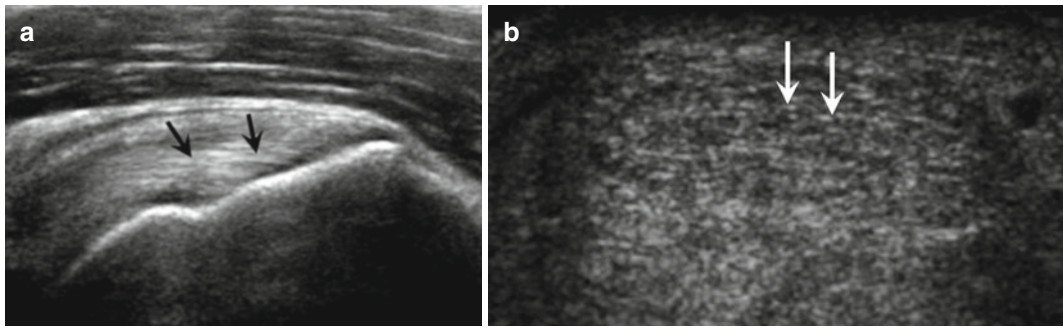

Fig. 5.1 Normal tendon. (**a**) Long-axis ultrasound image of the supraspinatus tendon demonstrates the normal hyperechoic appearance (*arrows*). (**b**) Short-axis ultrasound image of the Achilles tendon demonstrates normal hyperechoic appearance with visualization of individual tendon fibrils (*arrows*)

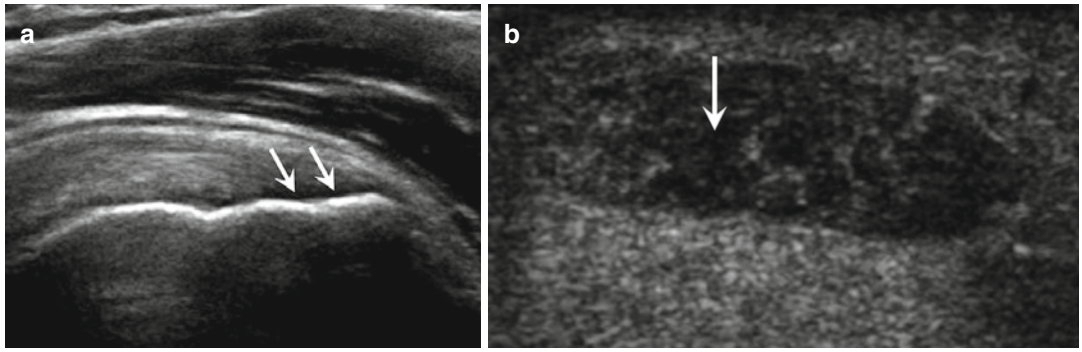

Fig. 5.2 Anisotropy. (**a**) Long-axis ultrasound image of the supraspinatus tendon shows insertional fibers are oblique to the ultrasound beam resulting in artificially decreased echogenicity (*arrows*). (**b**) Short-axis ultrasound image of the Achilles tendon with ultrasound beam angled obliquely to the tendon shows a falsely pathological, hypoechoic appearance (*arrow*)

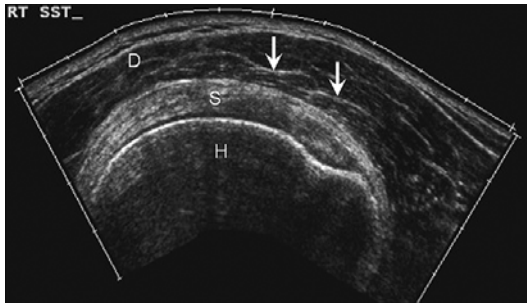

Fig. 5.3 Normal muscle. Short-axis ultrasound image using extended field of view of the deltoid muscle (*D*) shows hypoechoic appearance with echogenic striations reflecting the perimysium (*arrows*); humeral head (*H*), supraspinatus tendon (*S*)

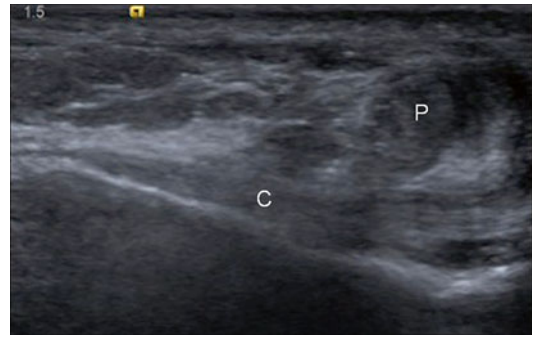

Fig. 5.4 Normal ligament. Normal echogenic ultrasound appearance of the calcaneofibular ligament (*C*) in long axis adjacent to peroneal tendons (*P*)

ropy (Fig. 5.2) (Crass et al. 1988). It is the dense, linear arrangement of the fibers that produces anisotropy. As the tendon is imaged at increasing or decreasing angles relative to the perpendicular, it becomes progressively hypoechoic.

Normal muscle appears hypoechoic with internal hyperechoic septations representing the perimysium that surrounds the bundles of muscle fibers (Fig. 5.3) (van Holsbeeck and Introcaso 2001). Muscles can present a characteristic multipennate appearance when viewed in long axis. Ligaments are typically hyperechoic and demonstrate a fibrillar structure similar to that of tendons (Fig. 5.4); however, the individual fibers are more tightly packed. Like tendons, ligaments demonstrate anisotropy when the ultrasound beam is not perpendicular to the structure. When surrounded by echogenic fat, ligaments may appear relatively hypoechoic (Jacobson 2002).

Peripheral nerves demonstrate a fascicular pattern with hypoechoic nerve fascicles surrounded by a hyperechoic connective tissue known as the epineurium (Fig. 5.5) (Silvestri et al. 1995). Only the surface (cortex) of the bone is visible with ultrasound. The cortex is smooth and hyperechoic with posterior acoustic shadowing (Fig. 5.6) (Jacobson 2002).

There are two types of cartilage within the musculoskeletal system, hyaline cartilage that lines the articular surfaces of the joints and fibrocartilage that comprises the labrum of the

shoulder and hip and the menisci of the knee. Hyaline cartilage is hypoechoic (Fig. 5.7), while the normal fibrocartilage is hyperechoic (Fig. 5.8) (Kazam et al. 2011; Lee and Bouffard 2001).

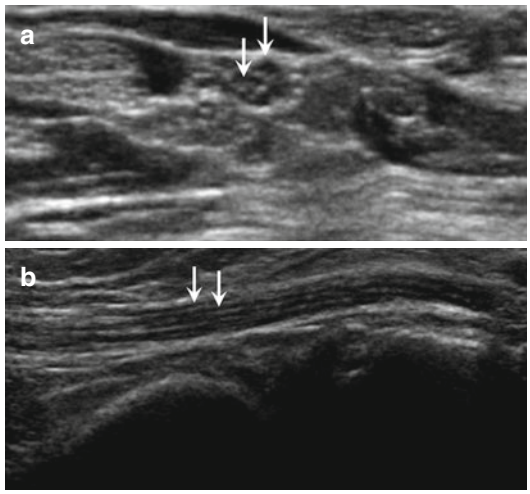

Fig. 5.5 Normal nerve. (**a**) Short-axis and (**b**) long-axis ultrasound images of a normal peripheral nerve demonstrating the hypoechoic fascicles surrounded by the echogenic epineurium (*arrows*)

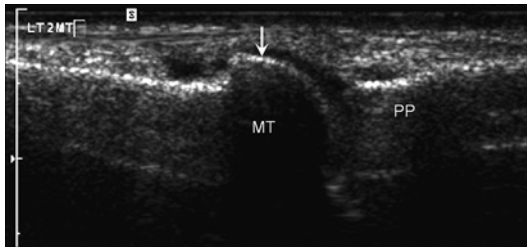

Fig. 5.6 Normal bone. Long-axis ultrasound image shows echogenic cortex (*arrow*) of the second metatarsal (*MT*) at the level of the metatarsophalangeal joint with posterior acoustic shadowing; proximal phalanx (*PP*)

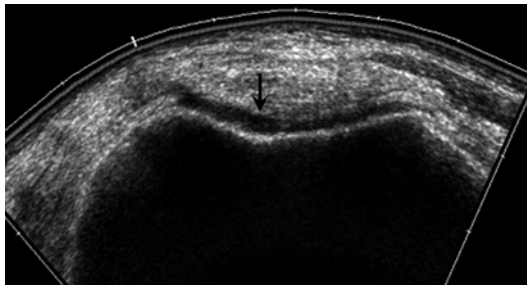

Fig. 5.7 Normal hyaline cartilage. Normal ultrasound appearance of the hypoechoic hyaline cartilage (*arrow*) lining the femoral trochlea

5.3 Ultrasound of Pathology in the Musculoskeletal System

5.3.1 Tendons

The pathology of tendons includes tendinosis or tendinopathy, partial tearing, and full-thickness tearing as well as the development of calcific deposits as seen in calcific tendinitis. Tendinosis manifests as abnormalities of both tendon morphology and echogenicity (Adler and Sofka 2003; Kainberger et al. 1990; Sell et al. 1996). There may be hypoechoic linear regions of diminished echogenicity as well as mucoid degeneration manifested by more globular regions of decreased echogenicity (Fig. 5.9). The

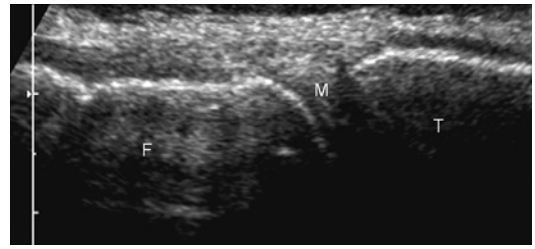

Fig. 5.8 Normal fibrocartilage. Long-axis ultrasound image of medial knee shows hyperechoic fibrocartilage of the meniscus of the knee (*M*); femur (*F*), tibia (*T*)

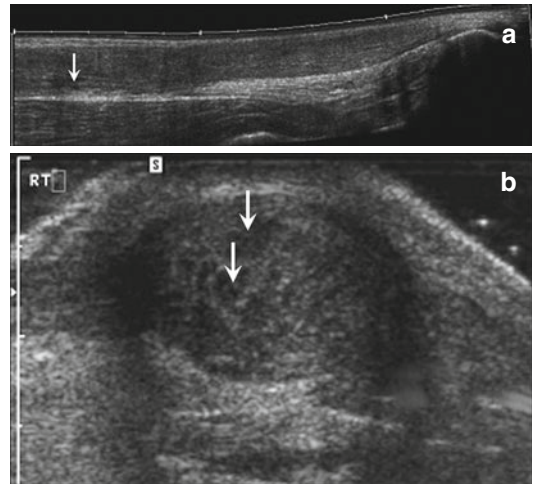

Fig. 5.9 Tendinosis. (**a**) Long- and (**b**) short-axis ultrasound images of the Achilles tendon show the tendon is enlarged and heterogeneous in echotexture with areas of decreased echogenicity (*arrows*)

tendon may be enlarged. In addition, areas of dystrophic calcification or ossification may also be seen (Adler and Finzel 2005).

Tears appear as discretely marginated defects within the tendon involving a portion of the tendon width (partial tear) (Fig. 5.10) or the entire width (full-thickness tear). The defects are well defined and hypoechoic or anechoic in appearance. Because tears and tendinosis can both appear hypoechoic, secondary signs may be necessary in differentiating these two entities (to be discussed later in this chapter) (Teefey et al. 2000a, b, c; Wiener and Seitz 1993).

Occasionally, areas of dystrophic calcification or ossification may develop within a tendon. These calcifications present as linear or globular foci of increased echogenicity with variable degrees of posterior acoustic shadowing (Fig. 5.11) (Adler and Finzel 2005; Farin and Jaroma 1995). The calcification represents deposits of calcium hydroxyapatite.

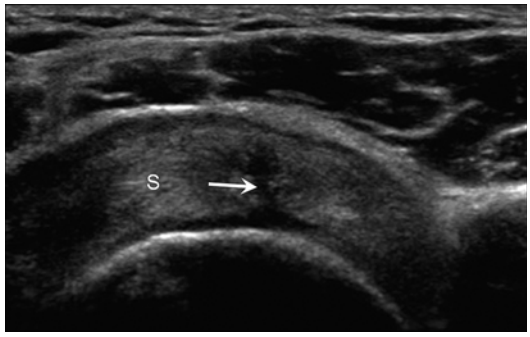

Fig. 5.10 Partial tear. Short-axis ultrasound image of the supraspinatus (*S*) demonstrates a discretely marginated linear defect (*arrow*) partially traversing the tendon width

Fig. 5.11 Calcific tendinitis. Short-axis ultrasound image shows linear echogenic calcification (++) with posterior acoustic shadowing (*arrow*) within the supraspinatus tendon (*S*)

5.3.2 Muscles

Abnormalities of the muscle in the setting of sports medicine may result from direct or indirect injury. Indirect injury may be caused by stretching of the muscle fibers during muscle contraction or may be due to excessive stretch alone (Speer et al. 1993). There are three grades of injury that may result in this setting. Grade 1 refers to muscle strain without frank tissue disruption. Grade 2 refers to partial-thickness tearing of the muscle. Grade 3 refers to a full-thickness tear of the muscle (Palmer et al. 1999). These types of injuries typically occur at the myotendinous junction and affect muscles that traverse two joints such as the hamstring muscles in the thigh or the gastrocnemius muscle in the calf (Garrett 1996).

Acute muscle injury may be associated with hemorrhage that appears hyperechoic (Fig. 5.12) in the acute setting (Blankenbaker and Tuite 2010; Lee and Healy 2004). Over time, the hematoma becomes more hypoechoic in appearance. Most frequently, hematomas are heterogeneous in appearance with areas of increased and decreased echogenicity (Lee and Healy 2004). Diffuse muscle edema also appears hyperechoic (Adler and Garofalo 2009). Partial tears manifest as incomplete disruption (Fig. 5.12) of the muscle fibers, while complete disruption of the muscle fibers reflects a full-thickness tear (Peetrons 2002). Over

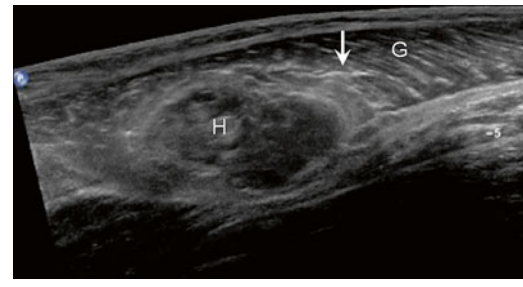

Fig. 5.12 Partial muscle tear. Long-axis ultrasound image shows grade 2 injury of the medial gastrocnemius muscle (*G*) with partial disruption of the normal muscle fibers (*arrow*) and an associated hematoma (*H*)

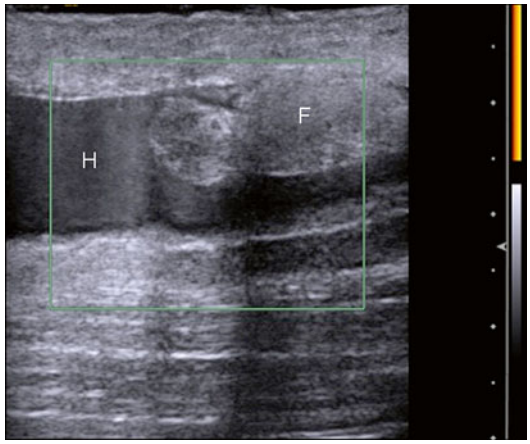

Fig. 5.13 Morel-Lavallee lesion. Long-axis ultrasound image of the lateral thigh shows a hypoechoic fluid collection (*H*) with lobular echogenic foci reflecting fat globules (*F*). No flow is present with power Doppler interrogation

time, the muscles may develop granulation tissue that displays vascularity on color or power Doppler flow imaging.

A special subtype of injury occurs when hemorrhage occurs between the deep surface of the subcutaneous fat and the subjacent musculature due to a shear injury, most frequently at the level of the hip. This is known as a Morel-Lavallee lesion (Mellado and Bencardino 2005). On ultrasound, these lesions are heterogeneous in the early stages, with irregular margins. Chronic lesions are smoother in contour and more homogeneous. They may contain hypoechoic or anechoic fluid and may contain echogenic globules of fat (Fig. 5.13). No flow should be demonstrated with color or power Doppler interrogation (Mukherjee et al. 2007; Neal et al. 2008; Parra et al. 1997).

Occasionally, following trauma, the injured muscle may ossify. This appears as a region of increased echogenicity that may show posterior acoustic shadowing (Fig. 5.14). Ultrasound may demonstrate early mineralization before changes are visible on plain radiography (Tyler and Saifuddin 2010).

Finally, a previously injured muscle or a muscle with an injury to its nerve supply may atrophy. This results in decreased muscle volume and increased echogenicity of the affected muscle (Fig. 5.15).

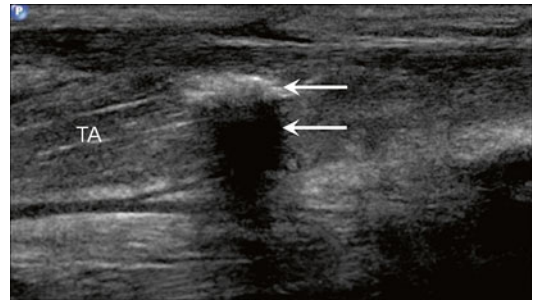

Fig. 5.14 Myositis ossificans. Long-axis ultrasound image of the tibialis anterior (*TA*) muscle several months following direct trauma shows linear echogenic focus with posterior acoustic shadowing (*arrows*) reflecting myositis ossificans at the site of prior injury

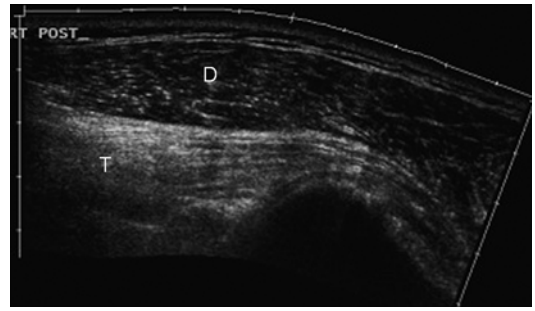

Fig. 5.15 Muscle atrophy. Long-axis ultrasound image of the shoulder shows denervation atrophy of the teres minor (*T*) with increased echogenicity of the muscle reflecting fatty replacement. Deltoid (*D*) demonstrates normal hypoechoic appearance of muscle with the normal echogenic perimysium

Atrophy may also occur in the setting of chronic tear of the associated tendon (Peetrons 2002).

5.3.3 Bones

As previously mentioned, the normal cortex of the bone is smooth and hyperechoic with posterior acoustic shadowing. In the setting of an acute fracture, there is focal discontinuity of the cortex (Fig. 5.16) with or without an associated cortical step-off (Crag et al. 1999). The sonographic appearance of stress fractures includes periosteal reaction with hyperemia on color or power Doppler interrogation. There may hypoechoic periosseous fluid and/or hemorrhage and possible cortical discontinuity (Bodner et al. 2005;

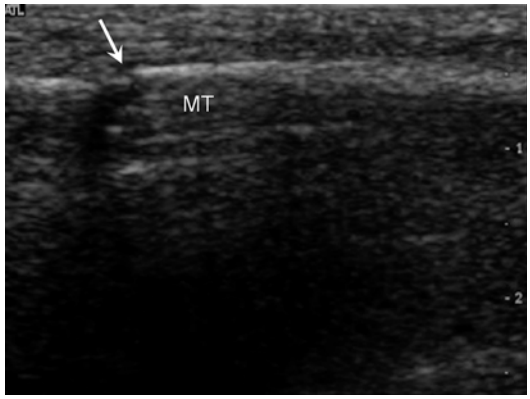

Fig. 5.16 Fracture. Long-axis ultrasound image shows focal cortical disruption (*arrow*) in a patient with a non-displaced fracture of the fifth metatarsal (*MT*)

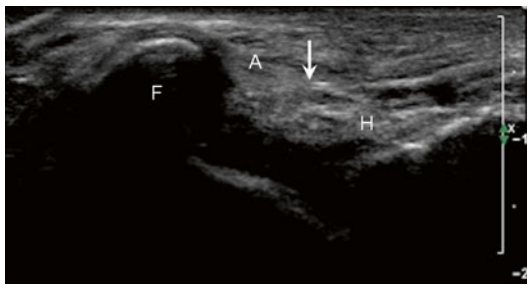

Fig. 5.17 Ligament tear. Long-axis ultrasound image shows the anterior talofibular ligament (*A*) with complete rupture with torn fibers (*arrow*) attached to the fibula (*F*) and hemorrhage (*H*) in gap

Drakonaki and Garbi 2010). Patients will typically report point tenderness with transducer pressure. The presence of modular increased echogenic soft tissue about the fracture site represents callous formation.

5.3.4 Ligaments

Abnormalities of the ligaments include partial and complete tears. Partial tears appear as areas of decreased echogenicity within a thickened ligament with some fibers remaining in continuity. A complete tear manifests as disruption of the ligament fibers or replacement of the fibers by heterogeneous, hypoechoic tissue representing fluid and/or hemorrhage and residual ligament (Fig. 5.17). Occasionally, a hyperechoic fleck of bone can be seen in the setting of an avulsion fracture. Remote sprains are characterized by thickening and enlargement of the ligament possibly associated with focal ossification (Peetrons et al. 2004). Scar remodeling or granulation tissue may appear as hypervascular soft tissue at the site of the tear.

5.3.5 Nerves

Abnormalities of the nerves may be caused by entrapment secondary to ligamentous or fibro-osseous structures or secondary to mass effect from anomalous muscles, tumors, or fluid collections. Alternatively, abnormal motion of a nerve can result in nerve pathology as seen in ulnar nerve subluxation. The abnormal nerve appears enlarged and hypoechoic with loss of the normal fascicular pattern (Fig. 5.18) (Bianchi 2008; Jacobson et al. 2010; Kermarrec et al. 2010). In the setting of a localized nerve injury, a posttraumatic neuroma may form. These appear as discrete hypoechoic nodules.

5.4 Shoulder Ultrasound

5.4.1 Rotator Cuff

The shoulder is the most frequently evaluated joint with sonography. The routine shoulder examination includes the assessment of the rotator cuff tendons (supraspinatus, infraspinatus subscapularis, teres minor), long head of the biceps brachii, and the acromioclavicular joint as well as the performance of dynamic maneuvers to assess for subacromial impingement (Jacobson 2013a). The most commonly affected tendon is the supraspinatus tendon. Pathology of the tendons ranges from tendinosis to full-thickness, full-width tears.

Tendinosis manifests as focal or diffuse decreased echogenicity of the tendon with possible enlargement of the affected tendon (Fig. 5.19) (Adler and Sofka 2003; Kainberger et al. 1990; Sell et al. 1996). Partial tears appear as focal hypoechoic or anechoic defects within the tendon

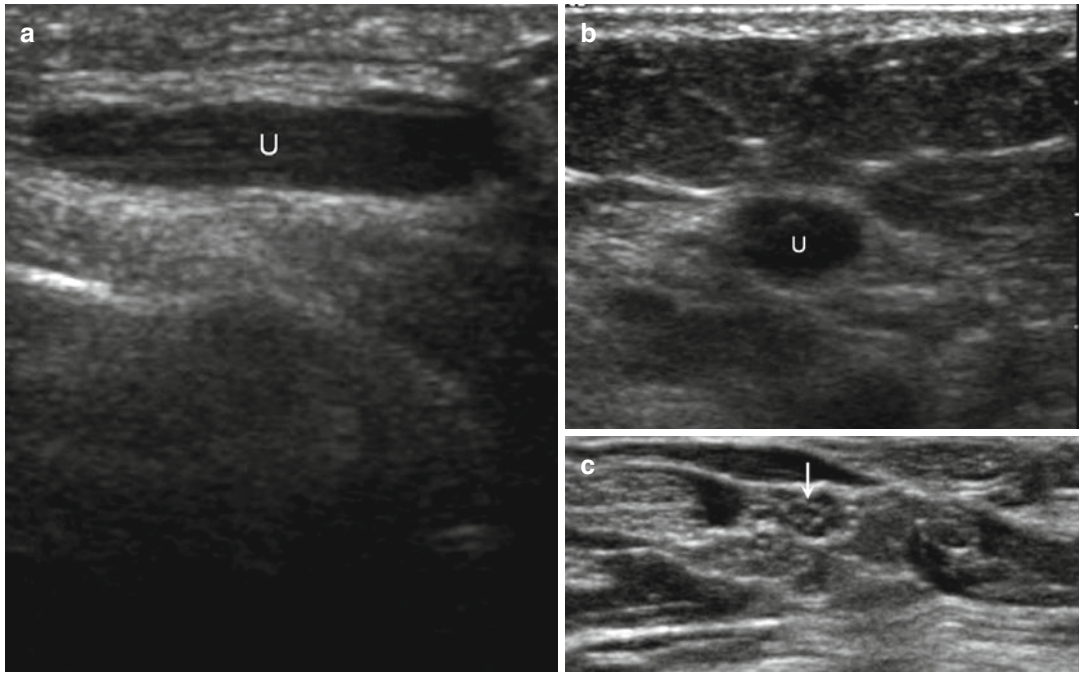

Fig. 5.18 Ulnar neuritis. (**a**) Long- and (**b**) short-axis ultrasound images of the ulnar nerve (*U*) in a patient with ulnar neuritis. The nerve is enlarged and hypoechoic with loss of the normal fascicles. (**c**) Compare to a normal peripheral nerve in short axis with hypoechoic fascicles surrounded by hyperechoic epineurium (*arrow*)

that involve only the bursal or articular surface of the tendon (Fig. 5.20) (Jacobson et al. 2004; van Holsbeeck et al. 1995). Partial tears may also be intrasubstance or interstitial, not extending to the articular or bursal surfaces.

The most commonly encountered partial, articular surface tear involves the anterior supraspinatus tendon distally at its insertion on the greater tuberosity (Fig. 5.20) (Schaeffeler et al. 2011; Tuite et al. 1998). Cortical irregularity or enthesopathic change involving the greater tuberosity may be present related to chronic rotator cuff degeneration (Fig. 5.21). This will not be present in the setting of an acute tear of an otherwise normal tendon or a tear involving the more proximal non-insertional tendon fibers (Jacobson et al. 2004; Wohlwend et al. 1998). In the setting of a partial, articular surface tear, the superficial surface of the tendon may maintain its normal convexity on ultrasound, without associated volume loss (Fig. 5.20) (Jacobson 2013a).

A special subtype of partial articular surface tear involving the most distal, insertional fibers of either the infraspinatus or supraspinatus is known as a rim-rent tear or PASTA lesion when it involves the supraspinatus (partial articular-sided supraspinatus tendon avulsion) (Fig. 5.22). This more frequently affects younger patients, such as athletes (Tuite et al. 1998; Vinson et al. 2007).

Like partial articular surface tears, bursal surface tears also appear hypoechoic or anechoic; however, these tears occur along the more superficial aspect of the tendon (Fig. 5.23) (Jacobson et al. 2004). Tears extending from the bursal surface through the tendon footprint to the greater tuberosity are still considered bursal surface tears (Jacobson 2013a).

Since tendon tears and tendinosis both may appear hypoechoic, secondary findings will be helpful in differentiating these entities. Indirect signs of a tear include diminished thickness of the tendon. In addition, the hypoechoic tear tends to be a more focal and well-defined defect, rather than the ill-defined hypoechoic areas seen in tendinosis (Teefey et al. 2000a, b, c; Wiener and Seitz 1993). The cartilage interface sign may assist in the diagnosis of partial articular surface tears. This finding occurs when the tear contacts

the hypoechoic hyaline cartilage along the humeral head, appearing as a hyperechoic curvilinear interface between the tear and the cartilage (Fig. 5.24) (Bouffard et al. 1993). Secondary signs of bursal surface partial tears include tendon thinning and herniation of the subacromial–subdeltoid bursa and peribursal fat into the defect with resultant loss in the normal convexity of the tendon (Fig. 5.25) (Bouffard et al. 1993; Thain and Adler 1999; Wiener and Seitz 1993). Tears may be accentuated in real time by direct compression with the transducer. This maneuver may be helpful when complex material fills the tear or in differentiating partial from full-thickness tears.

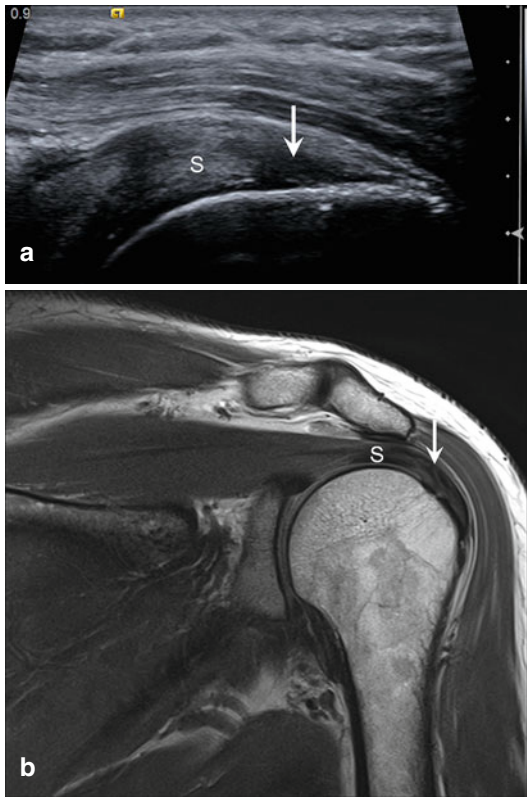

Fig. 5.19 Rotator cuff tendinosis. (**a**) Longitudinal ultrasound image of the supraspinatus (*S*) demonstrates decreased echogenicity and loss of the normal fibrillar pattern of the tendon (*arrow*). (**b**) Corresponding coronal proton density-weighted MRI demonstrates increased signal (*arrow*) in the supraspinatus (*S*) tendon due to tendinosis

Tendinosis and tears of the subscapularis tendon are less common than supraspinatus tears. Partial- and full-thickness tears have similar sonographic appearances as tears of the supraspinatus and infraspinatus tendon. The more common type of tear involves the superior fibers of the subscapularis associated with a tear of the anterior fibers of the supraspinatus. In the setting of a partial-thickness subscapularis tear, the long head biceps brachii tendon may subluxate or dislocate into the substance of the tear (Fig. 5.26). Full-thickness tears of the subscapularis may allow the biceps brachii tendon to dislocate into the glenohumeral joint (Fig. 5.27) (Farin and Jaroma 1996; Morag et al. 2011; Thain and Adler 1999). The multipennate nature of the subscapularis tendon seen in short axis should not be confused with tendon pathology.

5.4.2 Biceps

Biceps tendinosis appears diffusely hypoechoic on ultrasound (Fig. 5.28) (Adler and Sofka 2003; Kainberger et al. 1990; Sell et al. 1996).

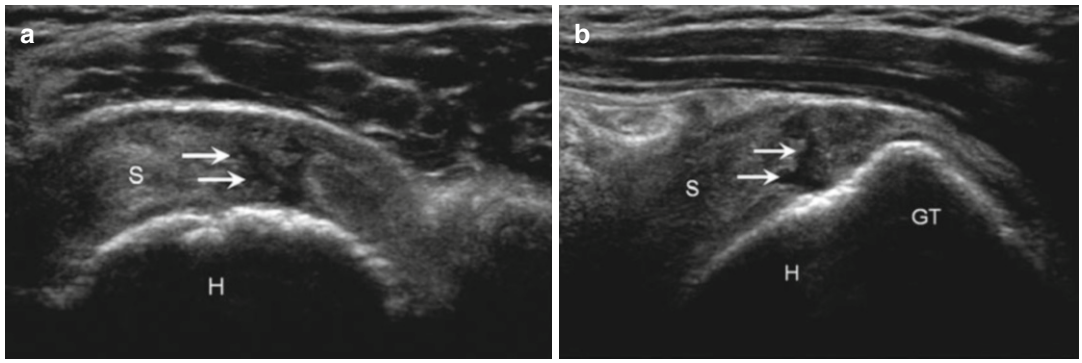

Fig. 5.20 Supraspinatus partial tear, articular surface. (**a**) Short- and (**b**) long-axis ultrasound images demonstrate a high-grade partial articular-sided tear (*arrows*) of the supraspinatus (*S*) tendon; humerus (*H*), greater tuberosity (*GT*)

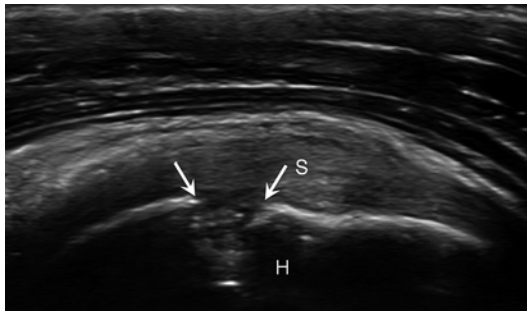

Fig. 5.21 Enthesopathy. Short-axis ultrasound image of the supraspinatus (*S*) tendon insertion demonstrates enthesopathic cyst formation (*arrows*) in the humeral head (*H*)

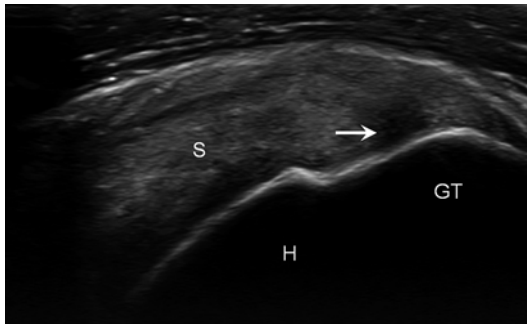

Fig. 5.22 Supraspinatus tear, rim rent. Long-axis ultrasound image of the supraspinatus (*S*) demonstrates a partial, rim-rent-type tear (*arrow*) at the insertion on the greater tuberosity (*GT*); humerus (*H*)

The biceps tendon may be enlarged, and there may be associated calcification manifesting as echogenic foci with posterior acoustic shadowing (Adler and Finzel 2005). Small calcifications may not shadow and may just appear as discrete echogenic foci. Partial or complete disruption of the tendon may occur. Additionally, linear regions of decreased echogenicity may also be present reflecting interstitial split tears (Thain and Adler 1999). As mentioned above, the biceps tendon may subluxate or dislocate secondary to partial- or full-thickness tears of the subscapularis tendon (Figs. 5.26 and 5.27). The biceps tendon may be perched on the lesser tuberosity in the setting of subluxation or translate more medially in the setting of a full-thickness subscapularis tear. In

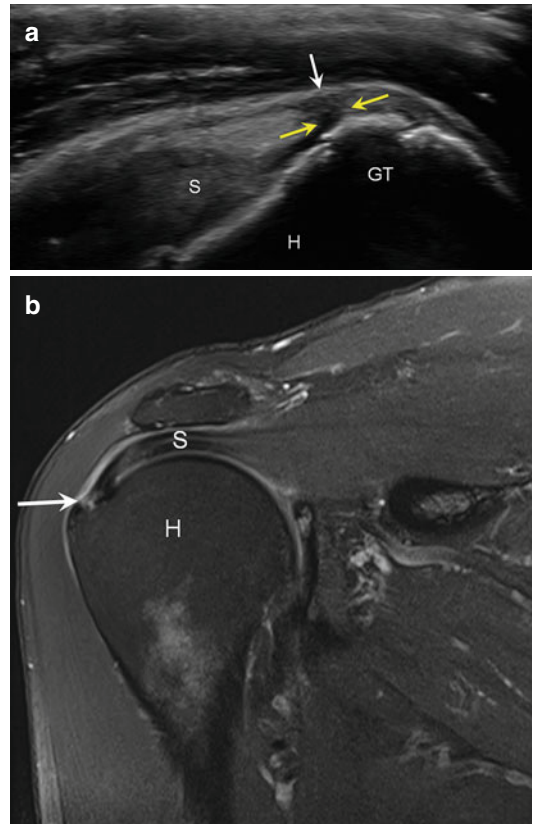

Fig. 5.23 Supraspinatus tear, bursal surface. (**a**) Long-axis ultrasound image of the supraspinatus (*S*) insertion shows a high-grade bursal surface tear (*yellow arrows*) extending from the collapsed subacromial bursa (*white arrow*) nearly to the greater tuberosity (*GT*); humerus (H). (**b**) Corresponding coronal fluid-sensitive MRI demonstrates the bursal tear (*white arrow*) of the supraspinatus (*S*); humerus (*H*)

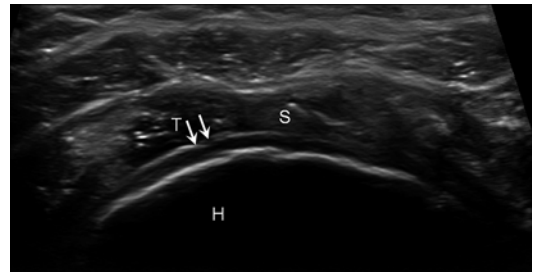

Fig. 5.24 Cartilage interface sign. Short-axis ultrasound image of the supraspinatus (*S*) demonstrates the cartilage interface sign (*arrows*) indicating extension of the tear (*T*) to the articular surface; humerus (*H*)

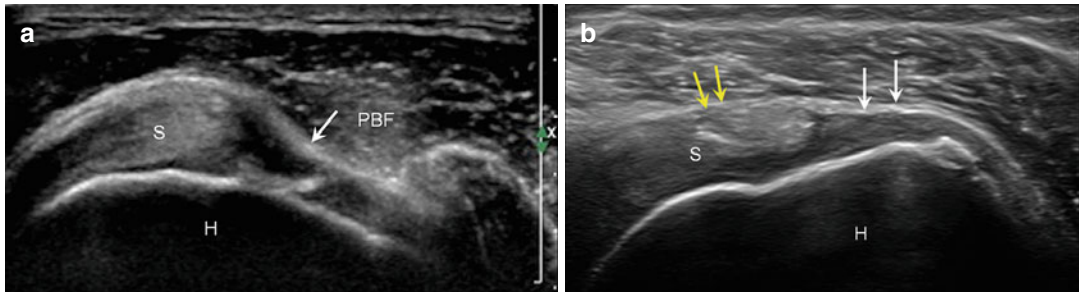

Fig. 5.25 Secondary sign, bursal tears. (**a**) Long-axis ultrasound image of the supraspinatus (*S*) shows herniation of the peribursal fat (*PBF*) and subacromial–subdeltoid bursa (*arrow*) into the bursal surface tear (*T*). (**b**) Long-axis ultrasound image of the supraspinatus (*S*) shows loss of the normal tendon convexity (*white arrows*) in a subtle bursal surface tear. Normal convex surface of tendon (*yellow arrows*); humerus (*H*)

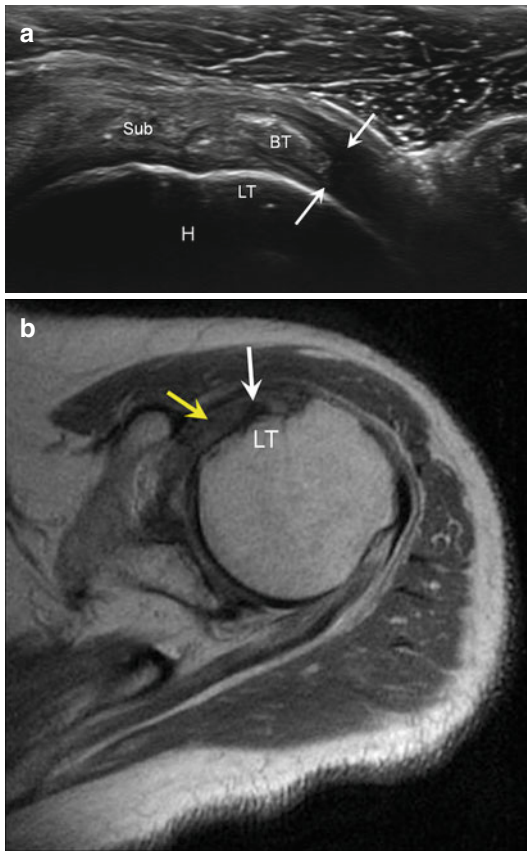

Fig. 5.26 Subscapularis partial tear. (**a**) Long-axis ultrasound image of the subscapularis (*Sub*) demonstrates mild medial subluxation of the biceps tendon (*BT*) into the high-grade tear (*arrows*); biceps is perched on lesser tuberosity (*LT*); humerus (*H*). (**b**) Corresponding axial proton density-weighted MRI shows medial subluxation of the biceps (*white arrow*) into a subscapularis tear (*yellow arrows*); lesser tuberosity (*LT*)

dynamic ultrasound imaging, placing the shoulder in external rotation can accentuate subluxation and dislocation of the biceps tendon (Farin et al. 1995a). Complete rupture of the biceps tendon results in an empty sheath (Fig. 5.29) (Thain and Adler 1999). Although a trace amount of fluid may normally be seen adjacent to the biceps tendon, when a greater amount of fluid is seen surrounding a focal segment of the tendon, this suggests tenosynovitis (Jacobson 2013a). These findings can be further confirmed with the use of power Doppler that will demonstrate hyperemia in the setting of inflammation as seen in tendinitis and tenosynovitis (Fig. 5.30) (Thoirs et al. 2008). Normal tendons and synovium about the shoulder should demonstrate minimal or no flow with power Doppler interrogation. A branch of the anterior humeral circumflex artery adjacent to the biceps tendon will cause a focus of blood flow on power Doppler imaging that should not be confused with tenosynovitis (Fig. 5.31) (Thain and Adler 1999). Because the biceps tendon sheath communicates with the glenohumeral joint, the joint should be assessed for an effusion so as not to mistake biceps tenosynovitis for normal decompression of joint fluid into the tendon sheath (Zubler et al. 2011).

5.4.3 Calcific Tendinitis

Calcific tendinitis develops due to the deposition of calcium hydroxyapatite in the rotator cuff

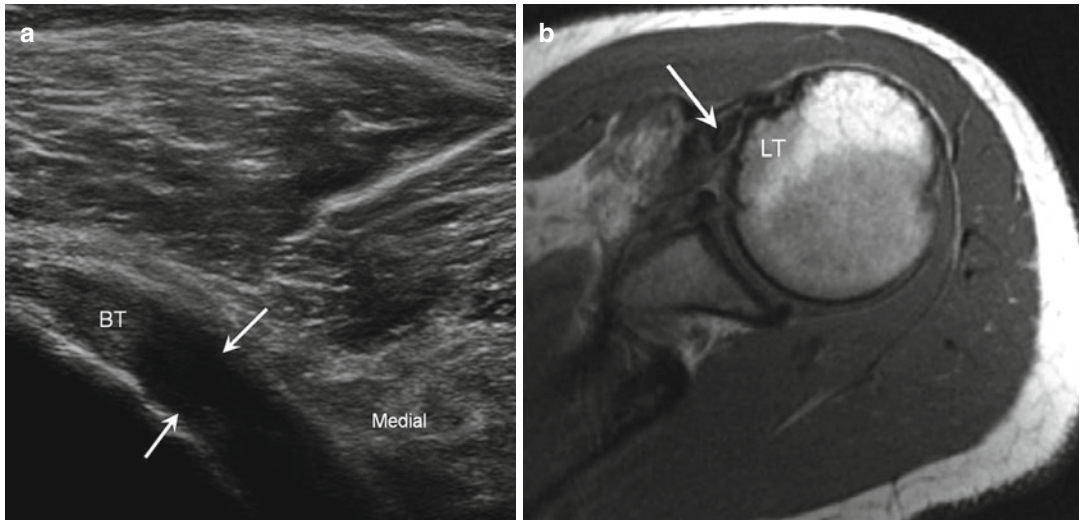

Fig. 5.27 Subscapularis complete tear. (**a**) Long-axis ultrasound image shows anechoic defect due to complete subscapularis tendon tear (*arrows*) with complete medial dislocation of the biceps (*BT*). Corresponding axial proton density-weighted MRI (**b**) shows medial dislocation of the biceps (*arrow*) beyond the lesser tuberosity (*LT*) due to the complete subscapularis tear

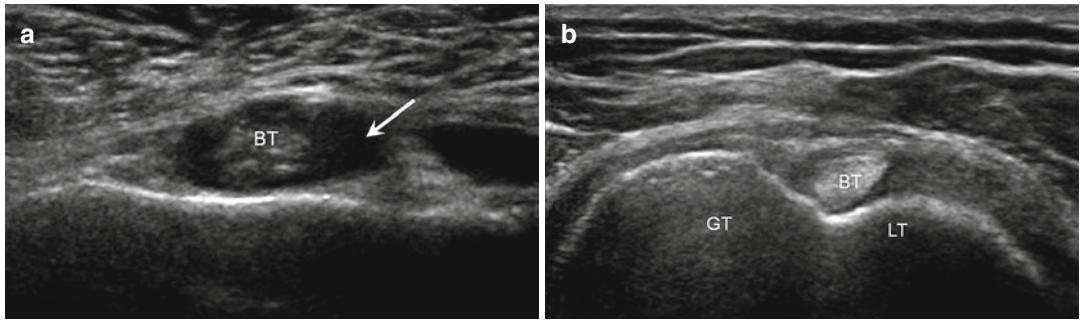

Fig. 5.28 Biceps tendinosis. (**a**) Short-axis ultrasound image of the biceps tendon (*BT*) shows an enlarged tendon with loss of the echogenic, fibrillar appearance; tendon sheath effusion (*arrow*). In (**b**), normal ellipsoid, echogenic appearance of the biceps tendon (*BT*) in short axis; greater tuberosity (*GT*), lesser tuberosity (*LT*)

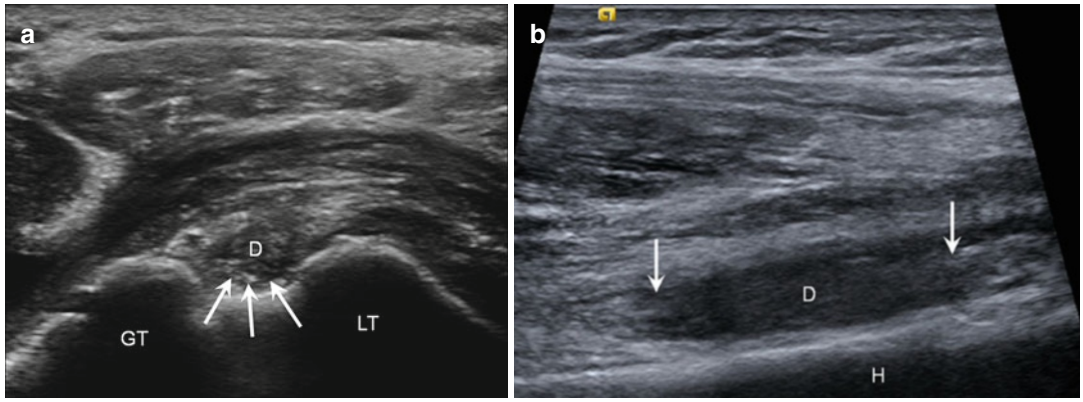

Fig. 5.29 Proximal biceps rupture. (**a**) Short-axis ultrasound image shows empty bicipital groove (*arrows*) due to rupture of the biceps with debris (*D*) in the sheath; greater tuberosity (*GT*), lesser tuberosity (*LT*). (**b**) Long-axis ultrasound image demonstrates retracted ends of torn tendon (*arrows*) with debris (*D*) in sheath; humerus (*H*)

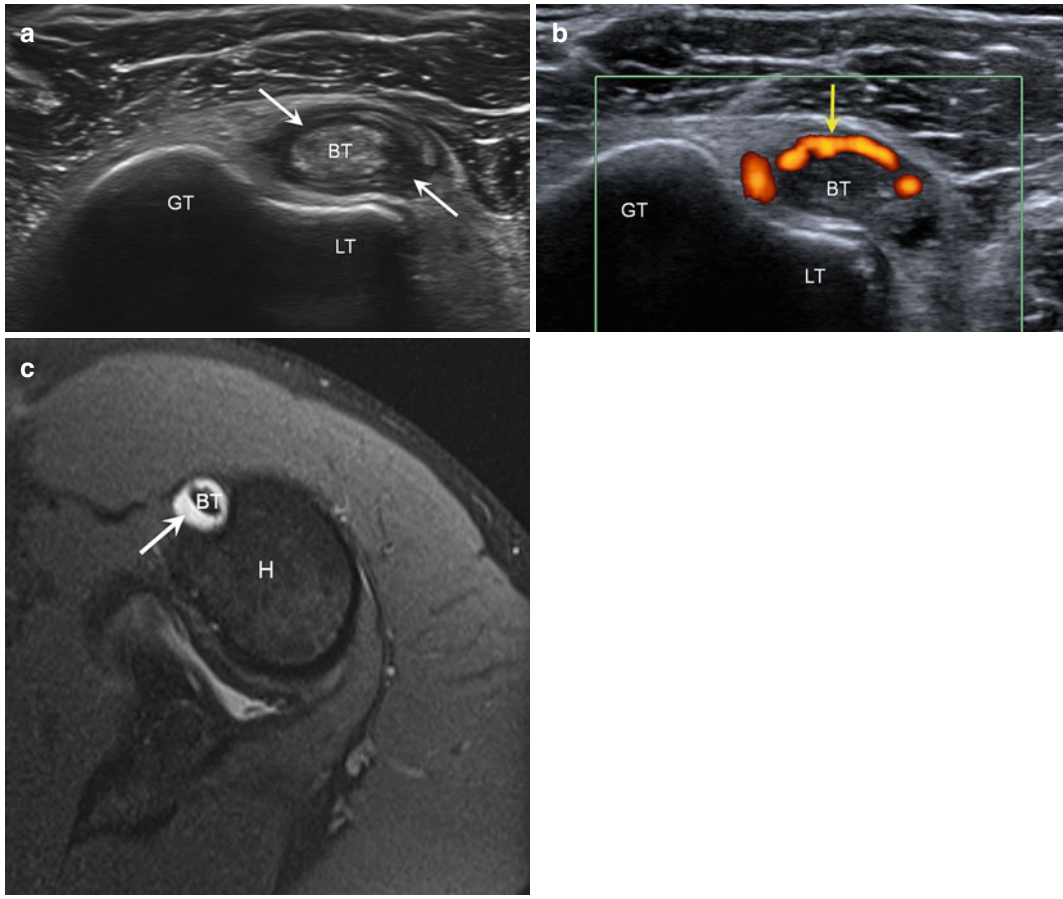

Fig. 5.30 Biceps tenosynovitis. (**a**) Short-axis ultrasound image of the biceps tendon (*BT*) shows an enlarged, heterogeneous tendon surrounded by hypoechoic fluid (*arrows*); greater tuberosity (*GT*), lesser tuberosity (*LT*). (**b**) Power Doppler ultrasound image demonstrates hyperemia (*yellow arrow*) due to tenosynovitis of the biceps tendon (*BT*); greater tuberosity (*GT*), lesser tuberosity (*LT*). (**c**) Corresponding axial fluid-sensitive MRI shows biceps tendon (*BT*) surrounded by fluid (*arrow*); humerus (*H*)

tendons. The supraspinatus is by far the most frequently affected tendon (80 %); however, the other rotator cuff tendons may also be affected (Bianchi and Martinoli 2007; Bosworth 1941; Mole et al. 1997). It is thought to be the result of local hypoxia within the tendon that results in metaplasia of the tendon and resultant calcification (Uhthoff and Sarkar 1989). Areas of calcification may appear as linear echogenic foci with posterior acoustic shadowing or more globular areas of echogenicity without shadowing (Fig. 5.32). These latter calcifications are typically more symptomatic and associated with hyperemia on power Doppler interrogation (Chiou et al. 2002). These calcifications may be treated with ultrasound-guided aspiration that will be discussed later in this chapter (Farin et al. 1995b; Howard et al. 1993).

5.4.4 Impingement

Impingement syndromes in the shoulder are readily evaluated with dynamic ultrasound imaging. Impingement occurs when the acromiohumeral interval through which the supraspinatus tendon passes is narrowed. This may be due to a thickened coracoacromial ligament, an acromioclavicular joint arthrosis, or a subacromial spur (Farin et al. 1990). On ultrasound, the supraspinatus tendon and subacromial–subdeltoid bursa become entrapped between the

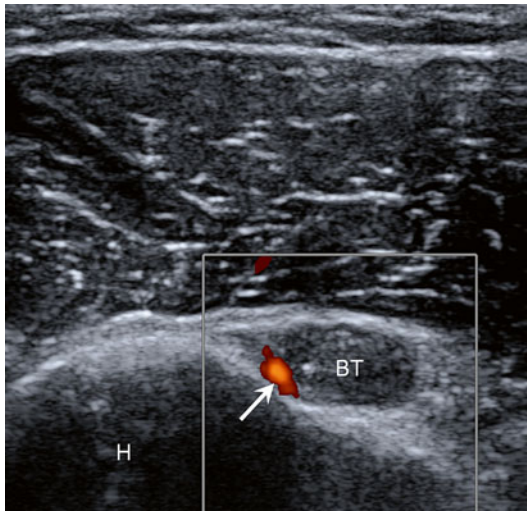

Fig. 5.31 Circumflex artery branch. Short-axis ultrasound image of the biceps tendon (*BT*) with normal branch of the anterior humeral circumflex artery (*arrow*) that should not be confused with hyperemia; humerus (*H*)

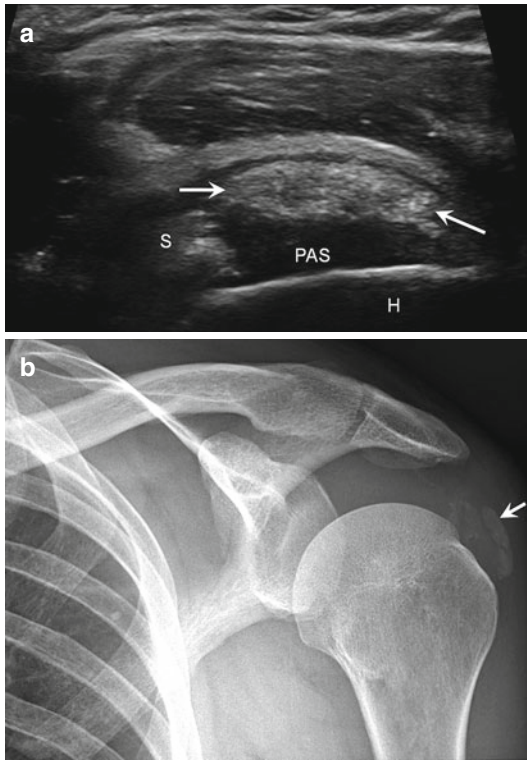

Fig. 5.32 Supraspinatus calcific tendinitis. Long-axis ultrasound image of the supraspinatus tendon (*S*) shows an ovoid echogenic focus (*arrows*) with posterior acoustic shadowing (*PAS*) reflecting calcific tendinitis; humerus (*H*). (**b**) Anteroposterior radiograph shows calcific deposit (*arrow*)

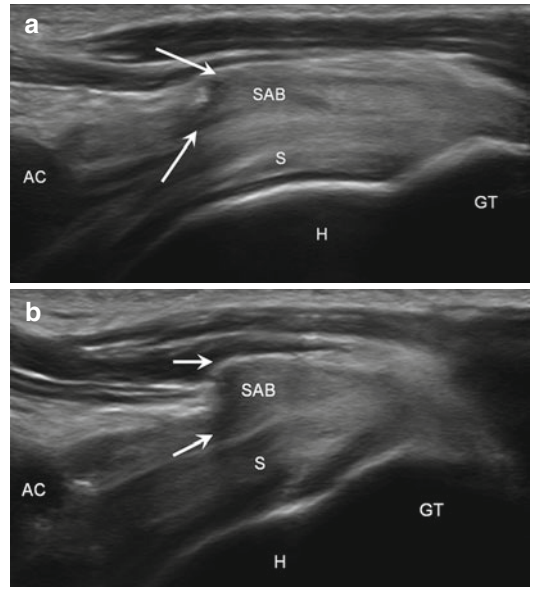

Fig. 5.33 Subacromial impingement. Long-axis ultrasound images of supraspinatus tendon (*S*) with (**a**) mild shoulder abduction show thickened subacromial bursa (*SAB*) becoming "bunched" (*arrows*) due to impingement under acromion (*AC*). With increased abduction in (**b**), the bursa demonstrates increased "bunching" (*arrows*); humerus (*H*), greater tuberosity (*GT*)

greater tuberosity and the structures of the coracoacromial arch (Farin et al. 1990). As the arm is abducted, there may be "bunching" of the supraspinatus tendon and subacromial–subdeltoid bursa as these structures attempt to pass under the coracoacromial arch (Fig. 5.33). There may also be pooling of fluid within the bursa with subacromial–subdeltoid bursitis (Farin et al. 1990). Abnormalities of the supraspinatus tendon may be seen in association with impingement including tendinosis and tears. Similar findings can be seen in subcoracoid impingement where there is narrowing of the coracohumeral interval, resulting in the entrapment of the subscapularis tendon during internal rotation of the shoulder (Troelsen et al. 2007).

5.4.5 Glenoid Labrum

As previously described, the normal glenoid labrum, composed of fibrocartilage, is hyperechoic (Fig. 5.34). The labrum attaches to the adjacent glenoid and appears as a triangular

structure (Talijanovic et al. 2000). Degeneration of the labrum appears as diffuse hypoechogenicity, while a tear appears as a discrete hypoechoic or anechoic defect (Tirman et al. 1994). While a portion of the posterior labrum can be visualized when scanning the infraspinatus tendon and the posterior joint recess, the anterior labrum is difficult to assess due to overlying structures. Therefore, MRI with or without intra-articular gadolinium should be considered to evaluate the labrum.

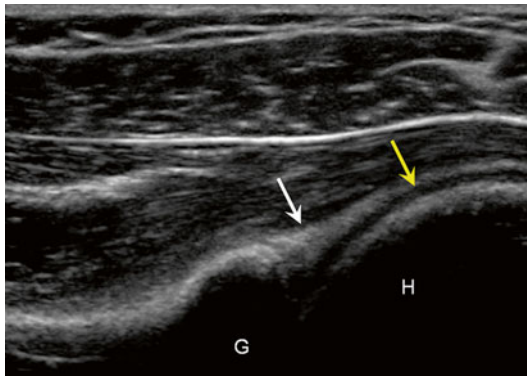

Fig. 5.34 Normal glenoid labrum. Longitudinal ultrasound image shows normal posterior labrum (*white arrow*) which appears as an echogenic triangle attached to the glenoid (*G*); normal hypoechoic articular cartilage (*yellow arrow*), humerus (*H*)

A paralabral cyst is a fluid collection that may develop when fluid from the glenohumeral joint extends through a labral tear into the surrounding tissues (Hashimoto et al. 1994). Around the shoulder, this may result in compression of the suprascapular nerve within the suprascapular or the spinoglenoid notch (Fehrman et al. 1995; Tirman et al. 1994; Tung et al. 2000). The cysts appear as round, anechoic sometimes multiloculated collections that can contain echogenic debris (Fig. 5.35). A communication through the associated labral tear may also be demonstrated. There may be associated atrophy of the infraspinatus or supraspinatus and infraspinatus muscles in the region of the spinoglenoid notch or suprascapular notch cysts, respectively (Fig. 5.36). These cysts may be aspirated under ultrasound guidance (see Sect. 5.10.1) often producing thick, clear material, although the cysts can recur if the underlying labral tear is not repaired.

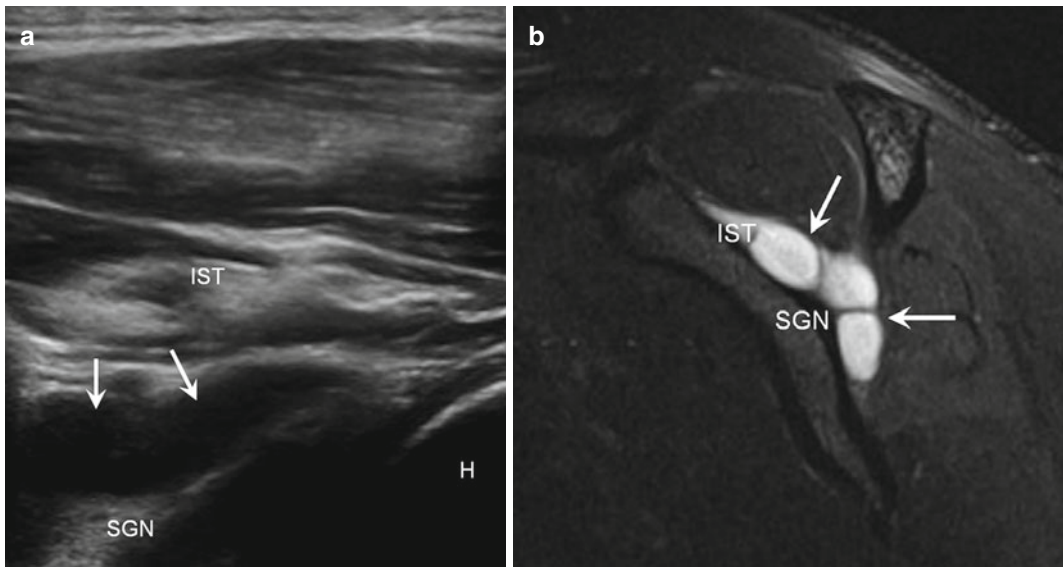

Fig. 5.35 Paralabral cyst. (**a**) Long-axis ultrasound image along the posterior shoulder at the spinoglenoid notch (*SGN*) demonstrates an anechoic collection (*arrows*) consistent with a paralabral cyst; infraspinatus (*IST*), humerus (*H*). In (**b**), corresponding sagittal fluid-sensitive MRI shows the spinoglenoid notch (*SGN*) with the paralabral cyst (*arrows*) and mild denervation edema in the infraspinatus muscle (*IST*)

5.4.6 Fractures

Fractures of the greater tuberosity can be diagnosed during evaluation of the shoulder following trauma. Nondisplaced fractures may be missed at plain radiography. Fractures appear as a focal disruption of the echogenic cortex with an associated step-off (Fig. 5.37) (Patten et al. 1992). There will typically be point tenderness on exam over the fracture site.

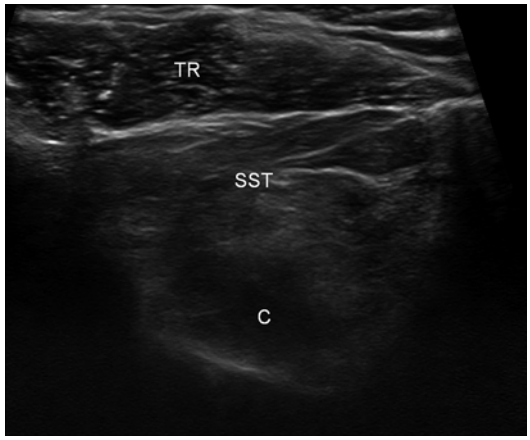

Fig. 5.36 Muscle atrophy. Short-axis ultrasound image of the supraspinatus muscle (*SST*) shows increased echogenicity due to denervation from the suprascapular notch paralabral cyst (*C*). Compare to normal echogenicity of the adjacent trapezius (*TR*)

5.4.7 Pectoralis Major

Although not routinely evaluated during a shoulder ultrasound examination, the pectoralis major muscle and tendon may be assessed as directed by the patient's clinical history or symptoms. The normal pectoralis major muscle has three heads, the clavicular, sternal, and abdominal heads. The tendons converge into a single tendon unit to insert on the bicipital groove of the humeral shaft, just lateral to the biceps tendon. The insertion extends over 5 cm in craniocaudal dimension (Rehman and Robinson 2005). Injury of the pectoralis muscle has become more common in high-performance athletes and is seen almost exclusively in men (Weaver et al. 2005). Injuries to the pectoralis include avulsion injuries at the tendon insertion with or without osseous avulsion or injury to the myotendinous junction or muscle belly (Miller 2003). As in the rotator cuff, injuries may be partial or full thickness. The most common injuries are partial tears involving both the sternal and clavicular heads (Connell et al. 1999; Lee et al. 2000). Injuries manifest as hypoechoic or anechoic regions within the tendon, at the myotendinous junction, or within the muscle belly with disruption of the tendon and/or muscle fibers (Fig. 5.38). Retraction indicates a full-thickness tear. There may be associated hematoma that can be hypoechoic or anechoic

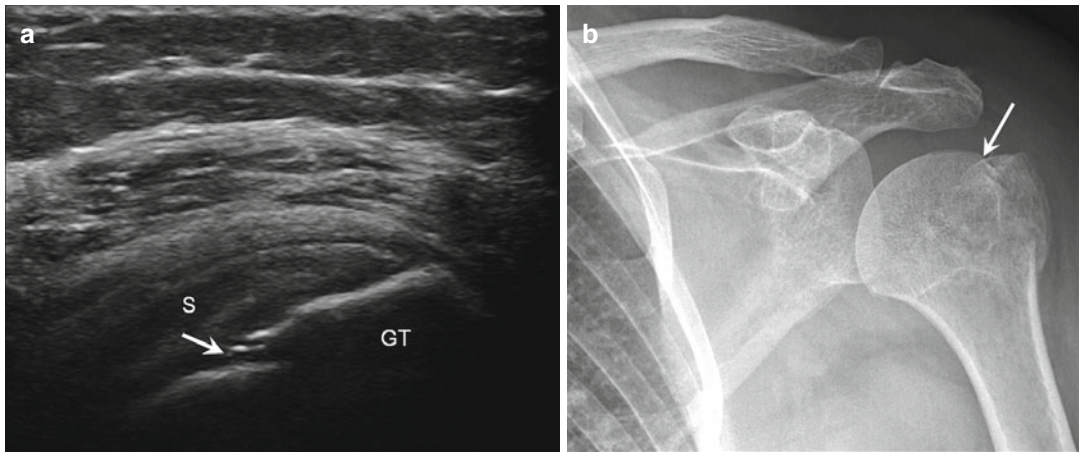

Fig. 5.37 Greater tuberosity fracture. (**a**) Long-axis ultrasound image of the supraspinatus tendon (*S*) and greater tuberosity (*GT*) demonstrates focal cortical disruption (*arrow*) due to a minimally displaced fracture. (**b**) Corresponding anteroposterior radiograph shows the fracture (*arrow*)

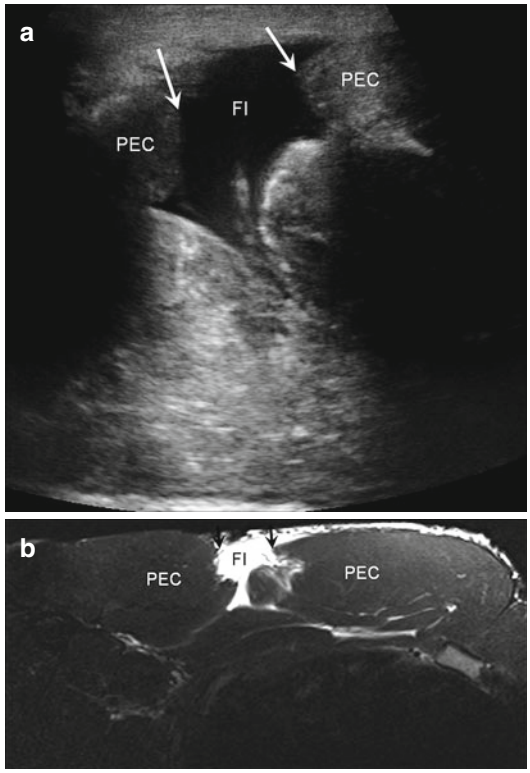

Fig. 5.38 Pectoralis muscle tear. (**a**) Long-axis ultrasound image of the pectoralis major muscle (*PEC*) demonstrates a myotendinous junction tear (*arrows*) with intervening fluid/hemorrhage (*Fl*). (**b**) Corresponding axial fluid-sensitive MRI shows the tear (*black arrows*) of the pectoralis (*PEC*) with a fluid-filled gap (*Fl*)

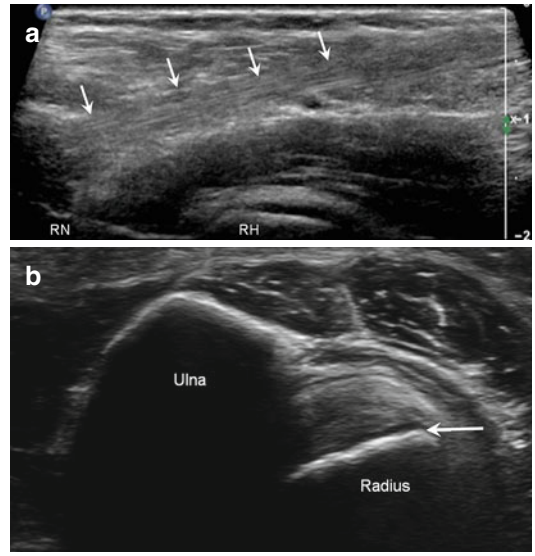

Fig. 5.39 Normal biceps insertion. (**a**) Long-axis ultrasound image shows the normal echogenic appearance of the biceps tendon insertion (*arrows*); radial neck (*RN*), radial head (*RH*). (**b**) Short-axis ultrasound image of the posterior forearm just below the elbow joint with the wrist in pronation shows the normal insertion of biceps (*arrow*); radius and ulna

(Weaver et al. 2005). There may be edema within the more proximal muscle bellies. Dynamic examination may accentuate the site of the tear.

5.5 Elbow Ultrasound

5.5.1 Biceps Brachii

Because many of the ligaments and tendons of the elbow are relatively superficial in location, they are readily evaluated with ultrasound. Evaluation of the distal biceps, however, can be difficult due to its oblique course, anisotropy, and the deeper location of the insertion on the radial tuberosity. Provocative maneuvers and dynamic imaging may be used to better visualize the insertion and to eliminate anisotropy (Fig. 5.39) (Chew and Giuffrè 2005; Miller and Adler 2000). Injuries of the biceps tendon typically occur 1–2 cm proximal to the insertion on the radial tuberosity. Tears can be complete or partial and may be associated with pre-existing tendinosis due to relative hypovascularity of the tendon in this region (Chew and Giuffrè 2005; Vardakas et al. 2001). Mechanical impingement between the radial tuberosity and proximal ulna during pronation may also predispose to biceps tendon tears (Fig. 5.40) (Chew and Giuffrè 2005; Seiler et al. 1995). There may be associated bicipitoradial bursitis manifesting as a hypoechoic fluid collection that may contain internal debris or echoes that insinuates between the insertional fibers of the biceps tendon and the adjacent radial tuberosity (Fig. 5.41) (Sofka and Adler 2004).

With partial tears, there is thickening of and decreased echogenicity within the tendon (Fig. 5.42). This may be difficult to differentiate from tendinosis. There may also be attenuation of the distal tendon in the setting of partial tearing. Tendon retraction will be absent. Dynamic imaging can help elucidate partial tears from

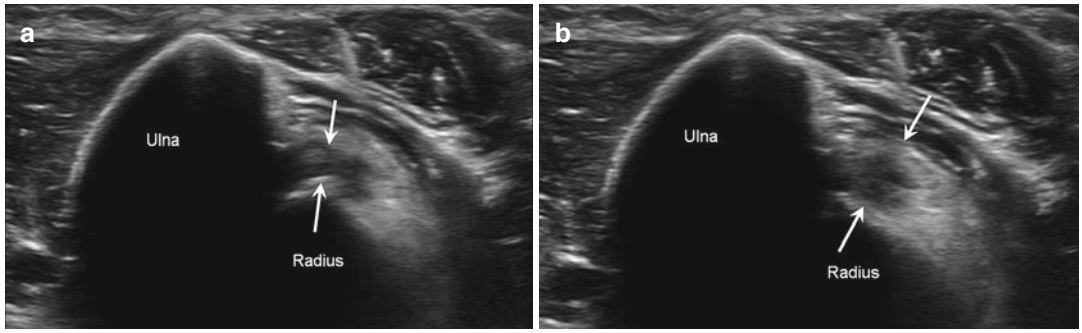

Fig. 5.40 Biceps impingement at insertion. Short-axis ultrasound images of the posterior forearm just below the elbow in (**a**) pronation and (**b**) supination show the biceps tendon insertion (*arrows*) becoming "bunched" in supination (**b**) due to impingement; radius and ulna

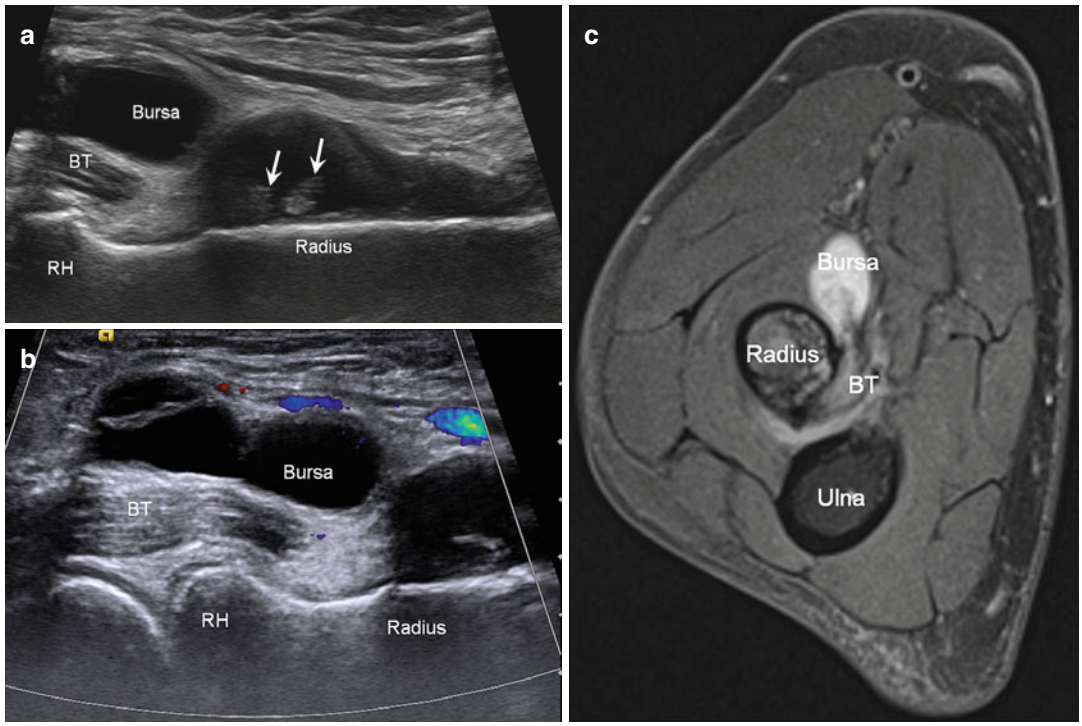

Fig. 5.41 Bicipitoradial bursitis. Long-axis ultrasound images without (**a**) and with (**b**) color Doppler demonstrate distension of the bicipitoradial bursa (*Bursa*) at the level of the biceps tendon (*BT*) insertion on the radius; radial head (*RH*), synovial hypertrophy (*arrows*). (**c**) Corresponding axial fluid-sensitive MRI shows the distended bicipitoradial bursa (*Bursa*) where biceps tendon (*BT*) inserts on the radius; ulna

tendinosis and nonretracted full-thickness tears (Chew and Giuffrè 2005; Hayter and Adler 2012; Kalume et al. 2009). With full-thickness tears, there will be complete disruption of the tendon fibers with a hypoechoic defect. There may be surrounding edema or hemorrhage in the acute setting (Fig. 5.43). If there is tearing of the bicipital aponeurosis, there will be proximal retraction of the tendon into the arm. This usually occurs in the setting of a single, forceful

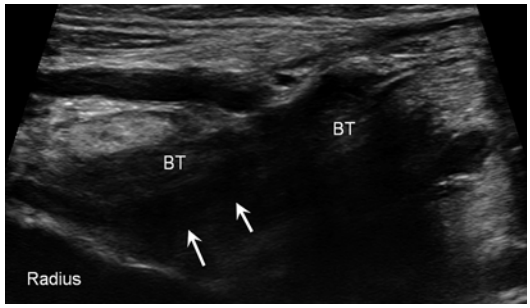

Fig. 5.42 Partial tear distal biceps. Long-axis ultrasound image of the biceps tendon (*BT*) insertion shows a hypoechoic defect (*arrows*) due to partial tearing; radius

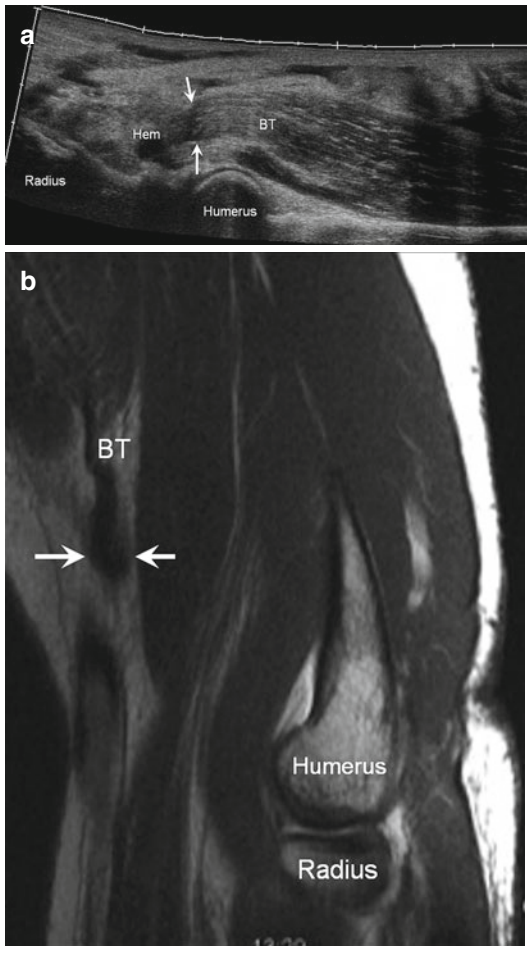

Fig. 5.43 Complete rupture distal biceps. (**a**) Longitudinal ultrasound image of the distal biceps tendon (*BT*) demonstrates complete rupture at the insertion on the radius (*Rad*) with retraction of the tendon (*arrows*) and intervening hemorrhage (*Hem*); humerus. (**b**) Sagittal proton density-weighted MRI shows the ruptured biceps tendon (*BT*) that is proximally retracted (*arrows*); humerus, radius

traumatic injury. Ultrasound may be used to locate the retracted tendon stump (Chew and Giuffrè 2005; Hayter and Adler 2012; Miller and Adler 2000).

5.5.2 Triceps Brachii

Triceps injury may result from direction impaction or tendon avulsion from the olecranon. Tears may be partial or complete, and there may be pre-existing tendinosis or enthesopathy (Fig. 5.44), or there may be associated olecranon bursitis. Tears appear as hypoechoic or anechoic defects in the tendon involving some (partial) or all (complete) of the tendon fibers (Fig. 5.45). There may be tendon retraction in full-thickness tears, and a linear focus of increased echogenicity reflecting an osseous fragment may be present in the setting of bone avulsion (Fig. 5.46). Tendinosis appears as tendon enlargement with decreased echogenicity of the tendon fibers without disruption (Downey et al. 2011; Hayter and Adler 2012; Jacobson 2013b).

5.5.3 Common Flexor and Extensor Tendons

The origins of the flexor and extensor tendons of the hand and wrist originate from the medial and lateral epicondyles, respectively. Disorders of the tendons including tendinosis and tearing are the sequelae of acute, traumatic, and chronic overuse injuries (Hayter and Adler 2012). The term lateral epicondylitis or "tennis elbow" refers to pathology of the common extensor tendons. Although acute or chronic inflammation is lacking, the term epicondylitis continues to be used. The underlying pathology involves tendinosis and tearing of the tendons (Nirschl and Pettrone 1979; Potter et al. 1995). At ultrasound, the tendons appear enlarged and hypoechoic (Connell et al. 2000). There may be foci of internal calcification within the tendon and enthesopathic change at the lateral epicondyle (Hayter and Adler 2012).

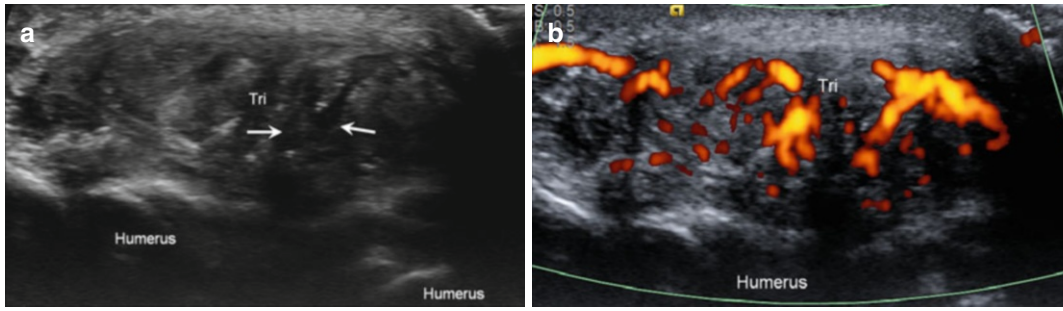

Fig. 5.44 Triceps tendinosis. (**a**) Transverse ultrasound image of the distal triceps tendon (*Tri*) shows enlargement and heterogeneity of the tendon with interstitial tearing (*arrows*). (**b**) Power Doppler image shows extensive hyperemia due to neovascularity in the setting of tendinosis; humerus

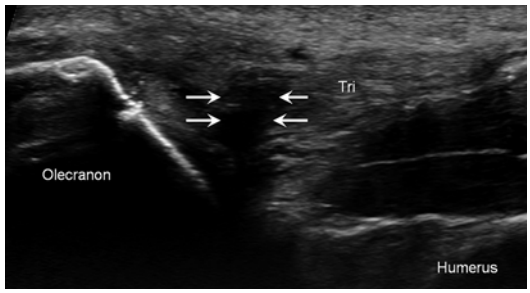

Fig. 5.45 Triceps tendon tear. Longitudinal ultrasound image demonstrates a high-grade partial, deep surface tear (*arrows*) of the distal triceps tendon (*Tri*); humerus (*Hum*), olecranon (*Olec*)

With power Doppler interrogation, there may be increased vascularity (Tran and Chow 2007). The most commonly and severely affected tendon is the extensor carpi radialis brevis. In the setting of tears, there is partial- or full-thickness discontinuity of the tendon fibers (Fig. 5.47) (Levin et al. 2005).

Medial epicondylitis or "golfer's elbow" refers to tendinopathy of the common flexor origin. This entity is much less common than lateral epicondylitis and is most frequently seen in overhead, throwing athletes such as baseball pitchers (Kaplan and Potter 2004). The findings of medial epicondylitis are similar to those of lateral epicondylitis (Fig. 5.48) (Kijowski and De Smet 2005; Miller et al. 2002). Ultrasound is

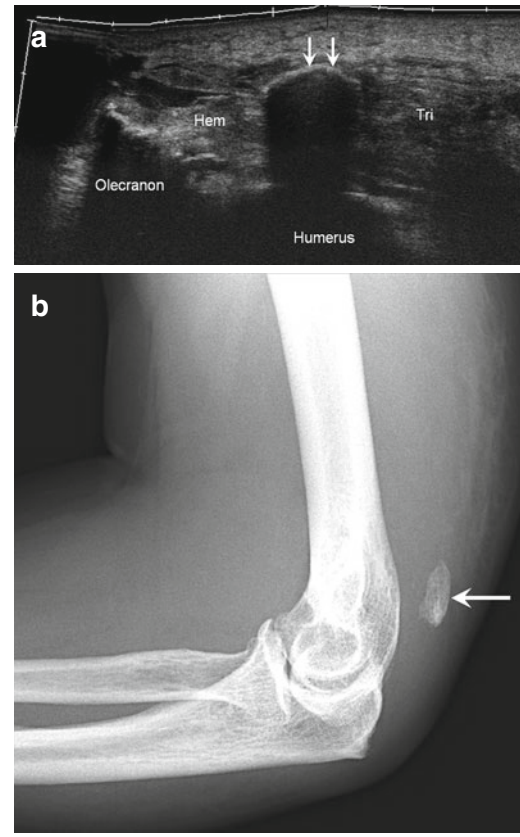

Fig. 5.46 Triceps tendon avulsion. (**a**) Longitudinal ultrasound image shows a complete avulsion of the distal triceps tendon (*Tri*) from the olecranon with an ossific avulsion (*arrows*) and hemorrhage (*Hem*); humerus. (**b**) Lateral radiograph of a different patient with similar findings of an avulsion fracture (*arrow*) due to a triceps tendon tear

useful in assessing both the findings of medial epicondylitis and concomitant pathology of the medial collateral ligament and the ulnar nerve that will be further described below (Martin and Schweitzer 1998).

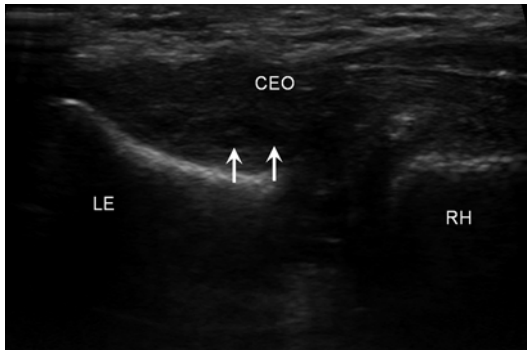

Fig. 5.47 Lateral epicondylitis. Longitudinal ultrasound image of the lateral elbow shows thickening of the common extensor tendon origin (*CEO*) with a partial deep surface tear (*arrows*); lateral epicondyle (*LE*), radial head (*RH*)

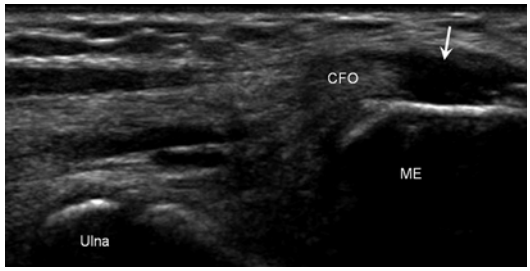

Fig. 5.48 Medial epicondylitis. Longitudinal ultrasound image of the medial elbow shows an anechoic defect (*arrow*) in the common flexor tendon origin (*CFO*) reflecting a high-grade tear; medial epicondyle (*ME*), ulna

5.5.4 Medial (Ulnar) Collateral Ligament and Lateral (Radial) Collateral Ligament Complex

The primary stabilizer of the medial elbow against valgus instability is the medial collateral ligament (MCL), composed of anterior, posterior, and transverse/oblique bundles (Morrey and An 1983). The anterior bundle is the most functionally important and frequently evaluated component of the MCL complex, extending from the undersurface of the medial humeral epicondyle to the sublime tubercle of the ulna (Hayter and Adler 2012). This segment of the MCL is the most commonly injured ligament in the elbow and may be injured acutely, or more commonly, as a result of chronic overuse as seen in overhead throwing athletes (Jobe and Nuber 1986). The normal appearance of the anterior bundle of the MCL is a smooth, hyperechoic band of tissue (Fig. 5.49). Due to anisotropy, the ligament may appear hypoechoic (Jacobson et al. 2003; Ward et al. 2003). Sprains of the ligament appear as decreased echogenicity with loss of the normal band-like appearance of the ligament. Partial- and full-thickness tears appear as hypoechoic or anechoic areas of discontinuity in the ligament fibers (Fig. 5.49). In the setting of hemorrhage, it may be difficult to distinguish partial- and full-thickness tears (Miller et al. 2004). Dynamic imaging is helpful in these situations by exerting valgus stress on the elbow in partial flexion and assessing for separation of the torn fibers as well as widening of the medial joint line. The contralateral side may be imaged concurrently to assess

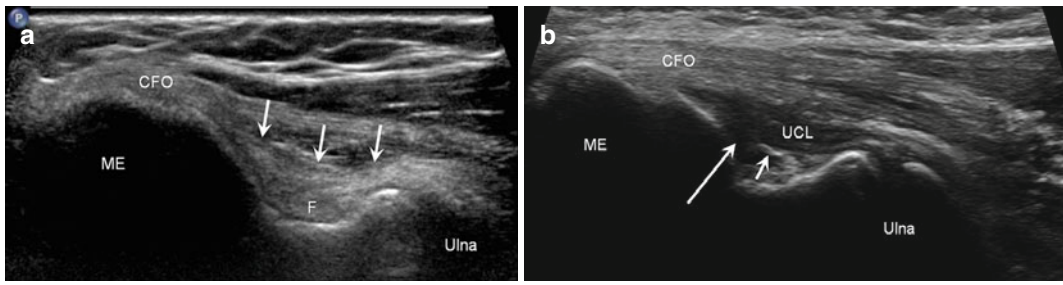

Fig. 5.49 Normal and torn ulnar collateral ligament. (**a**) Longitudinal ultrasound image of the medial elbow demonstrates the normal ulnar collateral ligament (*arrows*). (**b**) Long-axis ultrasound image of the medial elbow in a different patient shows an anechoic area reflecting a tear (*long arrow*) of the ulnar collateral ligament (*UCL*) at the origin with a small avulsion fracture (*short arrow*); common flexor origin (*CFO*), medial epicondyle (*ME*), ulna, fat (*F*)

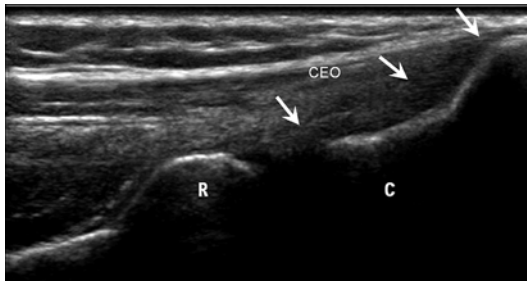

Fig. 5.50 Normal lateral structures of the elbow. Longitudinal ultrasound image of the lateral elbow shows the common extensor origin (*CEO*) superficial to, and nearly inseparable from, the radial collateral ligament (*arrows*). The lateral ulnar collateral ligament (not shown) is slightly posterior to the radial collateral ligament; radius (*R*), capitellum (*C*)

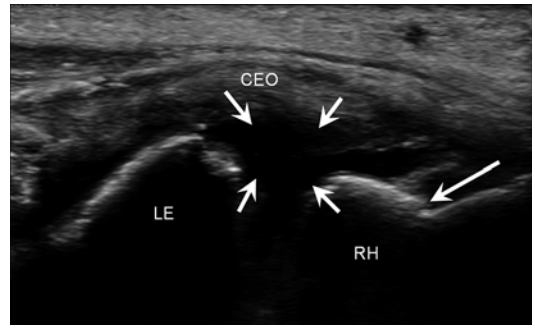

Fig. 5.51 Tear of lateral ligaments of the elbow. Longitudinal ultrasound image of the lateral elbow following dislocation shows complete disruption of the lateral ligaments (*short arrows*) with a focal cortical disruption at the radial head (*RH*)/neck junction (*long arrow*) indicating a fracture; common extensor origin (*CEO*), lateral epicondyle (*LE*)

for asymmetry (De Smet et al. 2002; Nazarian et al. 2003). In the setting of chronic MCL pathology due to overuse in overhead athletes, the ligament may be thickened and hypoechoic or may become remodeled and elongated due to the repetitive stress (De Smet et al. 2002; Nazarian et al. 2003). In the chronic setting, there may be associated signs of valgus extension overload or posteromedial impingement that can be seen in the throwing athlete. These include common flexor tendinopathy, medial joint line osteophytes, intra-articular bodies, or ulnar neuropathy. Due to increased compressive forces on the lateral joint line, there may be associated radiocapitellar arthritis (Gaary et al. 1997; Hayter and Adler 2012; Kijowski et al. 2005; Wilson et al. 1983).

The lateral collateral ligament complex is composed of the radial collateral ligament (RCL), the lateral ulnar collateral ligament (LUCL), and the annular ligament. The LUCL is the most important stabilizer against varus stress and posterolateral rotatory instability (Olsen et al. 1996). The LUCL originates from the posterior aspect of the lateral humeral epicondyle and curves around the posterior aspect of the radial head to insert on the supinator crest of the ulna. The RCL originates at the lateral humeral epicondyle and inserts along the annular ligament (Hayter and Adler 2012). The RCL and common extensor origin may be difficult to separate when both structures are normal. The normal ligaments should be echogenic and band-like in appearance (Fig. 5.50) (Jacobson 2013b).

The LUCL may be injured acutely following varus extension injury or a traumatic elbow dislocation, such as after a fall on an outstretched hand (Nestor et al. 1992). The ligament may also be injured iatrogenically following overaggressive debridement of the common extensor tendon for the treatment of lateral epicondylitis. In addition, severe cases of lateral epicondylitis may extend into and involve the lateral collateral ligament complex. Disruption of the LUCL results in posterolateral rotatory instability with posterior subluxation of the radial head with respect to the capitellum (O'Driscoll et al. 1992; Walz et al. 2010). Like the UCL, tears of the lateral ligamentous structures manifest as areas of decreased echogenicity with partial or complete disruption of the ligament fibers (Fig. 5.51).

5.5.5 Ulnar Neuropathy

The ulnar nerve traverses the posterior elbow within the cubital tunnel. The cubital retinaculum forms the roof of this tunnel, keeping the nerve within the tunnel through the range of motion of the elbow. Localized ulnar neuropathy at the elbow is known as cubital tunnel syndrome (Hayter and Adler 2012). Causes of ulnar neuropathy include acute trauma, chronic repetitive injury during

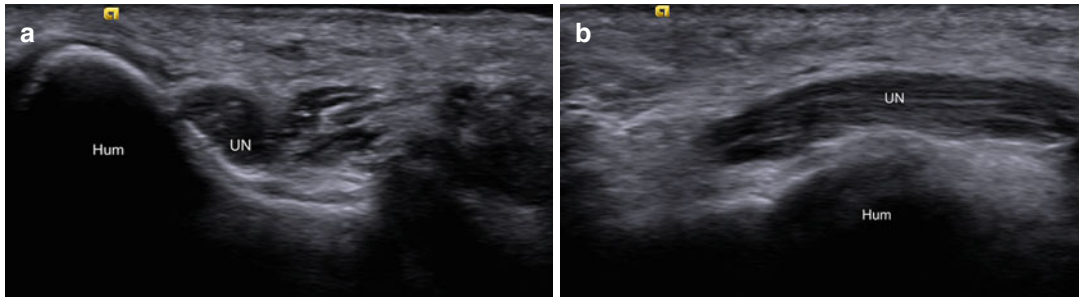

Fig. 5.52 Ulnar neuropathy. (**a**) Short- and (**b**) long-axis ultrasound images of the posterior elbow demonstrate enlargement of and decreased echogenicity within the ulnar nerve (*UN*) in the setting of ulnar neuropathy; humerus (*Hum*)

elbow flexion, ulnar nerve subluxation/dislocation, or the presence of an anconeus epitrochlearis muscle, an anatomic variant present in up to 23 % of the population (Husarik et al. 2009; Jacobson 2013b). With ulnar neuritis, the nerve is abnormally enlarged and diffusely decreased in echogenicity with loss of the normal fascicular pattern (Fig. 5.52) (Hayter and Adler 2012). A cross-sectional area of greater than 9 mm^2 is considered abnormal (Thoirs et al. 2008). Measurements, however, are not well established for the ulnar nerve.

The role of ultrasound is to evaluate for a potentially treatable cause of ulnar neuritis, to assess for subluxation or dislocation, and to provide guidance for therapeutic injection. Although frequently no cause of compression is seen, other causes besides an anconeus epitrochlearis include synovitis, soft tissue masses, and findings related to valgus extension overload as seen in the throwing athlete, including osteophytes and joint bodies (Wilson et al. 1983).

The advantage of ultrasound over MRI is the ability to perform dynamic imaging. This is particularly important in evaluating for ulnar nerve subluxation where the nerve abnormally dislocates medially over the medial epicondyle during flexion (Fig. 5.53) and "snapping triceps" where the medial head of the triceps subluxates medially during flexion, resulting in medial dislocation of the ulnar nerve. This latter entity has been described in weight lifters (Husarik et al. 2009; Jacobson et al. 2010; O'Driscoll et al. 1991; Okamoto et al. 2000).

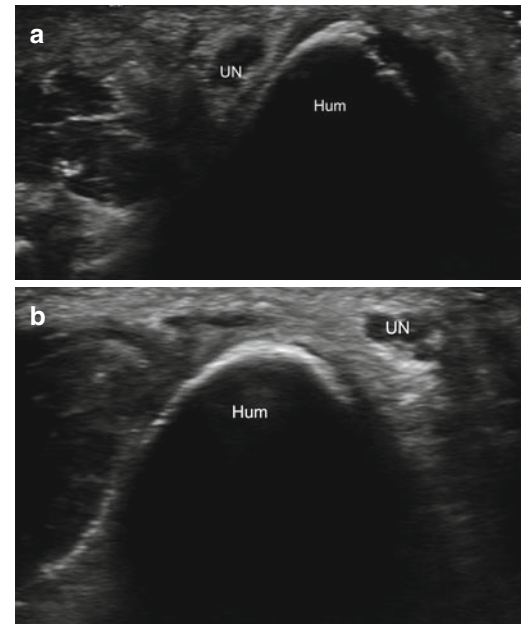

Fig. 5.53 Ulnar nerve subluxation. Short-axis ultrasound images of the posterior elbow in extension (**a**) and flexion (**b**) demonstrate subluxation of the ulnar nerve (*UN*) from lateral (**a**) to medial (**b**) with respect to the distal humerus (*Hum*)

5.5.6 Olecranon Bursitis

In addition to bicipitoradial bursitis, olecranon bursitis is readily assessed with ultrasound. In the athlete, this is frequently secondary to trauma. The collapsed bursa is not easily identified; however, in the setting of olecranon bursitis, there will be distension of the bursa with anechoic or hypoechoic fluid that may contain internal debris (Fig. 5.54). If the fluid is more hyperechoic, a

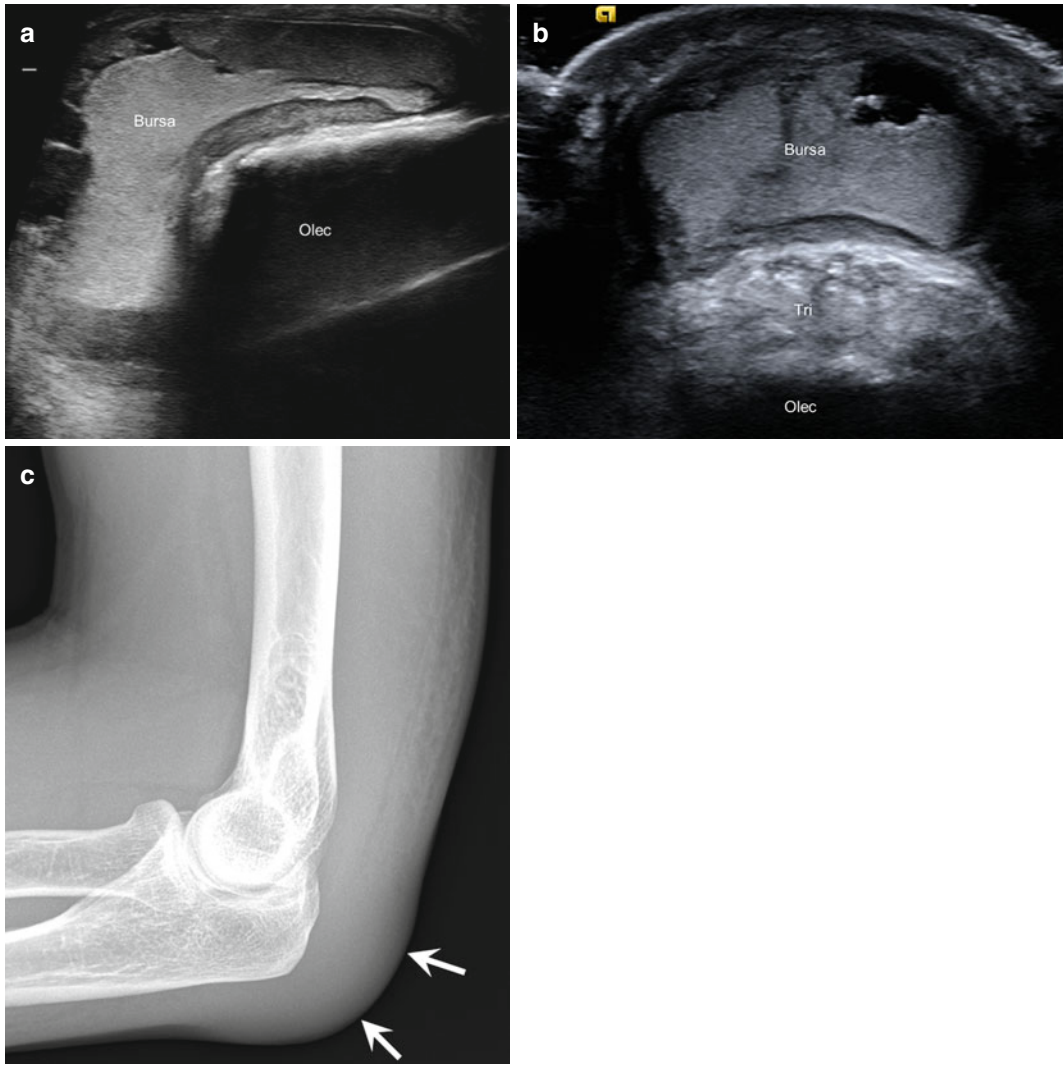

Fig. 5.54 Olecranon bursitis. (**a**) Long-axis extended field of view and (**b**) short-axis ultrasound images of the posterior elbow demonstrate marked olecranon bursitis with distension of the bursa (*Bursa*) with echogenic, hemorrhagic fluid; triceps tendon (*Tri*), olecranon (*Olec*). (**c**) Lateral radiograph of the elbow shows soft tissue swelling (*arrows*) in the location of the olecranon bursa

hemorrhagic bursitis should be considered (Jacobson 2013b).

5.6 Wrist and Hand (Including Finger) Ultrasound

Ultrasound is an ideal modality for the evaluation of sports-related injuries in the hand and wrist because of the development of high-frequency transducers and the superficial location of the structures (Teefey et al. 2000a, b, c). In addition, dynamic imaging may be performed to identify abnormalities of tendon motion or joint instability.

5.6.1 Scapholunate Ligament

The dorsal component of the scapholunate ligament is the more clinically relevant portion of the ligament and an important stabilizer of the carpus. The dorsal fibers are readily assessed with sonography appearing as a hyperechoic, fibrillar band. Tears appear as focal disruptions of the normal

hyperechoic ligament with a focal area of decreased echogenicity (Jacobson et al. 2002). In the setting of chronic, repetitive injury, the ligament may be abnormally thickened and hypoechoic (Jacobson et al. 2002; Renoux et al. 2009). There may be associated widening of the scapholunate interval that may be accentuated with clenching of the fist. A ganglion cyst (Fig. 5.55) may also develop adjacent to the tear with fluid decompressing from the joint through a tear (Cardinal et al. 1994). This may cause compression of the distal portion of the posterior interosseous nerve.

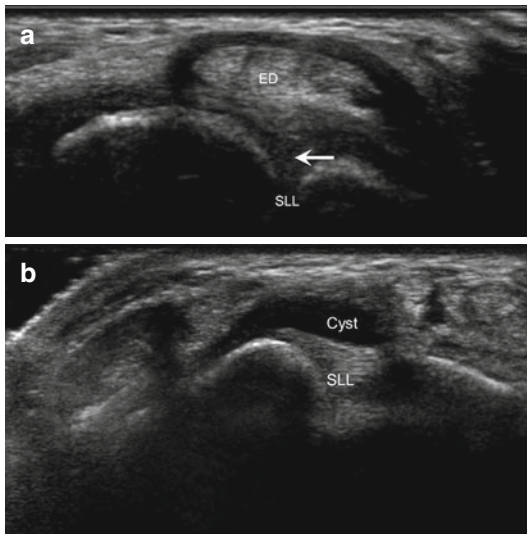

Fig. 5.55 Scapholunate ligament pathology. (**a**) Short-axis ultrasound image of the dorsal wrist demonstrates a hypoechoic tear (*arrow*) of the scapholunate ligament (*SLL*); extensor digitorum tendon (*ED*). (**b**) Short-axis ultrasound image of the scapholunate ligament (*SLL*) with an associated ganglion (*Cyst*)

5.6.2 Scaphoid Fracture

Fractures of the scaphoid may also be diagnosed with ultrasound with a fairly high degree of accuracy (Herneth et al. 2001). Findings include focal areas of periosteal reaction and cortical disruption or step-off (Herneth et al. 2001).

5.6.3 Extensor Tendons

Abnormalities of the tendons can be readily assessed with ultrasound including tenosynovitis, tendinosis, and tendon tears. Tenosynovitis refers to distension of the sheath surrounding a tendon with fluid and/or soft tissue (Fig. 5.56). The fluid may be anechoic or more heterogeneous and complex due to synovial hypertrophy, hemorrhage, or debris (Daenen et al. 2004; Teefey et al. 2000a, b, c). In the setting of synovial hypertrophy, there may be hyperemia as demonstrated in color or power Doppler interrogation (Fig. 5.56) (Breidahl et al. 1998; Teefey et al. 2000a, b, c).

Tendinosis manifests as focal or diffuse enlargement of the affected tendon with areas of decreased echogenicity (Fig. 5.56). Foci of calcification may be present (Daenen et al. 2004).

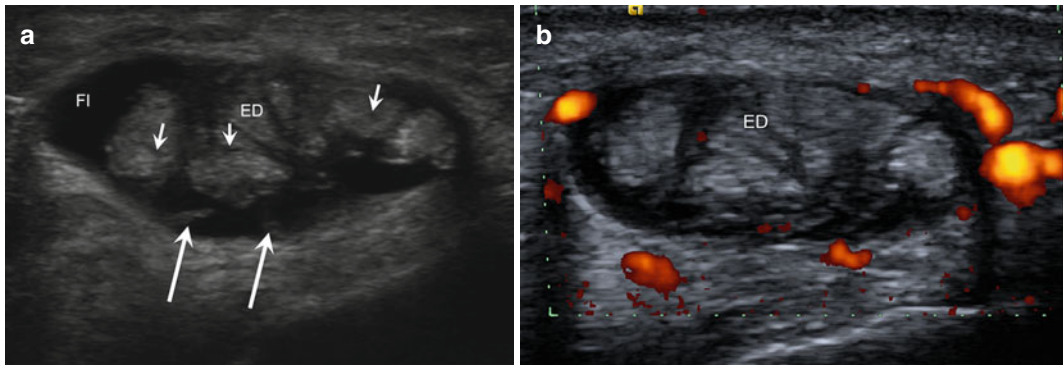

Fig. 5.56 Extensor tendinosis/tenosynovitis of the wrist. (**a**) Short-axis ultrasound image of the extensor digitorum tendon (*ED*) demonstrates mild tendinosis of the tendons with hypoechoic areas (*short arrows*) with fluid (*Fl*) distension of the tendon sheath and synovitis (*long arrows*). (**b**) Same image with power Doppler interrogation shows peritendinous hyperemia in the setting of inflammation

Tendon rupture may be partial or complete and appears as a fluid-filled cleft within the affected tendon with disruption of the normal fibers (Fig. 5.57) (Daenen et al. 2004). The fluid may be anechoic or hypoechoic and complex in the setting of hemorrhage due to acute injury. With complete rupture, there may be retraction and separation of the torn ends of the tendon (Daenen et al. 2004).

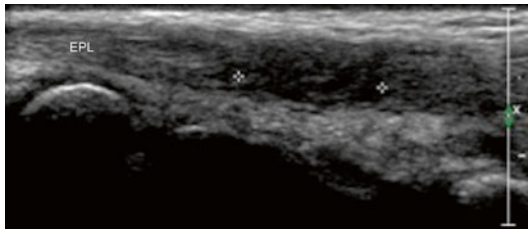

Fig. 5.57 Extensor pollicis longus tear. Longitudinal ultrasound image of the wrist shows a high-grade partial tear (++) of the extensor pollicis longus (*EPL*)

De Quervain's tenosynovitis is a common disorder that describes tendinosis and tenosynovitis of the first extensor compartment of the wrist that includes the abductor pollicis longus (APL) and extensor pollicis brevis (EPB) tendons. It is frequently seen due to chronic repetitive stress and overuse in athletes, such as tennis players (Daenen et al. 2004). At sonography, there will be tendinosis of the APL and EPB tendons with tendon enlargement and decreased echogenicity with loss of the normal fibrillar pattern. There may be linear foci of decreased echogenicity reflecting interstitial microtears (Daenen et al. 2004). There will be distension of the tendon sheath with anechoic or hypoechoic fluid (Fig. 5.58) (Daenen et al. 2004).

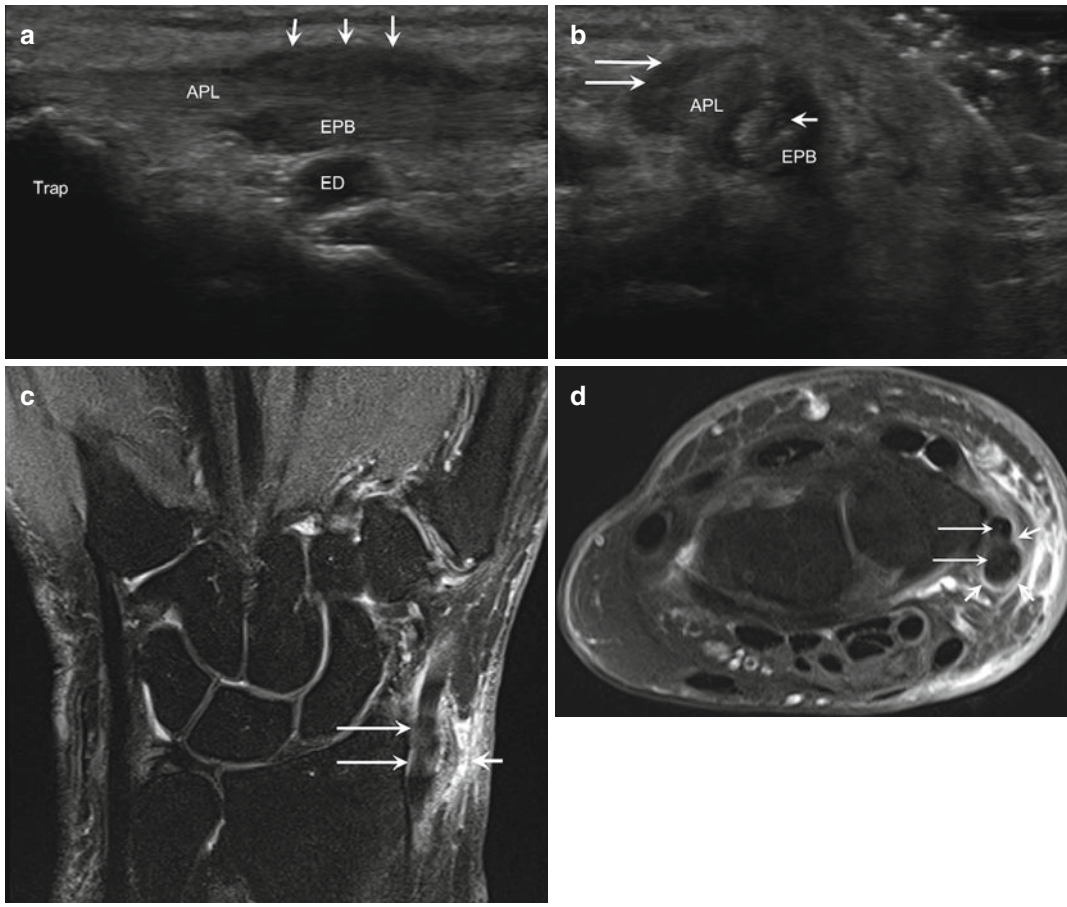

Fig. 5.58 De Quervain's tenosynovitis. (**a**) Long- and (**b**) short-axis ultrasound images of the first extensor compartment of the wrist show tendinosis of the abductor pollicis longus (*APL*) and extensor pollicis brevis (*EPB*) with a split tear (*short arrow*) of the EPB and synovial thickening (*long arrows*); trapezium (*Trap*), radial artery (*RA*). (**c**) Coronal and (**d**) axial fluid-sensitive MRIs of the same patient show findings of De Quervain's tenosynovitis including enlargement of the abductor pollicis longus and extensor pollicis brevis tendons (*long arrows*) with surrounding fluid (*arrow*)

This is often accompanied by thickening of the corresponding extensor retinaculum.

The extensor hood stabilizes the extensor tendons of the hand at the level of the metacarpophalangeal (MCP) joints, maintaining them in place through the range of motion during flexion and extension (Kichouh et al. 2011). The sagittal bands are the most important stabilizing structures of the extensor hood (Clavero et al. 2003; Drapé et al. 1994; Scott 2000; Young and Rayan 2000). Ruptures of the sagittal bands can occur following trauma to the MCP joint as seen in "boxer knuckle." This can result in subluxation or dislocation of the extensor tendon at the level of the MCP joint (Kichouh et al. 2011). On short-axis sonographic imaging, the normal sagittal bands appear as linear hyperechoic bands along both sides of the extensor tendon at the level of the MCP joint (Fig. 5.59) (Kichouh et al. 2011). Injury to the sagittal bands may appear as focal disruption of the normal hyperechoic band and/or focal hypoechoic thickening (Fig. 5.59) (Kichouh et al. 2011). There may be subluxation of the extensor tendon due to the injury. There may also be associated injuries to the extensor tendon itself (Kichouh et al. 2011).

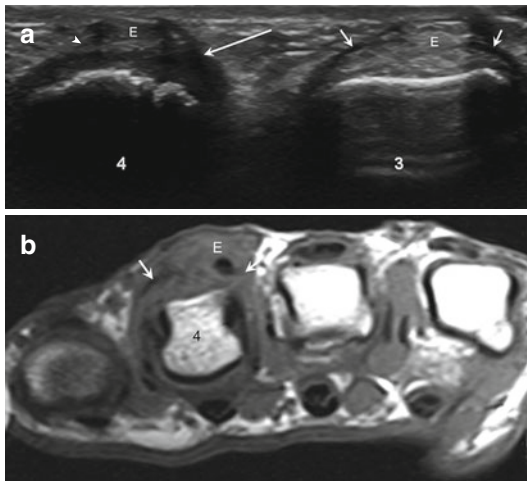

Fig. 5.59 Normal and torn extensor hood. (**a**) Short-axis ultrasound image shows disruption of the radial (*long arrow*) and ulnar (*arrowhead*) sagittal bands of the fourth finger (*4*) extensor hood. Normal-appearing sagittal bands (*short arrows*) are seen in the third finger (*3*); extensor tendon (*E*). (**b**) Axial proton density-weighted MRI shows disruption of the sagittal bands of the extensor hood (*arrows*) with subluxation of the extensor tendon (*E*) of the fourth finger (*4*)

5.6.4 Flexor Tendons

Abnormalities of the flexor tendons of the wrist and hand are similar to those affecting the extensor tendons, including tenosynovitis, tendinosis, and tendon tears. The sonographic findings of flexor tendon pathology are similar to those previously described in the extensor tendons (Fig. 5.60).

5.6.5 Triangular Fibrocartilage

The normal triangular fibrocartilage complex (TFCC) is a hyperechoic structure extending from the base of the ulnar styloid process to the radius. The deeper, radial attachment may be more difficult to see, although utilizing a lower-

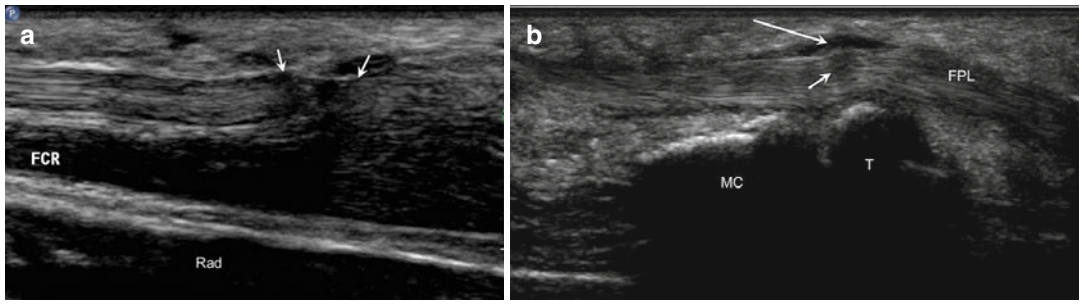

Fig. 5.60 Wrist flexor tendon pathology. (**a**) Longitudinal ultrasound image of the flexor carpi radialis tendon (*FCR*) shows a high-grade partial tear (*arrows*); radius (*Rad*). (**b**) Long-axis ultrasound image of the wrist in a different patient shows tendinosis and tenosynovitis (*long arrow*) of the flexor pollicis longus tendon (*FPL*) with interstitial tearing (*short arrow*); metacarpal (*MC*), trapezium (*T*)

frequency transducer may help (Chiou et al. 1998; Jacobson 2013c; Taljanovic et al. 2011). The ulnar attachment of the TFCC is located subjacent to the extensor carpi ulnaris tendon. Tears of the TFCC appear as areas of hypoechogenicity, typically linear, or areas of thinning of the TFCC (Fig. 5.61) (Keogh et al. 2004).

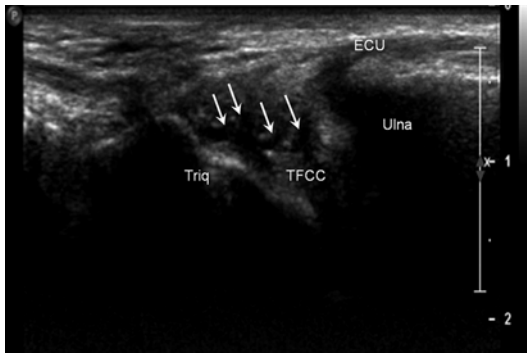

Fig. 5.61 Triangular fibrocartilage tear. Longitudinal ultrasound image of the medial wrist shows irregular hypoechoic tearing (*arrows*) of the triangular fibrocartilage complex (*TFCC*); triquetrum (*Triq*), extensor carpi ulnaris (*ECU*)

5.6.6 Ulnar Collateral Ligament of the Thumb

Injury to the ulnar collateral ligament (UCL) of the thumb is known as gamekeeper's thumb or skier's thumb (Moschilla and Breidahl 2002). The normal ulnar collateral ligament of the thumb appears as a hyperechoic fibrillar band along the ulnar aspect of the metacarpophalangeal joint of the thumb (Fig. 5.62). The ligament is located deep to the adductor aponeurosis that appears as a smooth, thin echogenic band. Tears of the UCL appear as partial or complete hypoechoic disruptions with loss of the normal ligament architecture (Fig. 5.62). The ligament may also appear enlarged and hypoechoic

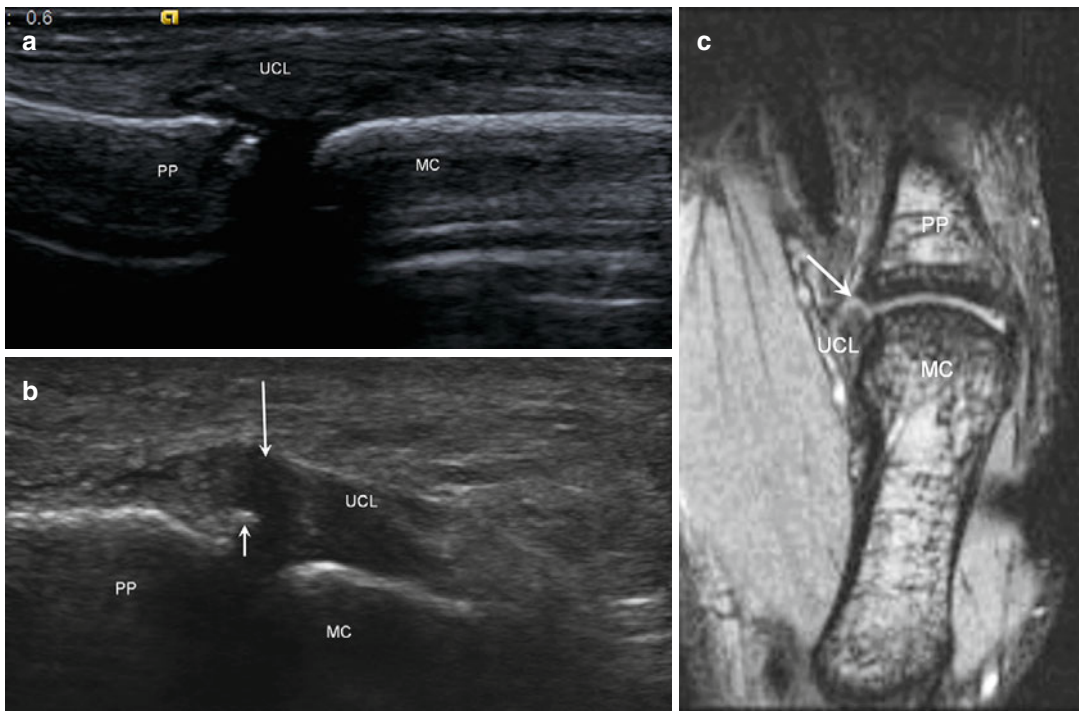

Fig.5.62 Ulnar collateral ligament, thumb. (**a**) Longitudinal ultrasound image of the thumb shows a normal, echogenic, and intact ulnar collateral ligament (*UCL*). (**b**) Longitudinal ultrasound image shows a complete, nonretracted tear (*long arrow*) of the UCL with a small avulsion fracture (*short arrow*). (**c**) Coronal gradient echo MRI shows a tear (*arrow*) at the insertion of the UCL; proximal phalanx (*PP*), metacarpal (*MC*)

(Ebrahim et al. 2006; Jacobson 2013c; Moschilla and Breidahl 2002). The torn ligament may be proximally retracted appearing as a round hypoechoic mass adjacent to the metacarpal head (Hergan et al. 1995). There may be an associated hyperechoic avulsion fragment from the base of the proximal phalanx that remains attached to the torn ligament (Fig. 5.62) (Moschilla and Breidahl 2002).

A subtype of gamekeeper's thumb is a Stener lesion that is defined as a full-thickness and displaced tear of the UCL. A Stener lesion is present when the torn, retracted UCL displaces superficial to the adductor aponeurosis (Ebrahim et al. 2006). This distinction is clinically relevant as Stener lesions are usually treated with surgery (O'Callaghan et al. 1994). Sonographic images demonstrate a nodular focus of tissue of mixed echogenicity at the level of the metacarpal head reflecting the proximally retracted UCL. The retracted ligament is displaced superficial to the adductor aponeurosis that becomes distorted and bulges with a convex surface due to the overlying retracted ligament (Fig. 5.63) (Ebrahim et al. 2006). The appearance has been referred to as a yo-yo on a string (Ebrahim et al. 2006).

Dynamic imaging with slight valgus stress placed on the MCP joint may help elucidate complete, nonretracted tears from partial tears (Jacobson 2013c).

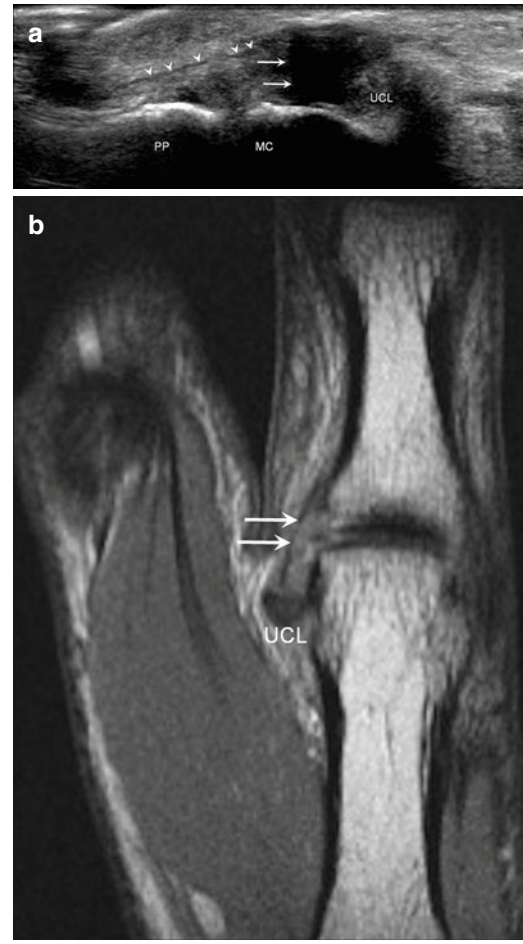

Fig. 5.63 Stener lesion. (**a**) Longitudinal ultrasound image of the thumb shows a complete tear (*arrows*) of the ulnar collateral ligament (*UCL*) with proximal retraction and partial displacement superficial to the adductor aponeurosis (*arrowheads*); proximal phalanx (*PP*), metacarpal (*MC*). (**b**) Coronal proton density-weighted MRI of the thumb demonstrates a Stener lesion with a torn, proximally retracted UCL superficial to the adductor aponeurosis (*arrows*)

5.6.7 Finger Pulleys

Ultrasound may also be used to evaluate the pulley system of the fingers (Boutry et al. 2005). The pulleys help to stabilize the flexor tendons during finger flexion and prevent subluxation or bowing (Boutry et al. 2005). The normal pulley (Fig. 5.64) appears as a linear hyperechoic band located superficial to the flexor tendon, although it may appear relatively hypoechoic adjacent to fat (Boutry et al. 2005; Martinoli et al. 2000). They may demonstrate anisotropy (Boutry et al. 2005). The A2 pulley located along the proximal phalanx is the most commonly injured pulley. This injury is typically seen in rock climbers but may be seen in other athletes such as football players (Moschilla and Breidahl 2002). Ultrasound shows focal hypoechoic disruption of the normal hyperechoic pulley. There may be thickening of and diffuse hypoechogenicity within the injured pulley. There will be volar displacement of the flexor tendon that becomes more pronounced during finger flexion known as bowstringing (Fig. 5.64) (Jacobson 2013c; Klausner et al. 2002; Martinoli et al. 2000; Moschilla and Breidahl 2002).

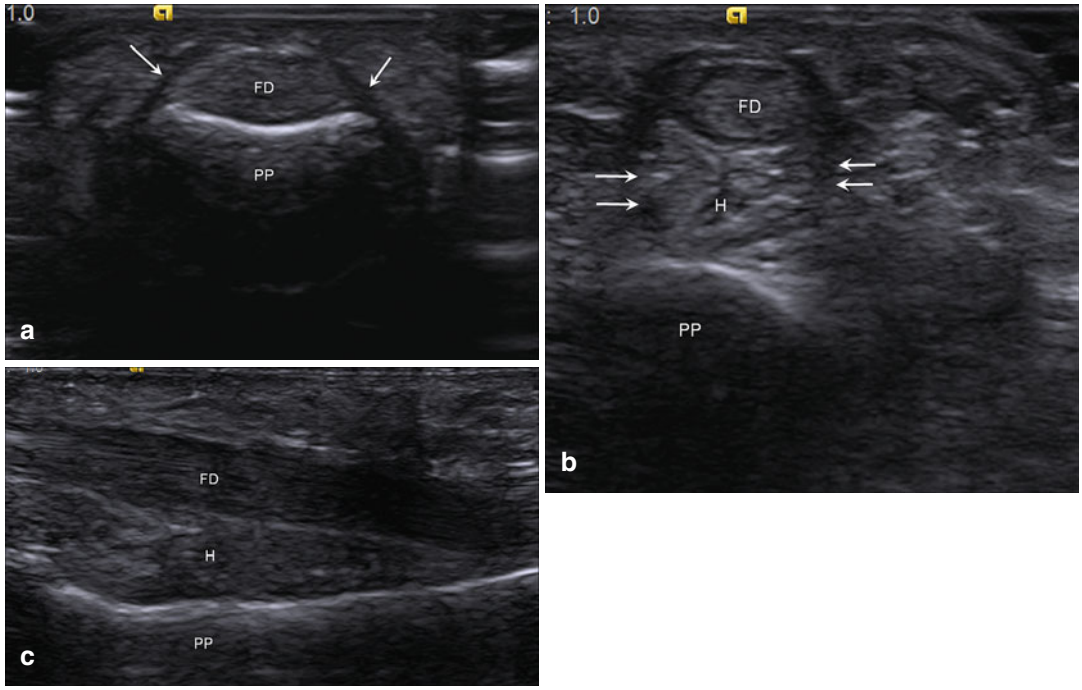

Fig. 5.64 Pulley apparatus of the finger. (**a**) Short-axis ultrasound image of the index finger shows the normal A2 pulley (*arrows*) maintaining the flexor digitorum tendons (*FD*) adjacent to the proximal phalanx (*PP*). (**b**) Short- and (**c**) long-axis ultrasound images in the setting of a completely disrupted A2 pulley (*arrows*) with displacement of the flexor tendons (*FD*) away from the proximal phalanx (*PP*) with intervening hemorrhage (*H*)

5.6.8 Carpal Tunnel

The carpal tunnel may also be assessed sonographically. Carpal tunnel syndrome is an entrapment neuropathy of the median nerve within the fibro-osseous carpal tunnel (Sernik et al. 2008). Anything that results in decreased size of the tunnel or increase in the tunnel contents may result in compression of the median nerve. These include tenosynovitis of the flexor tendons, masses, or trauma although frequently a cause is not found (Chen and Liang 1997; Duncan et al. 1999).

On imaging, there is enlargement of the median nerve within the carpal tunnel with decreased echogenicity and loss of the normal honeycomb appearance. Enlargement of the nerve of greater than 12 mm^2 is considered abnormal (Fig. 5.65) (Chen et al. 1997; Klauser et al. 2009). Values between 10 and 12 mm^2 are indeterminate. There may be flattening of the nerve with bowing of the overlying flexor retinaculum (Chen et al. 1997).

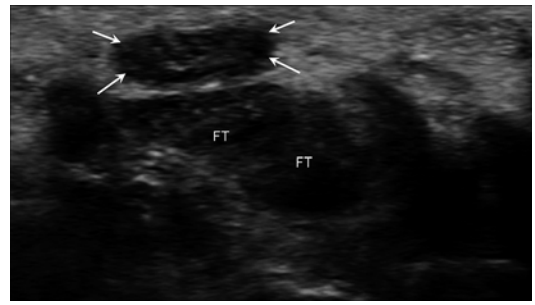

Fig. 5.65 Carpal tunnel syndrome. Short-axis ultrasound image of the wrist demonstrates an enlarged, hypoechoic median nerve (*arrows*) within the carpal tunnel adjacent to the flexor tendons (*FT*)

5.6.9 Ganglia of the Wrist and Hand

Ganglion cysts frequently occur in the hand and wrist and may be evaluated sonographically. Most commonly, they occur along the dorsal aspect of the wrist, superficial to the scapholunate ligament (Fig. 5.66) (Bianchi et al. 1994a).

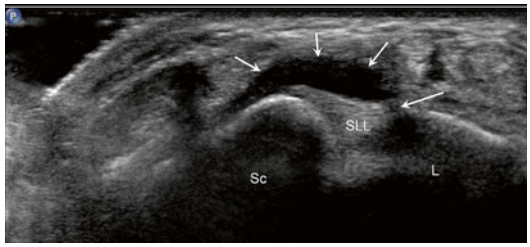

Fig. 5.66 Dorsal wrist ganglion cyst. Short-axis ultrasound image of the dorsal wrist demonstrates a ganglion cyst (*short arrows*) arising from a tear (*long arrow*) in the scapholunate ligament (*SLL*); scaphoid (*Sc*), lunate (*L*)

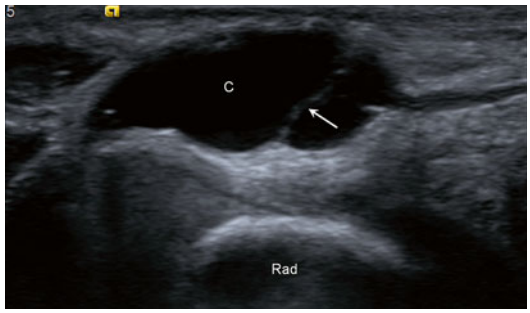

Fig. 5.67 Volar wrist ganglion cyst. Short-axis ultrasound image of the volar wrist shows a slightly complex ganglion cyst (*C*) with a thin internal septation (*arrow*) superficial to the radius (*Rad*)

Along the volar aspect of the wrist, ganglion cysts commonly occur between the radial artery and flexor carpi radialis tendon (Fig. 5.67) (Bianchi et al. 1994a). Within the fingers, ganglia may occur as retinacular cysts related to the A1 or A2 pulleys. Ultrasound may be used to guide aspiration and therapeutic injection with corticosteroid as a treatment for ganglion cysts (Breidahl and Adler 1996).

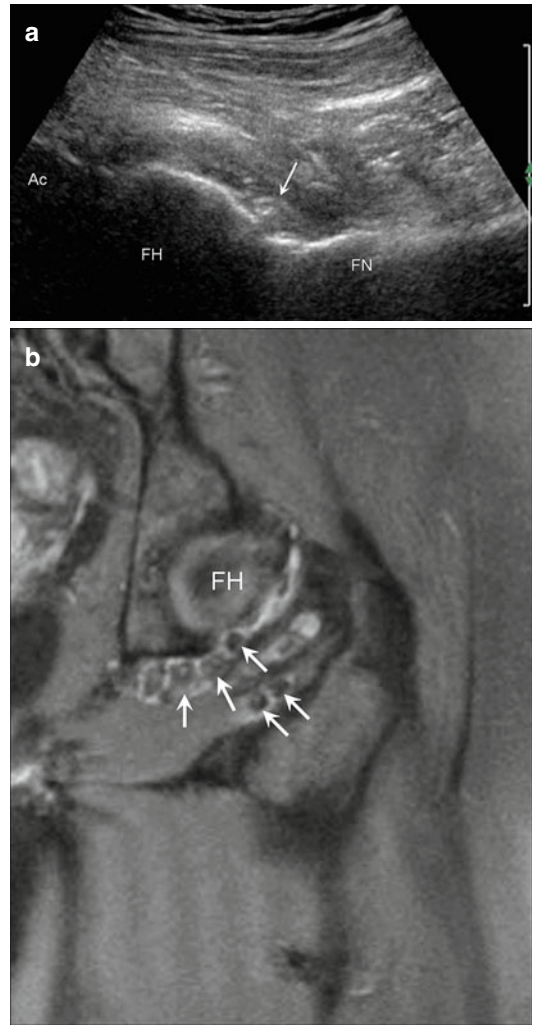

Fig. 5.68 Hip intra-articular bodies. (**a**) Long-axis ultrasound image along the anterior hip shows an echogenic intra-articular body (*arrow*) adjacent to the femoral head (*FH*)/femoral neck (*FN*) junction; acetabulum (*Ac*). (**b**) Coronal fluid-sensitive MRI in a different patient with the same pathology shows multiple hypointense joint bodies (*arrows*) adjacent to the femoral head (*FH*)

5.7 Hip and Thigh Ultrasound

5.7.1 Snapping Hip Syndrome

Snapping hip syndrome is an abnormal snapping or clicking sensation associated with certain hip motions. It is frequently seen in young, athletic adults and is more common in women. There may be pain associated with the snapping sensation (Deslandes et al. 2008). The syndrome can be further subdivided into intra-articular causes, including labral tears, chondral abnormalities, or joint bodies (Fig. 5.68), and extra-articular causes. The extra-articular causes may involve the iliopsoas tendon anteriorly (internal snapping hip) or the iliotibial band and gluteus maximus tendons laterally (external snapping hip) (Choi et al. 2002; Pelsser et al. 2001;

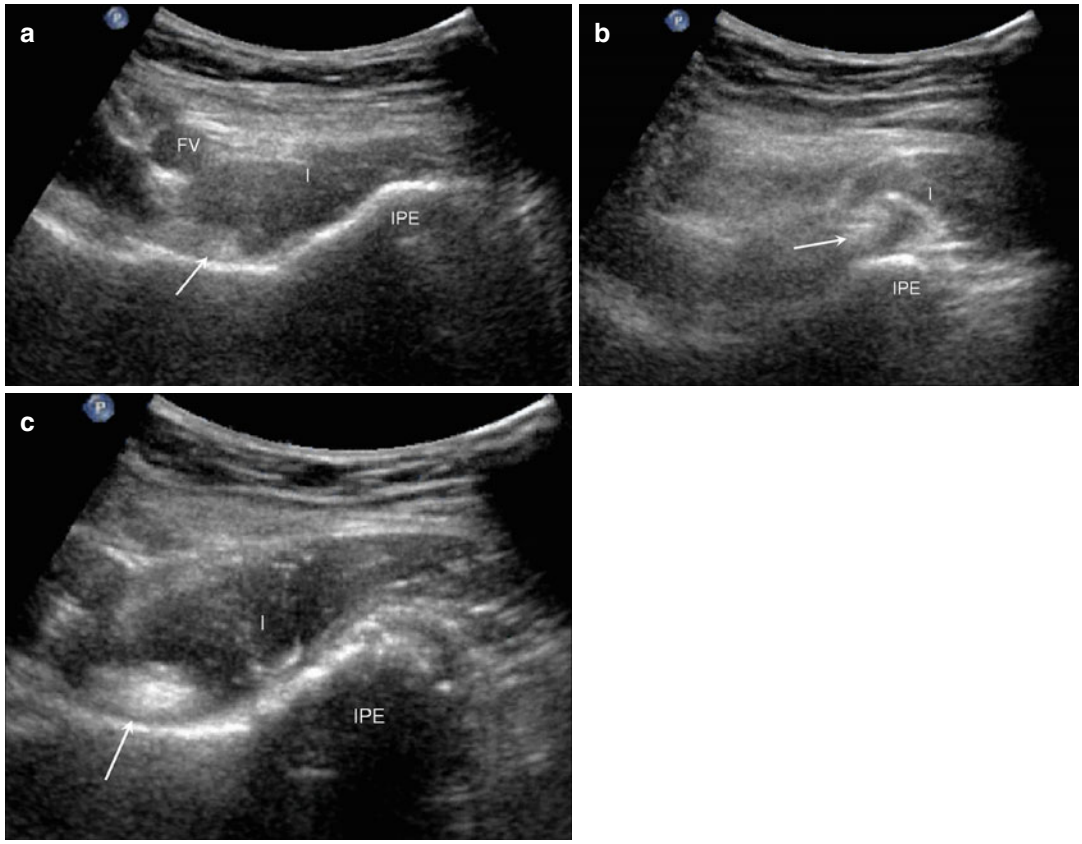

Fig. 5.69 Snapping iliopsoas tendon. Short-axis ultrasound images (**a**) in extension, (**b**) in flexion, and (**c**) return to extension show snapping of the iliopsoas tendon (*arrow*) laterally over the iliopectineal eminence (*IPE*); iliacus (*I*), femoral vessels (*FV*)

Schaberg et al. 1984). Although there may be bursitis and tendinopathy associated with the affected tendons, frequently these findings are absent, and the only abnormality is the pathologic motion of the tendons. The kinematic nature of snapping hip limits the utility of MRI in these patients, making dynamic ultrasound critical to the diagnosis of snapping hip syndromes (Pfirrmann et al. 2008).

Under normal circumstances, the psoas muscle glides laterally, rolling over the medial border of the iliacus muscle. With internal snapping hip, during abduction/flexion/external rotation, the iliopsoas tendon moves abruptly over the iliacus muscle, which becomes entrapped between the tendon and the iliopectineal eminence. As the hip returns to the neutral position, the tendon "snaps" over the muscle onto the subjacent pubic bone (Fig. 5.69) (Deslandes et al. 2008). The tendon may also abruptly flip over the femoral vessels during abduction/flexion/external rotation (Fig. 5.70). In addition to the findings at dynamic imaging, there may be iliopsoas tendinosis with enlargement and decreased echogenicity of the tendon with fluid distension of the bursa (Pelsser et al. 2001).

In the setting of external snapping hip, either the posterior margin of the proximal iliotibial band or the anterior margin of the gluteus maximus tendon snaps over the greater trochanter as the hip moves from flexion to extension. There may be thickening of and decreased echogenicity within the iliotibial band or gluteus maximus tendon, and there may be associated greater trochanteric bursitis (Fig. 5.71) (Pelsser et al. 2001).

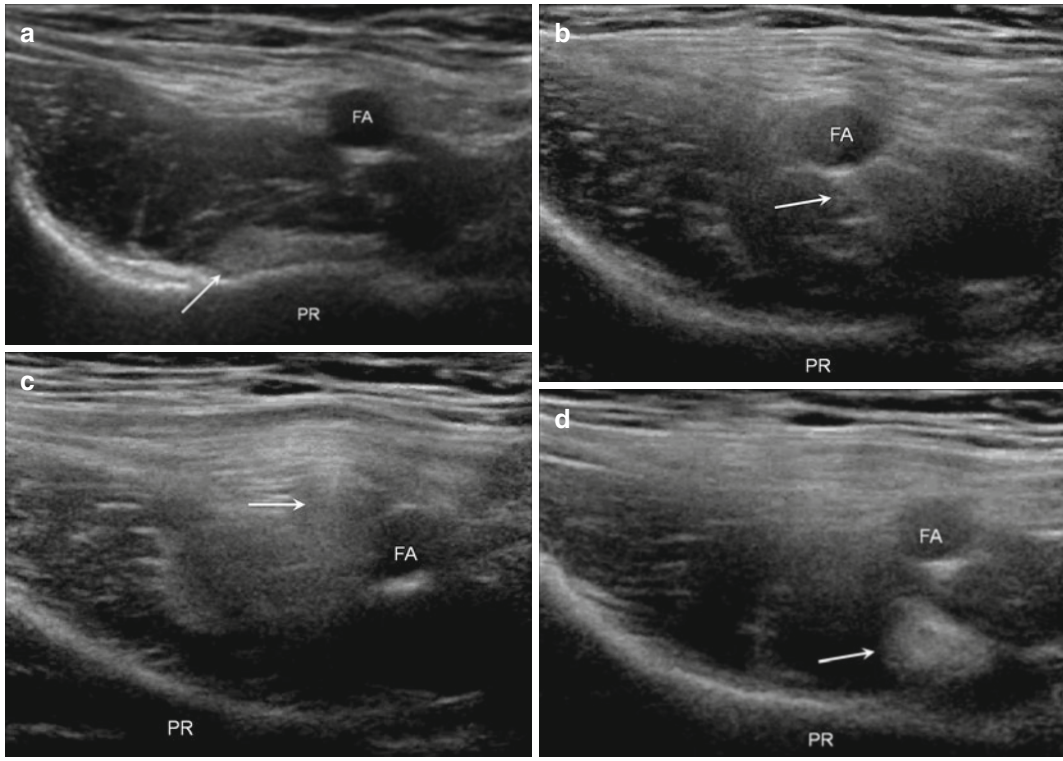

Fig. 5.70 Snapping iliopsoas tendon over femoral vessels. Short-axis ultrasound images (**a**) in extension, (**b**) partial flexion, (**c**) full flexion, and (**d**) return to extension demonstrate snapping of the iliopsoas tendon (*arrow*) over the femoral artery (*FA*); pubic ramus (*PR*)

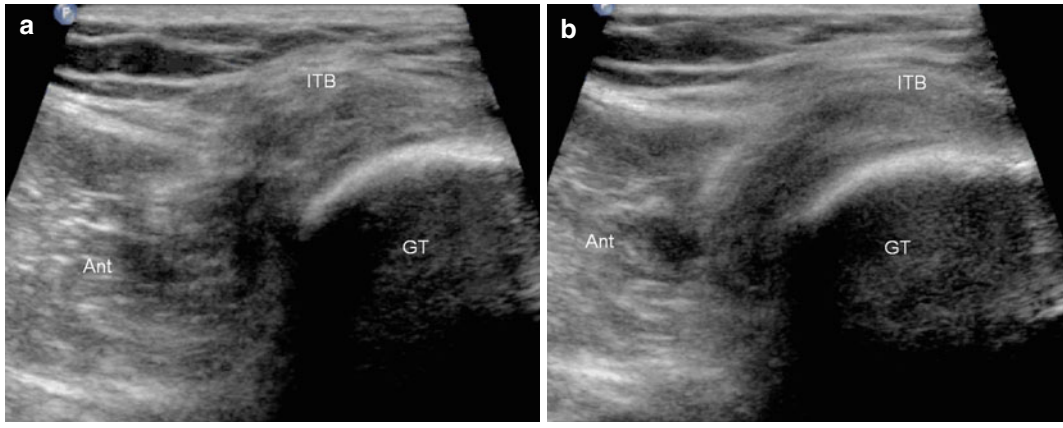

Fig. 5.71 External snapping hip. Short-axis ultrasound images (**a**) in flexion and (**b**) in extension show snapping of the proximal iliotibial band (*ITB*) over the greater trochanter (*GT*); anterior (*Ant*)

5.7.2 Calcific Tendinitis Around the Hip

Although calcific tendinitis and bursitis occur much more frequently in the rotator cuff, tendons about the hip may also be affected, including the gluteus maximus, gluteus medius, and rectus femoris tendons, as well as the greater trochanteric bursa. Imaging findings are similar to those in the rotator cuff with echogenic foci

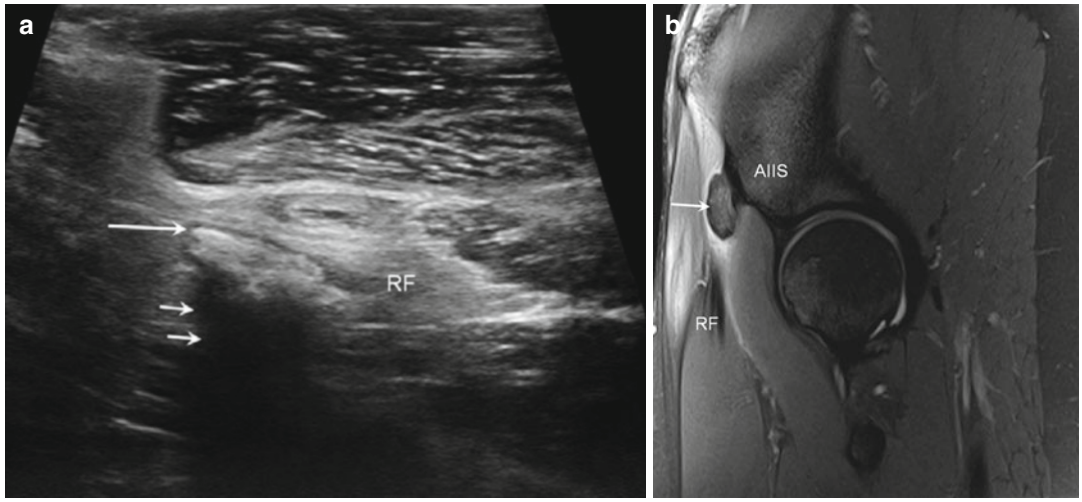

Fig. 5.72 Rectus femoris calcific tendinitis. (**a**) Long-axis ultrasound image of the anterior hip shows an ovoid echogenic region of calcification (*long arrow*) with posterior shadowing (*short arrows*) at the origin of the rectus femoris tendon (*RF*). (**b**) Corresponding sagittal fluid-sensitive MRI in the same patient shows the hypointense calcification (*arrow*) at the origin of the rectus femoris (*RF*) on the anterior inferior iliac spine (*AIIS*)

demonstrating posterior acoustic shadowing and possible hyperemia with power Doppler interrogation (Fig. 5.72). As in the rotator cuff, percutaneous aspiration with ultrasound guidance may be employed for treatment (Chiou et al. 2002; Farin et al. 1995b; Howard et al. 1993).

5.7.3 Labral Pathology and Femoroacetabular Impingement

Although traditionally evaluated on MRI, the labrum of the hip can be visualized with ultrasound. It appears as a hyperechoic, triangular structure attached to the anterior rim of the acetabulum (Cho et al. 2000). Tearing of the labrum is suggested by a hypoechoic cleft through the base of the labrum (Fig. 5.73), absence of the labrum, abnormal morphology of the labrum, or paralabral cyst formation (Fig. 5.74) (Troelsen et al. 2007). There are limitations of ultrasound evaluation of the hip labrum due to the depth of the structure and a limited acoustic window (Troelsen et al. 2007, 2009).

Femoroacetabular impingement (FAI) may also be assessed with ultrasound. FAI results from morphologic abnormalities of the proximal femur and/or acetabular rim resulting in abnormal contact between these structures. This may result in labral pathology, premature cartilage loss, and osteoarthrosis (Ganz et al. 2003). In cam-type FAI, there is an abnormal osseous protuberance at the femoral head/neck junction that abuts against the acetabular rim resulting in early cartilage and labral pathology (Buck et al. 2011; Ganz et al. 2008). With sonography, the osseous contour deformity (Fig. 5.75) may be documented as well as potential labral pathology (Buck et al. 2011; Cho et al. 2000). Dynamic imaging allows direct observation of the osseous protuberance along the femoral head/junction abutting the labrum and acetabular rim.

5.7.4 Proximal Hamstring and Quadriceps Injuries

The hamstring and quadriceps muscles and tendons are prone to the same pathology as other muscles and tendons throughout the body. The tendons are prone to tendinopathy that appears as decreased echogenicity and tendon enlargement. There may also be associated dystrophic

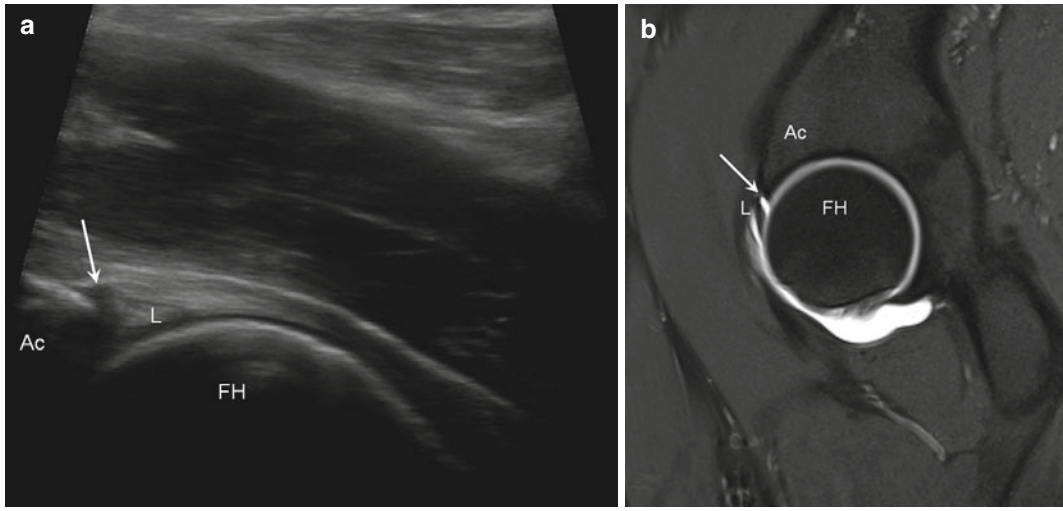

Fig. 5.73 Hip labral tear. (**a**) Longitudinal ultrasound image of the anterior hip demonstrates a hypoechoic tear (*arrow*) at the base of the anterosuperior labrum (*L*). (**b**) Sagittal fat-suppressed T1-weighted MR arthrogram image in the same patient shows fluid undermining the labrum (*L*) due to a tear (*arrow*); acetabulum (*Ac*), femoral head (*FH*)

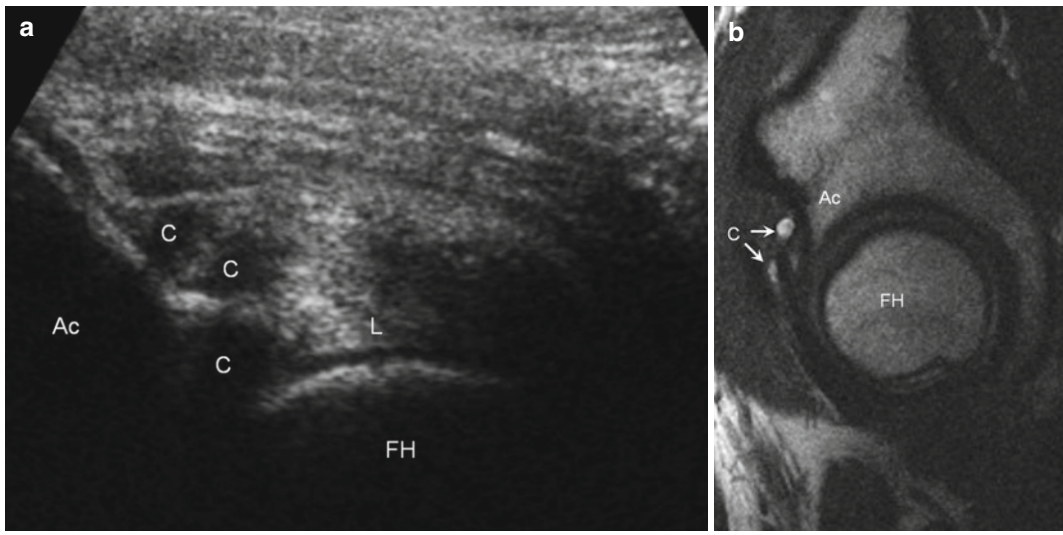

Fig. 5.74 Hip paralabral cyst. (**a**) Longitudinal ultrasound image of the anterior hip shows a hypoechoic, multiloculated paralabral cyst (*C*) undermining the labrum (*L*). (**b**) Sagittal proton density-weighted MRI shows the cyst (*C*, *arrows*); acetabulum (*Ac*), femoral head (*FH*)

calcification or ossification (Adler and Finzel 2005). Partial- and full-thickness tears of the tendons may occur with or without distal retraction of the tendons (Fig. 5.76). Injuries to the hamstring tendons may involve the entire hamstring complex or selectively involve the semimembranosus tendon along the lateral border of the ischium or the conjoint tendon posteromedially, composed of the biceps femoris and semitendinosus tendons (Fig. 5.77) (Koulouris and Connell 2005).

Injuries to the muscles may also occur. There are three grades of muscle injury. Grade 1 refers to muscle strain without frank tissue

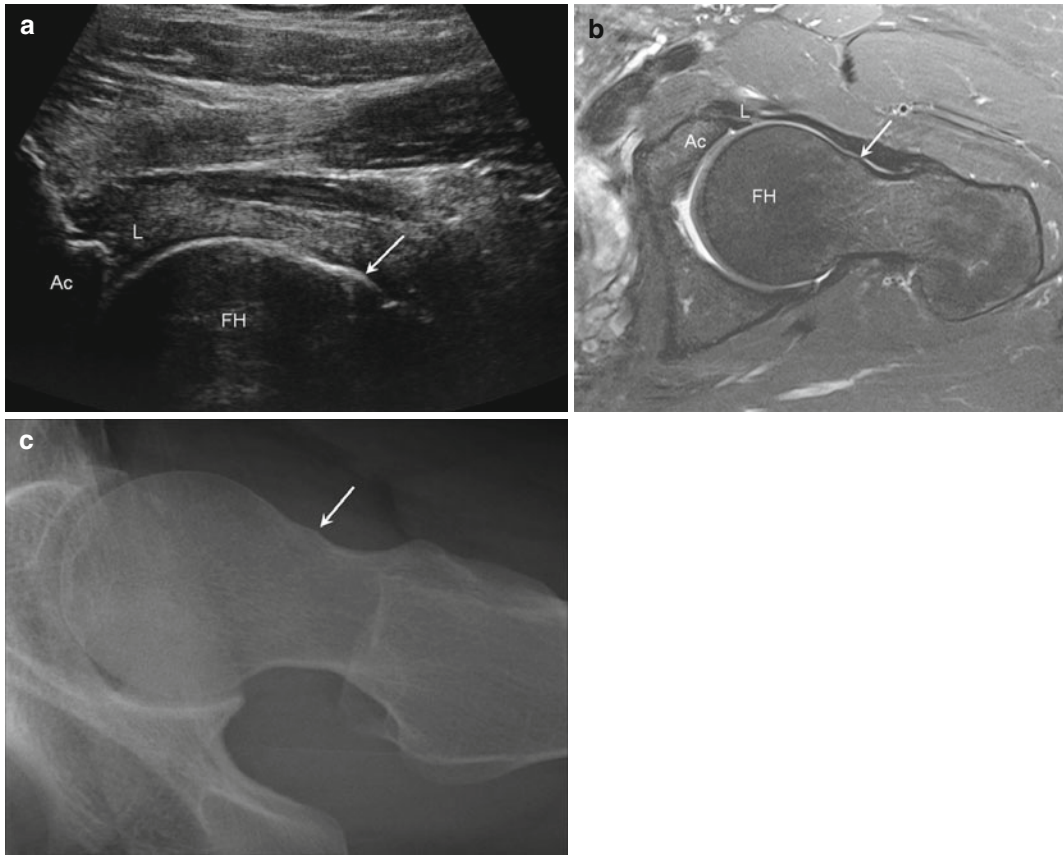

Fig. 5.75 Femoroacetabular impingement. (**a**) Long-axis ultrasound image of the anterior hip demonstrates abnormal convexity (*arrow*) at the femoral head (*FH*)/femoral neck junction in a patient with femoroacetabular impingement. (**b**) Corresponding axial oblique fluid-sensitive MRI showing the same findings; acetabulum (*Ac*), labrum (*L*). (**c**) Cross table lateral radiograph of the hip shows the convexity (*arrow*)

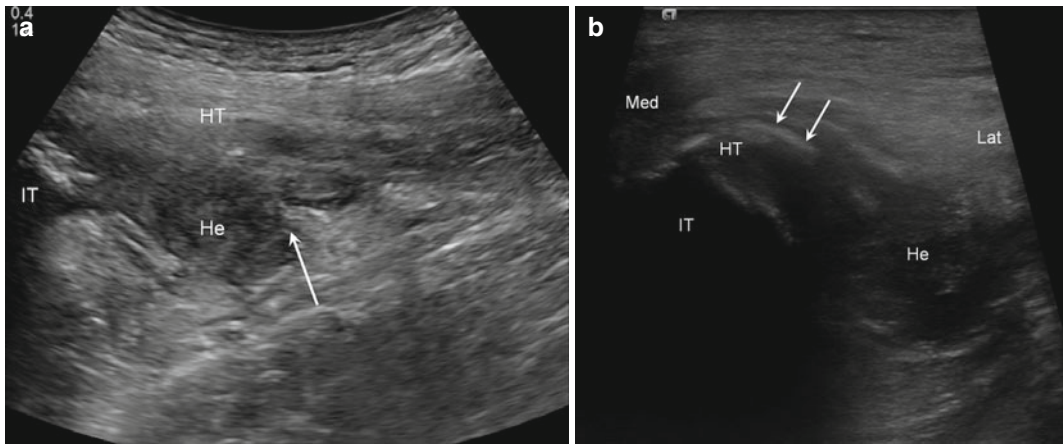

Fig. 5.76 High-grade tear involving conjoint and semimembranosus tendons at the hamstring origin. (**a**) Long-axis ultrasound image of the posterior hip showing a high-grade partial, deep surface retracted tear (*arrow*) of the entire hamstring tendon (*HT*) origin from the ischial tuberosity (*IT*) with intervening hemorrhage (*He*). (**b**) Short-axis ultrasound image shows enthesopathic calcification (*arrows*) at the origin from the ischial tuberosity (*IT*) adjacent to the remaining intact tendon fibers (*HT*); medial (*Med*), lateral (*Lat*)

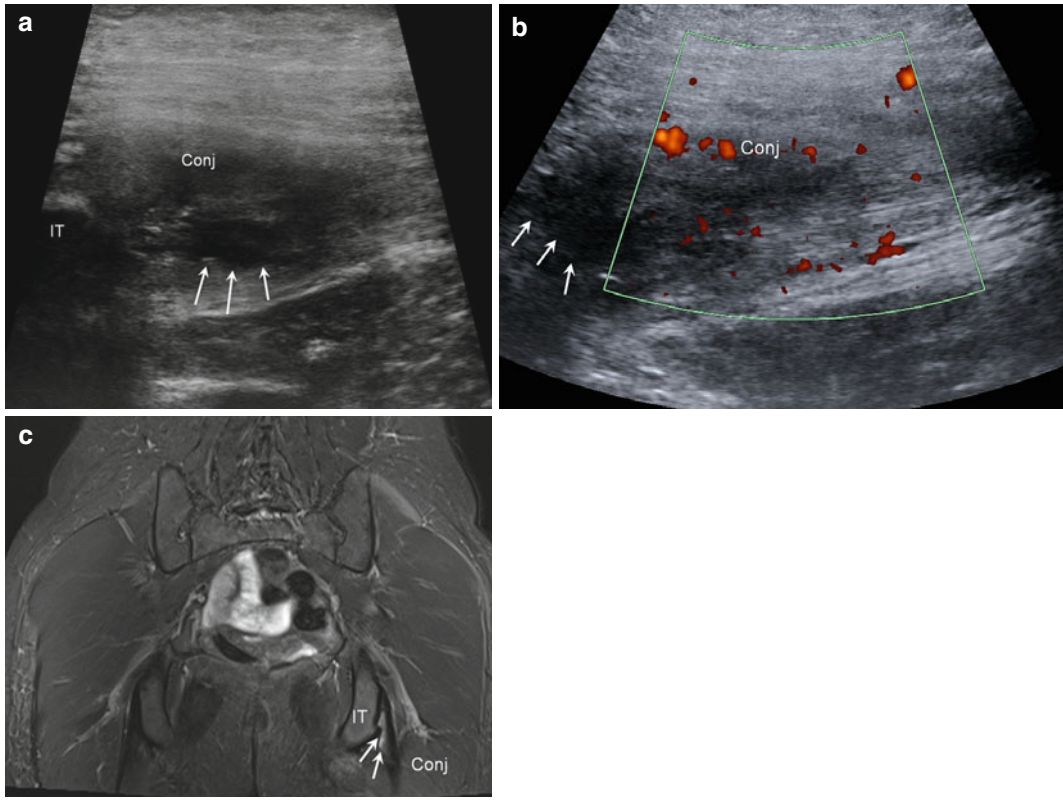

Fig. 5.77 Partial tear of conjoint tendon only at the hamstring origin. Longitudinal images (**a**) without and (**b**) with power Doppler interrogation show a low-grade partial, deep surface tear (*arrows*) of the conjoint tendon (*Conj*) from the ischial tuberosity (*IT*). Hyperemia in (**b**) is related to associated tendinopathy and neovascularity. (**c**) Corresponding coronal fluid-sensitive MRI of the pelvis shows the partial tear (*arrows*) of the conjoint tendon (*Conj*) from the ischial tuberosity (*IT*)

disruption. Grade 2 refers to partial-thickness tearing of the muscle (Fig. 5.78). Grade 3 refers to a full-thickness tear of the muscle (Palmer et al. 1999). These types of injuries typically occur at the myotendinous junction and affect muscles that traverse two joints such as the hamstring muscles and the rectus femoris (Garrett 1996).

In the setting of chronic tendinopathy of the hamstrings, cortical irregularity and pitting may occur at the tendon origin along the ischial tuberosity (Koulouris and Connell 2005; Linklater et al. 2010).

The rectus femoris is the most commonly injured muscle of the quadriceps muscle group. Injuries to the tendon may occur at the origin at the anterior inferior iliac spine. Because the rectus femoris crosses two joints, it is prone to myotendinous junction injuries. These injuries manifest as regions of decreased echogenicity along the central myotendinous aponeurosis within the substance of the muscle (Bianchi et al. 2006). More severe injuries will result in partial or complete disruption of the muscle fibers, appearing as hypoechoic defects that may contain more hyperechoic hemorrhage in the acute setting (Fig. 5.79) (Douis et al. 2011). Infiltrative hemorrhage or edema will make the muscle appear swollen and more echogenic.

Direct impaction of the muscle may result in an intramuscular hematoma, appearing as a hyperechoic ill-defined region initially and becoming more hypoechoic over time (Lee and Healy 2004). This may be complicated by heterotopic ossification in the healing stages (Fleckenstein and Shellock 1991). While strain

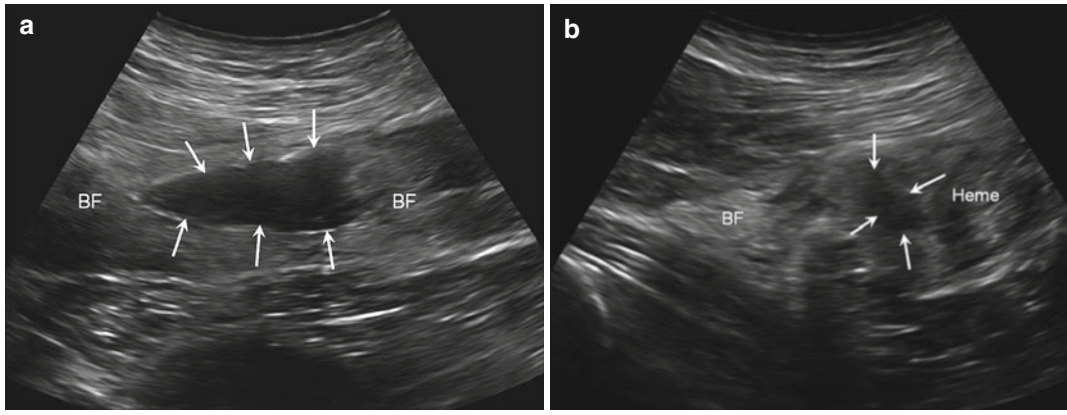

Fig. 5.78 Grade 2 strain of the biceps femoris. (**a**) Long- and (**b**) short-axis ultrasound images of the biceps femoris muscle (*BF*) demonstrate a high-grade strain with fluid replacing the muscle fibers (*arrows*) and more echogenic hemorrhage (*Heme*)

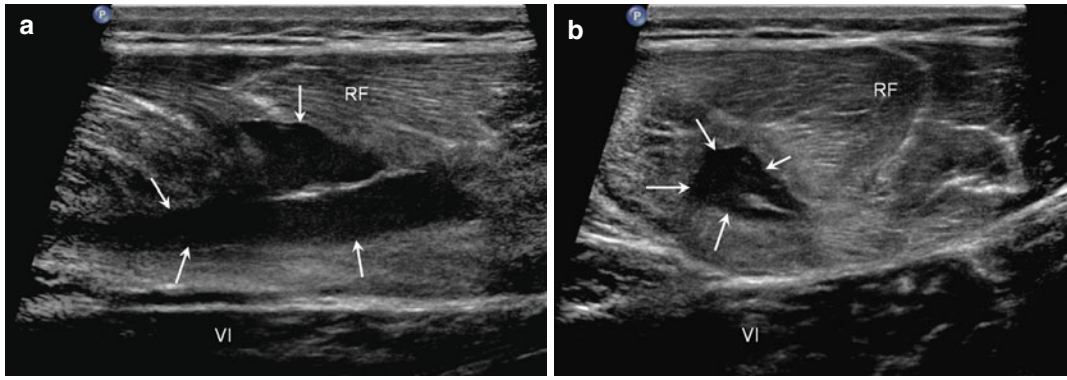

Fig. 5.79 Grade 2 strain of the rectus femoris. (**a**) Long- and (**b**) short-axis ultrasound images of the rectus femoris muscle (*RF*) show a high-grade strain with fluid replacing the muscle fibers (*arrows*); vastus intermedius (*VI*)

injuries more frequently involve superficial muscles, direct impact injuries more frequently affect the deeper muscles. Thus, in the thigh, the vastus intermedius muscle that is located immediately adjacent to the femur is the most frequently injured in the setting of direct trauma (Stoller 2007a). Mature myositis ossificans appears sonographically as an echogenic focus or foci with posterior acoustic shadowing within the previously injured muscle (Fig. 5.80) (Abate et al. 2011). In the early phases of injury, painful intramuscular hematomas may be treated with ultrasound-guided aspiration that will be discussed later (Lee and Healy 2004).

5.7.5 Adductor Muscles and Sports Hernia

Injuries of the adductor muscle group most frequently involve the adductor longus at the pubis. These types of injuries most frequently occur in high-level, elite athletes (Shortt et al. 2008). A subtype of injury occurring in this patient population is the "sports hernia" or athletic pubalgia. This involves tendinosis and/or partial tearing of the adductor longus origin with associated pathology of the common aponeurosis between the adductor longus and rectus abdominis. The spectrum of athletic pubalgia also includes pathology of the symphysis pubis including osteitis pubis and

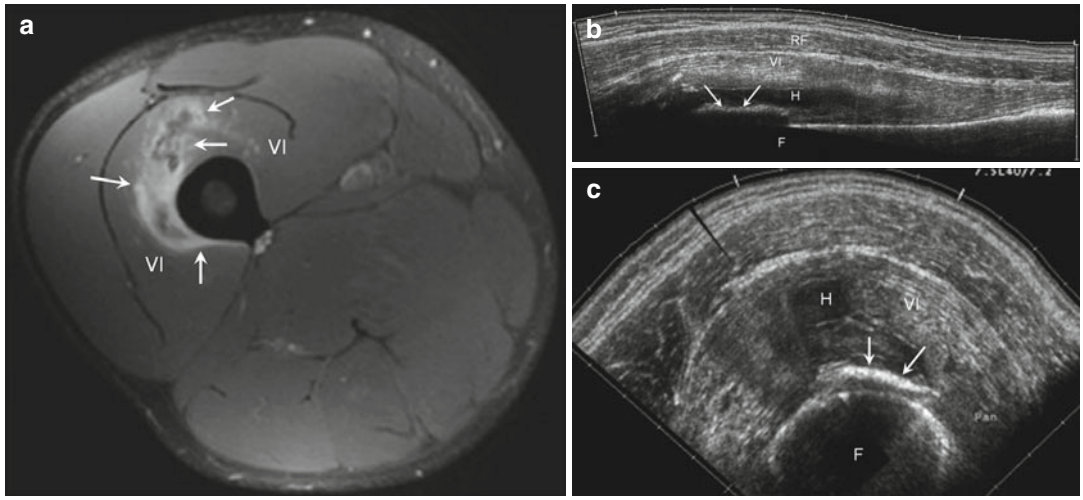

Fig. 5.80 Vastus intermedius heterotopic ossification. (**a**) Axial fluid-sensitive MRI of the thigh immediately following a direct impact with fluid and edema (*arrows*) in the vastus intermedius (*VI*); femur (*F*). (**b**) Long- and (**c**) short-axis ultrasound images 6 weeks following the injury show resolving hemorrhage (*H*) in the vastus intermedius (*VI*) with early development of linear heterotopic ossification (*arrows*); femur (*F*), rectus femoris (*RF*)

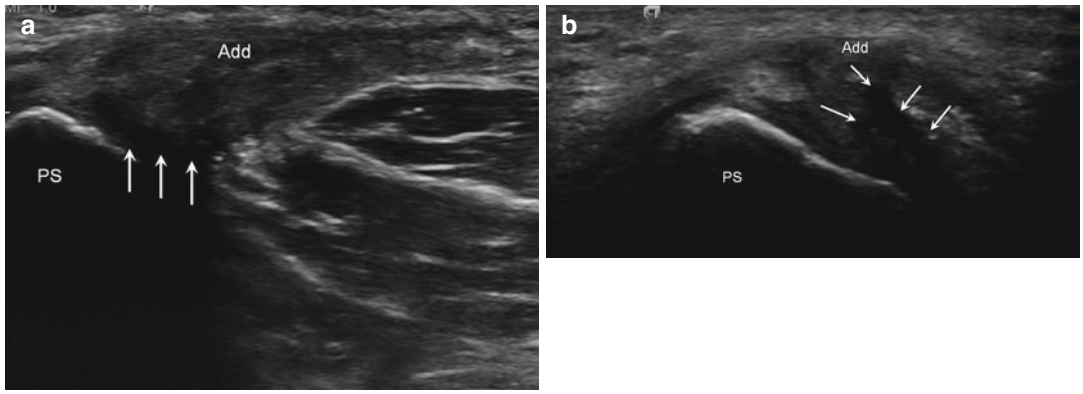

Fig. 5.81 Sports hernia. (**a**) Long- and (**b**) short-axis ultrasound images at the adductor tendon (*Add*) origin at the pubic symphysis (*PS*) demonstrate a high-grade partial, deep surface tear (*arrows*) in this athlete with a sports hernia

parasymphyseal stress injuries (Robinson et al. 2011; Shortt et al. 2008; Zoga et al. 2008). At ultrasound imaging, the adductor longus tendon may be thickened and hypoechoic. A hypoechoic or anechoic cleft may be seen undermining the tendon origin in partial tearing (Fig. 5.81) (Campbell 2013). In complete tearing, the tendon will be retracted distally and a surrounding hematoma of mixed echogenicity may be present in the acute setting (Campbell 2013). Pathology of the symphysis pubis as seen in symphyseal degeneration may include bony irregularity or productive change with adjacent soft tissue calcification (Campbell 2013). Ultrasound is frequently used to guide for therapeutic injections into the symphysis (Campbell 2013).

5.7.6 Abductor and Gluteus Muscles

Historically, lateral hip pain was frequently believed to be the result of trochanteric bursitis. It is now believed that the underlying pathology is most commonly related to tendinopathy of the gluteus medius and minimus tendons, with

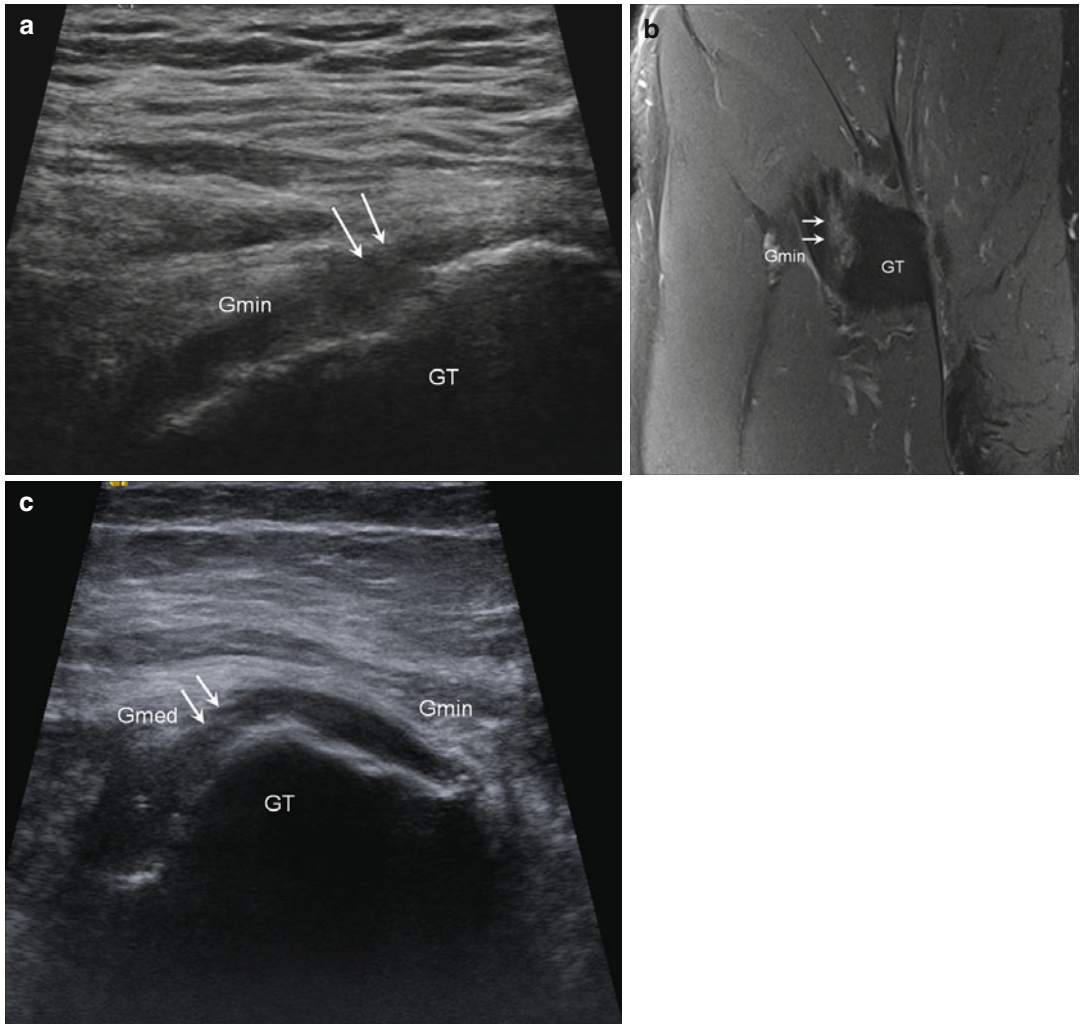

Fig. 5.82 Gluteal tendon pathology. (**a**) Longitudinal ultrasound image demonstrates thickening of and decreased echogenicity within (*arrows*) the gluteus minimus (*Gmin*) insertion on the greater trochanter (*GT*) due to tendinopathy. (**b**) Corresponding sagittal fluid-sensitive MRI in the same patient shows increased signal (*arrows*) at the gluteus minimus (*Gmin*) insertion. (**c**) Short-axis ultrasound image in a different patient shows thickening of and decreased echogenicity within (*arrows*) both the gluteus medius (*Gmed*) and gluteus minimus (*Gmin*) tendons at the greater trochanter (*GT*)

associated bursitis only rarely present (Kong et al. 2007; Westacott et al. 2011). The complex of symptoms including lateral hip pain, point tenderness over the greater trochanter, and weakness of hip abduction has been termed greater trochanteric pain syndrome (Kong et al. 2007). Other causes of greater trochanteric pain syndrome include hip arthrosis, stress injuries, and referred pain from the spine (Klausner et al. 2013). Although gluteal tendinopathy is most frequently seen in middle-aged women, tendinopathy and tears of these tendons can also be seen in athletes. Ultrasound is useful in the diagnosis of gluteal tendon pathology and may assist in guiding treatment of symptoms, including image-guided therapeutic injections (Klausner et al. 2013). At imaging, the tendons may appear thickened and heterogeneous with hypoechoic areas (Fig. 5.82). Tears manifest as attenuation of the tendons with partial- or full-thickness anechoic defects. Tears

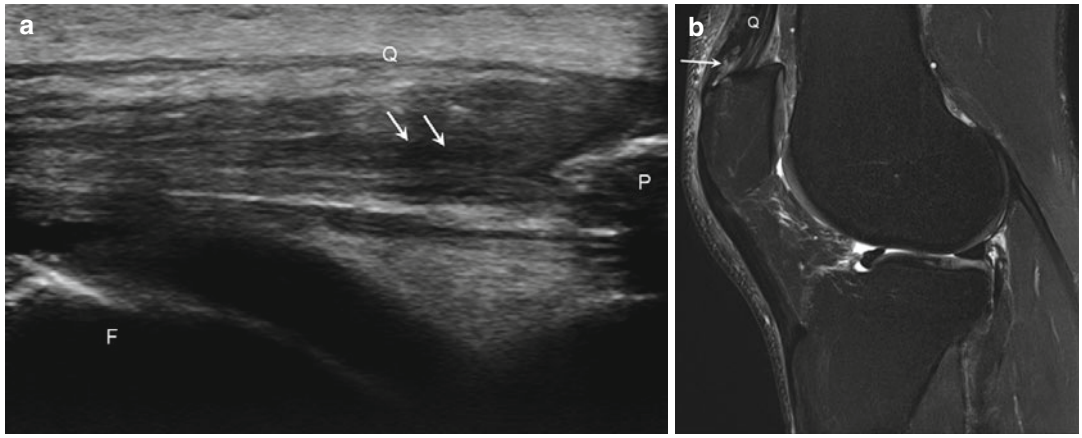

Fig. 5.83 Distal quadriceps tendinosis. (**a**) Longitudinal ultrasound image of the distal quadriceps tendon (*Q*) shows thickening of the tendon with interstitial tearing (*arrows*); femur (*F*), patella (*P*). (**b**) Corresponding sagittal fluid-sensitive MRI shows the thickened quadriceps tendon (*Q*) with increased interstitial signal (*arrow*)

most frequently affect the deep fibers of the tendon, specifically the gluteus medius tendon (Klausner et al. 2013), or hypoechoic distension of the bursa may also be present. The individual facets of the greater trochanter may also be identified with ultrasound that allows for precise determination of the affected tendon (Kong et al. 2007). The abductor tendons are a common site of calcific tendinosis and are amenable to percutaneous treatment. It should be noted that multiple bursae exist about the hip abductors. Ultrasound can be valuable in individually targeting these bursae.

5.8 Knee and Calf Ultrasound

5.8.1 Quadriceps Tendon

Anterior knee pain is a frequent problem in athletes. Because the quadriceps and patellar tendons are superficial structures, they are amenable to evaluation with sonography (Friedman et al. 2003). Sonographic findings of tendinosis demonstrate an enlarged tendon with hypoechoic areas without discontinuity of the tendon fibers (Fig. 5.83). Dystrophic calcifications may also be present (Friedman et al. 2003; Pfirrmann et al. 2008). With power or color Doppler interrogation, there may be hyperemia. Regions of hyperemia

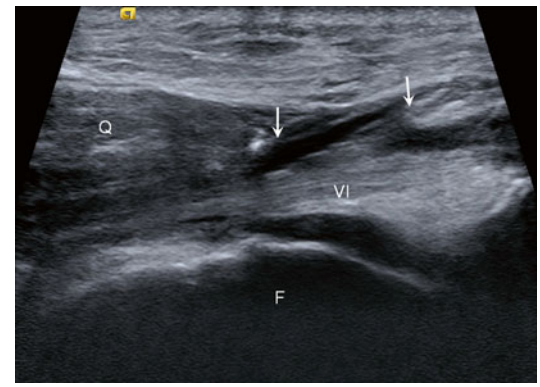

Fig. 5.84 Distal quadriceps partial tear. Longitudinal ultrasound image of the distal quadriceps tendon (*Q*) shows the edges of a high-grade partial tear (*arrows*) of the superficial layers of the tendon with intact deep fibers of the vastus intermedius (*VI*); femur (*F*)

frequently correspond to symptomatic areas of point tenderness in the patient. Similar to tears involving other tendons, tears of the quadriceps tendon appear as hypoechoic or anechoic defects (Fig. 5.84) involving portions of the tendon (partial thickness) or the entire width of the tendon (full thickness) (La et al. 2003). With full-thickness tears at the tendon insertion, there may be an associated avulsion fracture of the patella appearing as a curvilinear echogenic focus (Fig. 5.85) attached to the torn tendon fibers (Bianchi et al. 2011; Friedman et al. 2003). In cases where hematoma in the tendon gap may be

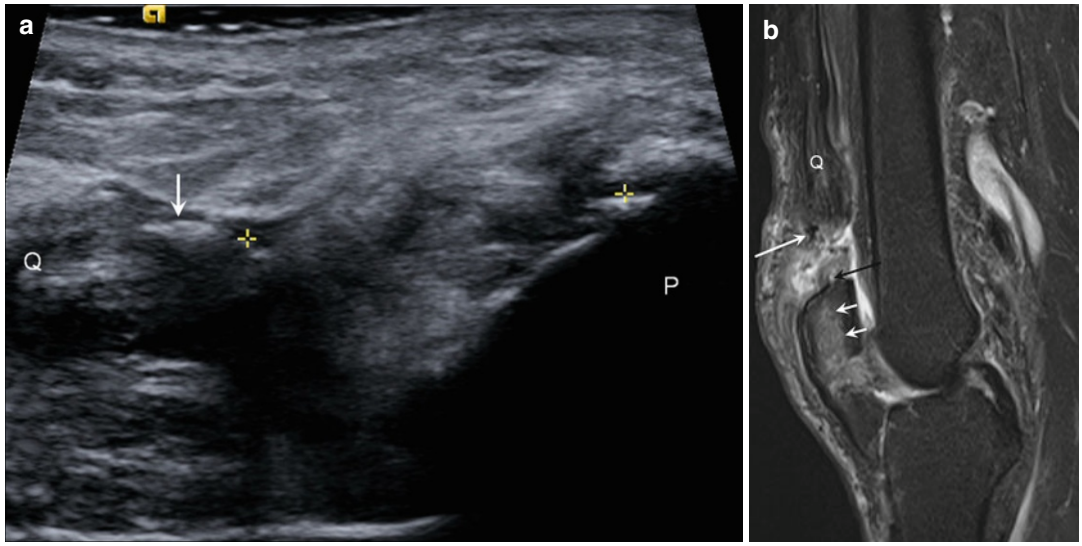

Fig. 5.85 Distal quadriceps avulsion with osseous fragment. (**a**) Long-axis ultrasound image of the distal quadriceps tendon (*Q*) shows complete avulsion of the tendon from the patella (*P*) with retraction (++) and an associated osseous avulsion fragment (*arrow*). (**b**) Corresponding sagittal fluid-sensitive MRI shows the torn, retracted quadriceps tendon (*Q*) with the hypointense avulsion fragment (*white long arrow*) from the patellar donor site (*black arrow*) and bone marrow edema in the patella (*white short arrows*)

confused with an incomplete tear, dynamic assessment of the tendon in extension and flexion can help identify the edges of the torn tendon (Friedman et al. 2003). These maneuvers will also be useful in subacute and chronic injuries when granulation tissue and fibrous scar tissue fill the gap between the torn fibers, mimicking a partial tear (La et al. 2003).

5.8.2 Patellar Tendon

Patellar tendon pathology is similar to that seen in the quadriceps tendon. The patellar tendon, however, is more prone to injuries, particularly in the young, athletic population (Miller 2013). In patellar tendinopathy, the tendon will appear enlarged and heterogeneous in echotexture with areas of decreased echogenicity. The fibers, nevertheless, remain in continuity. This entity has been referred to as jumper's knee (Khan et al. 1996). Focal hypoechoic or anechoic defects reflect tears that may involve a portion of the tendon or the full width and thickness of the tendon (Fig. 5.86) (Friedman et al. 2003). With power or color Doppler evaluation, there will be increased vascularity and hyperemia that again corresponds to the more symptomatic area in the patient (Fig. 5.87) (Hoksrud et al. 2008). Dynamic imaging may also be used to accentuate tendon retraction in the setting of a full-thickness tear with gentle flexion of the knee (Friedman et al. 2003).

5.8.3 Iliotibial Band

The iliotibial band friction syndrome is a commonly seen entity in sports medicine. It is most frequently seen in runners, particularly long-distance runners; however, it is also seen in other athletes, especially those who engage in activities involving repetitive knee flexion and extension, such as rowers, cyclists, and football players (Bonaldi et al. 1998). In this disorder, repetitive flexion and extension at the knee result in chronic friction between the iliotibial band (ITB) and the lateral femoral condyle. This results in abnormalities of the ITB and development of ill-defined edema or adventitial bursa

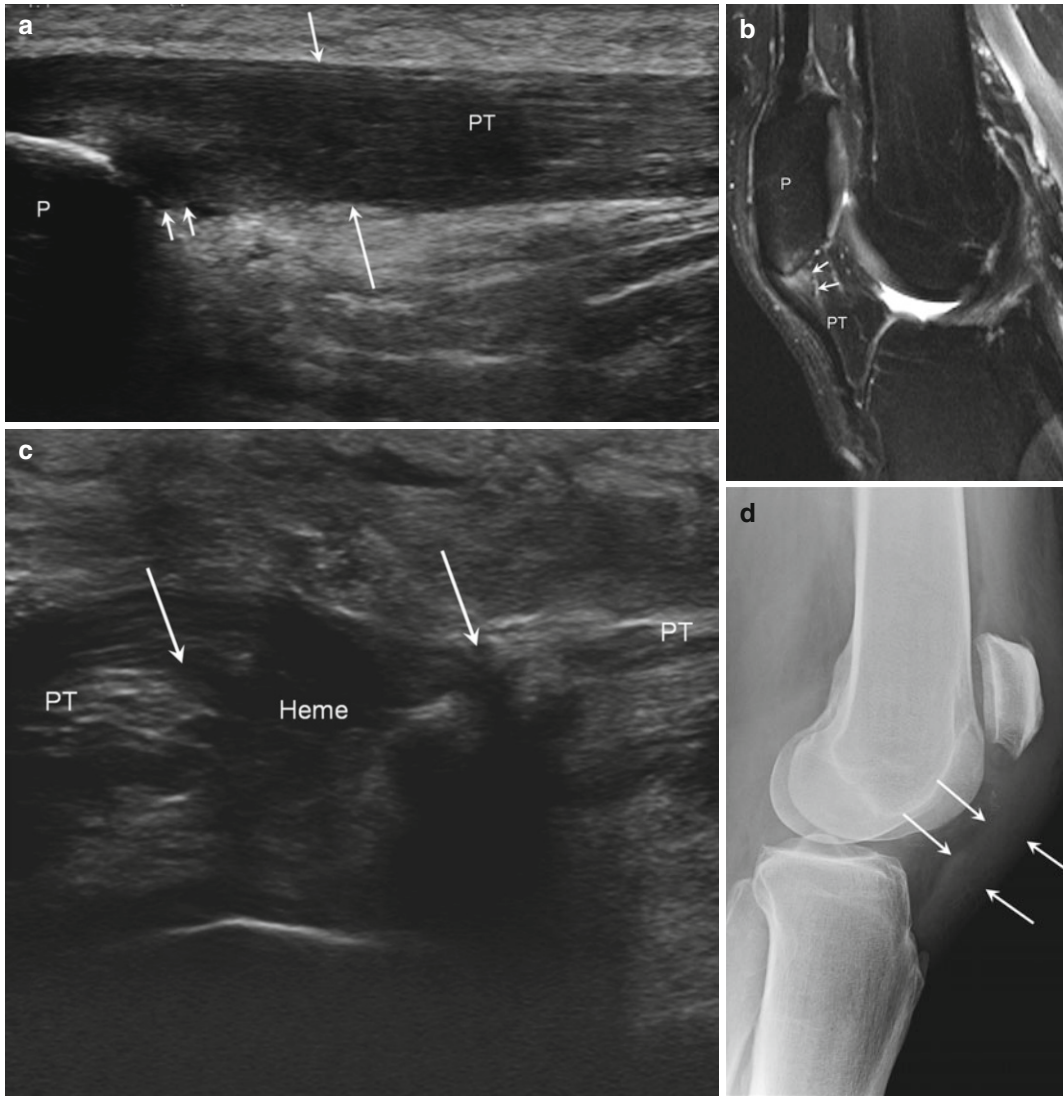

Fig. 5.86 Patellar tendon tears. (**a**) Long-axis ultrasound image of the patellar tendon (*PT*) shows thickening of the tendon (*long arrows*) with an anechoic defect (*short arrows*) reflecting a partial deep surface tear at the patella (*P*). (**b**) Corresponding sagittal fluid-sensitive MRI shows the partial deep surface tear (*arrows*) of the patellar tendon (*PT*) at the patella (*P*). (**c**) Long-axis ultrasound image in a different patient shows a complete, retracted tear (*arrows*) with intervening hemorrhage (*Heme*) involving the patellar tendon (*PT*); tibia (*Tib*). (**d**) Corresponding lateral radiograph shows patella alta with soft tissue swelling (*arrows*) due to the torn tendon with hemorrhage

formation deep to the ITB (Muhle et al. 1999). At ultrasound, the ITB will be thickened and hypoechoic. Within the intervening fat between the ITB and the lateral femoral condyle, there may be ill-defined hypoechoic edema or a more well-defined anechoic fluid collection reflecting adventitial bursa formation (Fig. 5.88) (Bonaldi et al. 1998).

5.8.4 Medial Collateral Ligament and Other Knee Ligaments

Although the anterior and posterior cruciate ligaments are far better evaluated with magnetic resonance imaging due to their intra-articular location, the superficial ligaments of the knee may be assessed sonographically. The ligaments

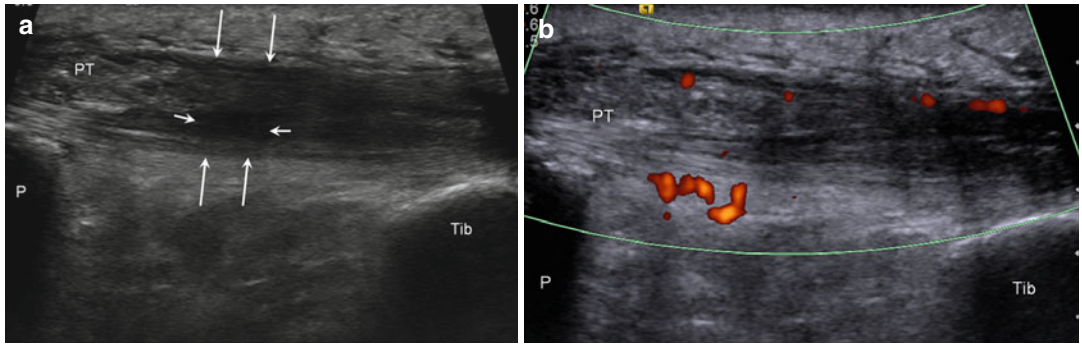

Fig. 5.87 Patellar tendinitis with hyperemia. Long-axis ultrasound images (**a**) without and (**b**) with power Doppler interrogation showing thickening (*long arrows*) of the patellar tendon (*PT*) with interstitial tearing (*short arrows*) and hyperemia in (**b**); patella (*P*), tibia (*Tib*)

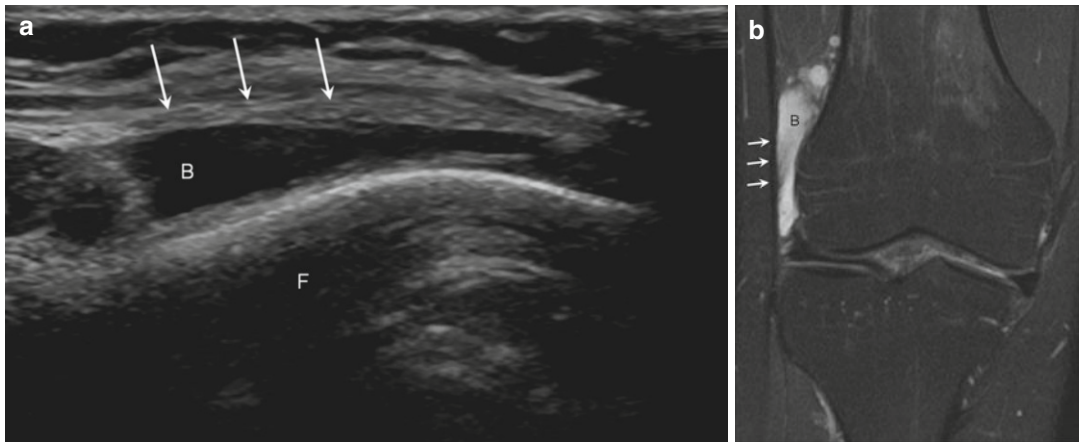

Fig. 5.88 Iliotibial band syndrome. (**a**) Long-axis ultrasound image of the lateral knee shows a patient with iliotibial syndrome with a bursitis (*B*) deep to the iliotibial band (*arrows*); femur (*F*). (**b**) Corresponding coronal fluid-sensitive MRI shows the bursitis (*B*) deep to the iliotibial band (*arrows*)

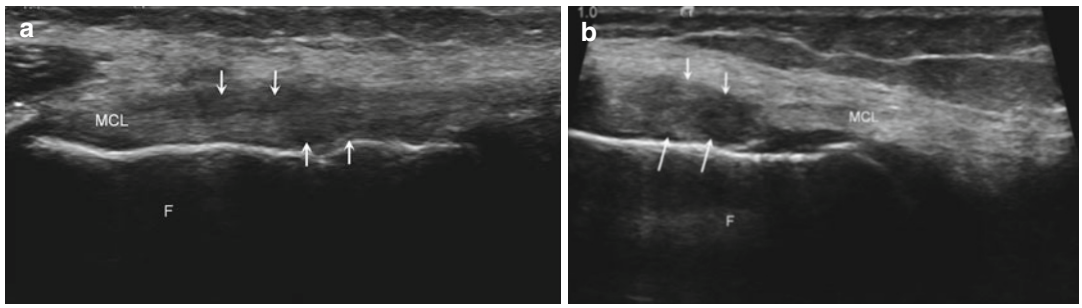

Fig. 5.89 MCL injury. Longitudinal ultrasound images of the medial aspect of the knee show (**a**) low-grade and (**b**) moderate-grade sprains of the proximal medial collateral ligament (*MCL*) with thickening of and decreased echogenicity within the ligament (*arrows*); femur (*F*)

most amenable to ultrasound evaluation are the medial and lateral collateral ligaments (De Maeseneer et al. 2002). Injuries of the medial collateral ligament (MCL) vary in appearance based on the severity of the injury (Fig. 5.89). Low-grade injuries manifest as periligamentous fluid without fiber disruption. Higher-grade injuries include partial or complete fiber disruption

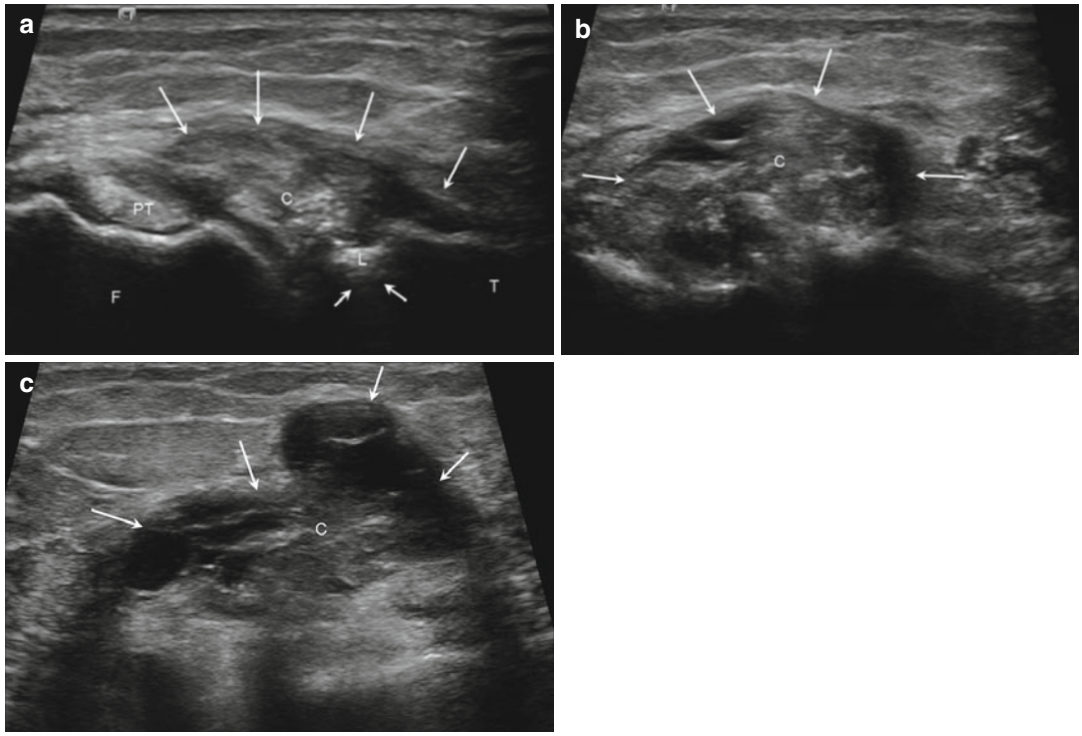

Fig. 5.90 Knee parameniscal cyst. (**a**–**c**) Longitudinal ultrasound images along the lateral knee demonstrate a complex parameniscal cyst (*C*, *long arrows*) with internal echogenic debris. Lateral meniscus (*L*) has a blunted, torn free edge (*short arrows*); popliteus tendon (*PT*), femur (*F*), tibia (*T*)

with associated hypoechoic or anechoic fluid separating the torn fibers. Remote injuries result in thickening of the ligament with or without associated calcification (Friedman et al. 2001) Dynamic imaging with gentle valgus stress may be utilized to accentuate the gap between the torn fibers (Lee et al. 1996).

The lateral collateral ligament, an important part of the posterolateral corner complex, may also be evaluated sonographically (Sekiya et al. 2010). The injured ligament will be thickened and hypoechoic or may be discontinuous (Sekiya et al. 2010).

5.8.5 Meniscal Pathology

While comprehensive evaluation of the menisci is limited due to their intra-articular location, ultrasound is capable of diagnosing some tears, particularly those located at the periphery or posterior aspect of the meniscus (Azzoni and Cabitza 2002; Wareluk and Szopinski 2012). The normal meniscus appears as a homogeneous, hyperechoic triangular structure (Grobbelaar and Bouffard 2000). Tears of the menisci present as linear hypoechoic or anechoic clefts within the substance of the meniscus (Friedman et al. 2003). Parameniscal cysts may also be identified with sonography. They appear as hypoechoic or anechoic fluid collections closely apposed to the meniscus. They may be of varying size (Seymour and Lloyd 1998). Often cysts contain varying amounts of internal echogenic debris and may mimic a solid lesion (Fig. 5.90) (Friedman et al. 2003). A communication between the cyst and a meniscal tear may be, but is not always, demonstrated with ultrasound. MRI remains the preferred imaging modality for meniscal evaluation (Azzoni and Cabitza 2002; Friedman et al. 2003).

5.8.6 Gastrocnemius and Plantaris Muscles

Within the calf, one of the most commonly injured muscles is the medial head of the gastrocnemius

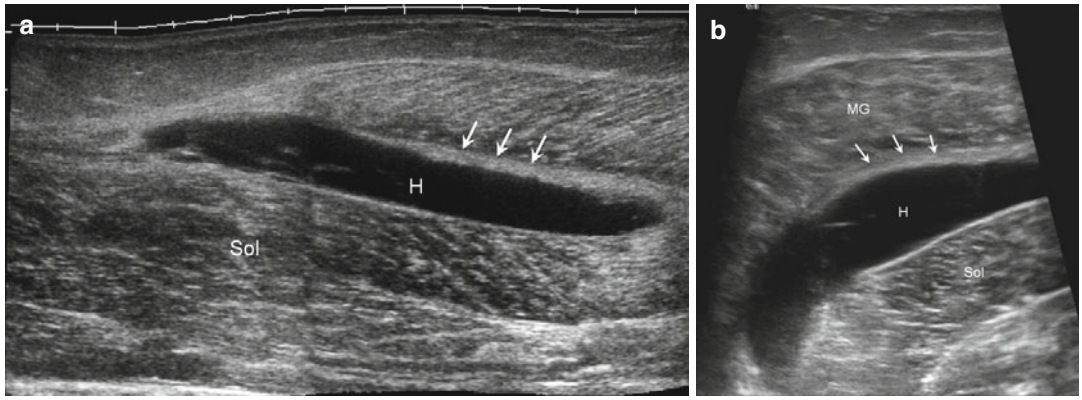

Fig. 5.91 Medial gastrocnemius muscle tear. (**a**) Long- and (**b**) short-axis ultrasound images of the medial gastrocnemius (*MG*) demonstrate a high-grade tear at the myotendinous junction (*arrows*) with intervening fluid/hemorrhage (*H*); soleus (*Sol*)

at the myotendinous junction. This entity has been termed "tennis leg" (Bianchi et al. 1998). Although this more frequently occurs in middle-aged persons involved in sports activities, these injuries may also occur in high-level athletes (Bianchi et al. 1998). Ultrasound is well suited to diagnose tears of the gastrocnemius. In addition, ultrasound is also useful in excluding other disorders that may clinically mimic gastrocnemius tears such as plantaris muscle tears (see below), deep vein thrombosis, ruptured popliteal cysts, or Achilles tendon pathology (Bianchi et al. 1998; Jamadar et al. 2002). The sonographic appearance varies based upon the severity of the injury. On imaging, tears appear as ill-defined hypoechoic areas at the myotendinous junction with varying degrees of muscle fiber disruption (Fig. 5.91). There may be increased echogenicity within the surrounding, intact muscle due to edema (Bianchi et al. 1998; Kwak et al. 2006). Complete tears result in tendon retraction (Bianchi et al. 1998).

The plantaris muscle courses from the lateral femoral condyle between the medial gastrocnemius and soleus muscles, inserting medial to the Achilles along the posterior calcaneus (Jamadar et al. 2002). Tears of the plantaris are less frequent than medial gastrocnemius tears and may simulate clinically injury to the latter muscle (Bianchi et al. 1998). Tears of the plantaris typically occur at the level of the mid-calf. Sonographic evaluation demonstrates discontinuity of the tendon with a surrounding hypoechoic fluid collection located between the medial gastrocnemius and soleus muscles (Fig. 5.92). The fluid collection resulting from a plantaris tear is typically located more proximally within the calf compared to the fluid accumulating following a medial gastrocnemius tear (Khy et al. 2012).

5.8.7 Stress Fractures

Stress fractures of the lower extremity are common in athletes and have increased in frequency in recent years (Khy et al. 2012). These fractures may occur in the femur, tibia, fibula, tarsal bones, and metatarsal bones. MRI is the modality of choice for the diagnosis of stress injuries as its sensitivity and specificity are greater than other modalities in all phases of stress injury, including early injury when plain radiographs may be normal (Khy et al. 2012). Ultrasound has recently been proven useful in the diagnosis of stress fractures in the aforementioned osseous structures where the cortical surface is visible sonographically, such as the anterior tibia (Khy et al. 2012). Sonographic imaging of stress fractures reveals hypoechoic periosteal thickening with a small adjacent hypoechoic fluid collection and soft tissue edema (Fig. 5.93). Hyperemia with color or power Doppler interrogation is also present. Occasionally a focal disruption of the hyperechoic cortex is present. As the healing process progresses, hyperechoic callous formation

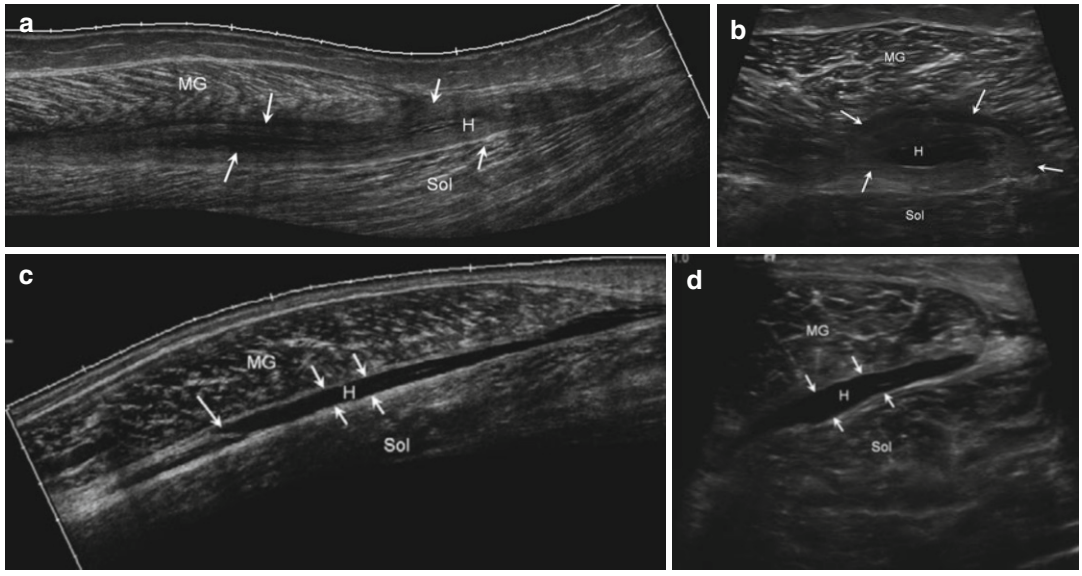

Fig. 5.92 Plantaris muscle tear. (**a**) Long- and (**b**) short-axis ultrasound images of a patient with a complete rupture of the plantaris tendon (*arrows*) with intervening hemorrhage (*H*); medial gastrocnemius (*MG*), soleus (*Sol*). (**c**) Long- and (**d**) short-axis ultrasound images in a different patient show complete rupture of the plantaris tendon (*short arrows*) with intervening hemorrhage (*H*). The retracted tendon stump (*long arrow*) can be seen in (**c**)

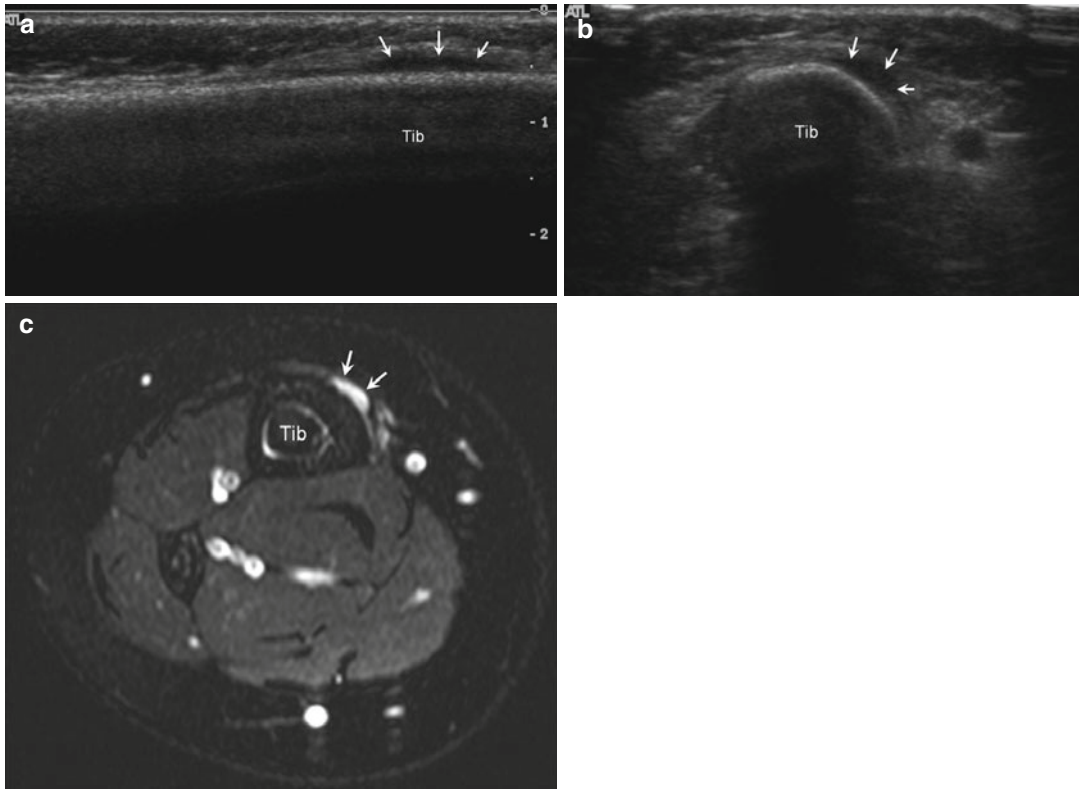

Fig. 5.93 Stress injury of the tibia. (**a**) Long- and (**b**) short-axis ultrasound images of the anterior tibia (*Tib*) show subperiosteal fluid (*arrows*) in a patient with an early stress injury. (**c**) Corresponding axial fluid-sensitive MRI shows hyperintense fluid (*arrows*) along the surface of the tibia (*Tib*)

develops at the fracture site (Bodner et al. 2005; Khy et al. 2012).

5.9 Foot and Ankle Ultrasound

5.9.1 Achilles Tendon

The Achilles tendon is readily examined with ultrasound due to its superficial location. In addition, extended field-of-view imaging allows the entire tendon to be rapidly assessed from the myotendinous junction to the enthesis by extending the range over which the information may be displayed. This technique provides a panoramic image of the tendon to illustrate bony and soft tissue landmarks as well as the relationship of any pathology to the surrounding tissues (Fig. 5.94) (Adler and Finzel 2005; Barbarie et al. 1998). Ultrasound may also be used to assess the peritendinous tissues including the paratenon and the retrocalcaneal bursa.

The pathology of the Achilles includes tendinosis, partial-thickness tearing, and full-thickness tearing. Tendinosis of the Achilles manifests as focal or diffuse, fusiform enlargement of the tendon with areas of decreased echogenicity (Fig. 5.95)

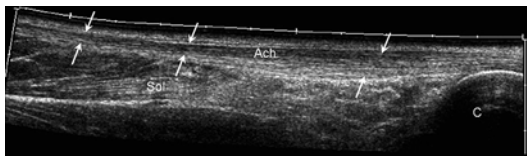

Fig. 5.94 Extended field of view of the Achilles tendon. Longitudinal ultrasound image of a normal Achilles (*Ach*) tendon using extended field-of-view imaging to include the entire tendon (*arrows*) from the myotendinous junction with the soleus (*Sol*) to the insertion on the calcaneus (*C*)

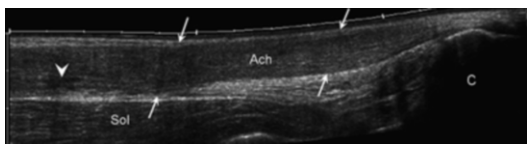

Fig. 5.95 Achilles tendinosis. Longitudinal ultrasound image of the Achilles tendon (*Ach*) in a patient with tendinosis with diffuse thickening of the tendon (*long arrows*) and a focal interstitial split tear (*arrowhead*); soleus (*Sol*), calcaneus (*C*)

(Aström et al. 1996). In addition, hyperemia with power or color Doppler interrogation may be present in the setting of tendinosis due to neovascularity. This finding, not present in a normal tendon, correlates directly with the site of the patient's symptoms (Fig. 5.96) (Richards et al. 2005). Enlargement of the tendon, greater than 6 mm, is considered abnormal (Bleakney et al. 2007).

Partial-thickness tears appear as focal hypoechoic or anechoic regions within the tendon that involve only some of the tendon fibers. These tears are usually superimposed on a background of tendinosis. Tears may be intrasubstance or extend to a surface (Fig. 5.97) (Bleakney et al. 2007). Enlargement of the tendon, greater than 10 mm, with marked intrasubstance abnormality suggests a partial-thickness tear (Aström et al. 1996).

Full-thickness tears are defined as complete disruption of the Achilles tendon fibers. These most frequently occur approximately 2–6 cm proximal to the enthesis in the critical zone of the tendon, corresponding to a zone of diminished vascularity (Hartgerink et al. 2001). There may be intervening hemorrhage between the torn edges of the tendon. There may also be herniation of adjacent echogenic fat into the gap (Fig. 5.98) (Jacobson et al. 2005). There may be retraction of the torn edges. The use of dynamic ultrasound in the setting of full-thickness tears allows the Achilles tendon to be quickly assessed in both neutral and plantar flexion to assess how closely approximated the torn edges are to determine if the patient may be treated conservatively. One caveat in the evaluation of full-thickness tears is that the plantaris tendon frequently remains intact and may mimic a partial-thickness tear. Thus it is important to track the plantaris in its entirety (Alfredson 2011).

The Achilles tendon does not have a true tendon sheath; however, inflammation of the surrounding tissues may occur resulting in paratenonitis. This manifests as hypoechoic soft tissue swelling surrounding the tendon (Calleja and Connell 2010). Retrocalcaneal or retro-Achilles bursitis may also be present in the setting of Achilles pathology with anechoic fluid distension along the deep or superficial surfaces of the tendon (Fig. 5.99) (Calleja and Connell 2010).

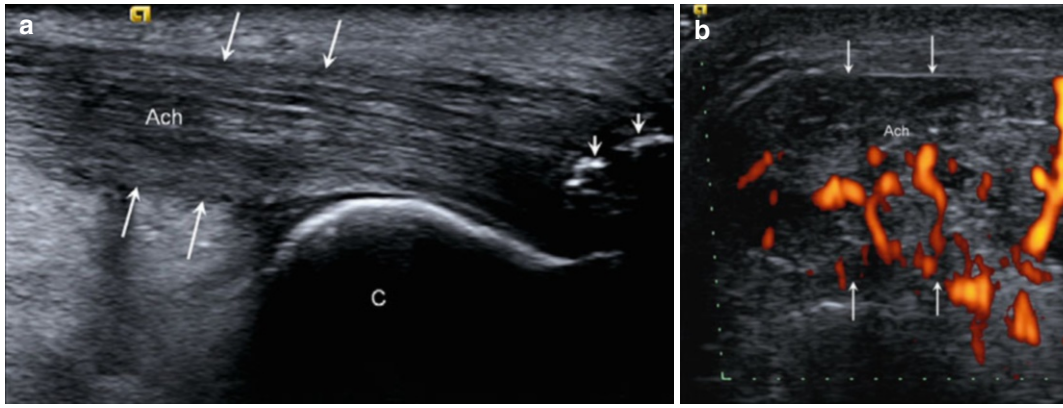

Fig. 5.96 Achilles tendinitis with hyperemia. (**a**) Long-axis ultrasound image of the Achilles tendon (*Ach*) shows a thickened tendon (*long arrows*) due to tendinosis with intratendinous calcifications (*short arrows*); calcaneus (*C*). (**b**) Short-axis ultrasound image shows the thickened (*arrows*) Achilles tendon (*Ach*) with diffuse hyperemia with power Doppler interrogation

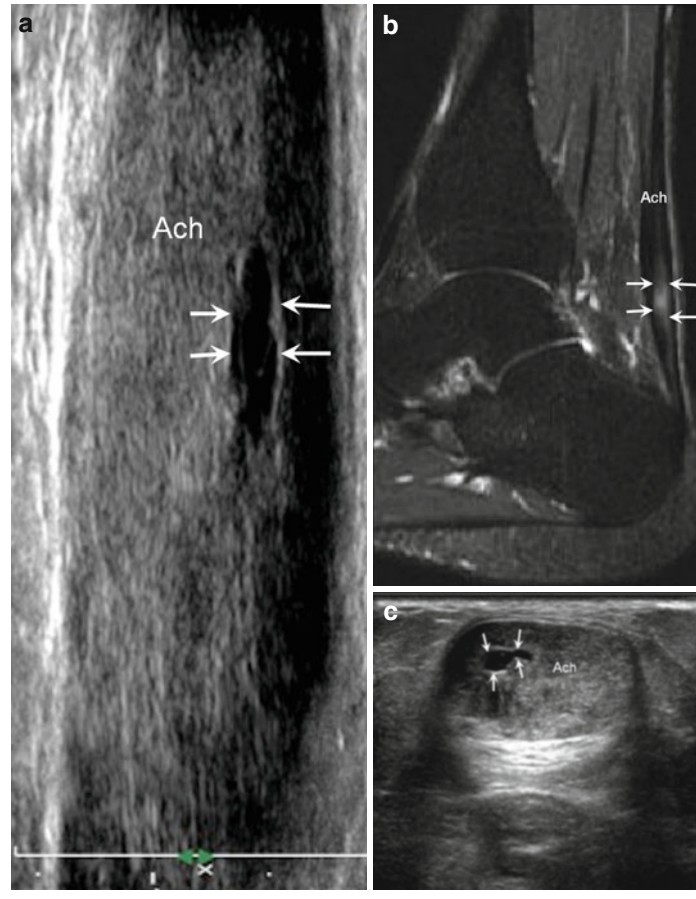

Fig. 5.97 Achilles tendon partial tear. (**a**) Longitudinal ultrasound image of the Achilles tendon (*Ach*) with thickening of the tendon and an intrasubstance tear (*arrows*). (**b**) Sagittal fluid-sensitive MRI in a different patient with similar pathology shows a thickened Achilles tendon (*Ach*) with an intrasubstance tear (*arrows*). (**c**) Short-axis ultrasound image shows the thickened Achilles tendon (*Ach*) with the intrasubstance tear (*arrows*)

5.9.2 Medial Flexor Tendons

The medial flexor tendons of the ankle include the posterior tibialis (PT), flexor digitorum longus, and flexor hallucis longus. The most frequently encountered pathology involves the posterior tibialis tendon. Tenosynovitis appears as hypoechoic or anechoic fluid distension of the tendon sheath. There may be associated synovial hypertrophy within the fluid that appears more hyperechoic (Fig. 5.100). A small volume of fluid within the PT tendon sheath is normal; however, a volume greater than 5.8 mm indicates PT tendon pathology (Chen and Liang 1997).

Power Doppler can be used to differentiate complex fluid from hypoechoic synovial thickening. The presence of hyperemia with power Doppler imaging indicates the presence of synovial thickening (Breidahl et al. 1998). In the competitive athlete, tenosynovitis is most frequently mechanical or traumatic.

As previously described in other tendons, tendinosis manifests as enlargement of the affected tendon with hypoechoic areas without fiber disruption (Premkumar et al. 2002). The tendon is most frequently abnormal at the level of the medial malleolus (Premkumar et al. 2002). Partial-thickness tears present as hypoechoic or anechoic regions of disruption of the tendon fibers (Kong and Van Der Vliet 2008). A variant of partial tearing of PT tendon is the longitudinal or intrasubstance split tear which results in the appearance of two separate tendon bundles with intervening anechoic or hypoechoic fluid. The tear may be completely intrasubstance or may extend to the tendon surfaces (Fig. 5.101) (Miller et al. 1996). Full-thickness tears involve the

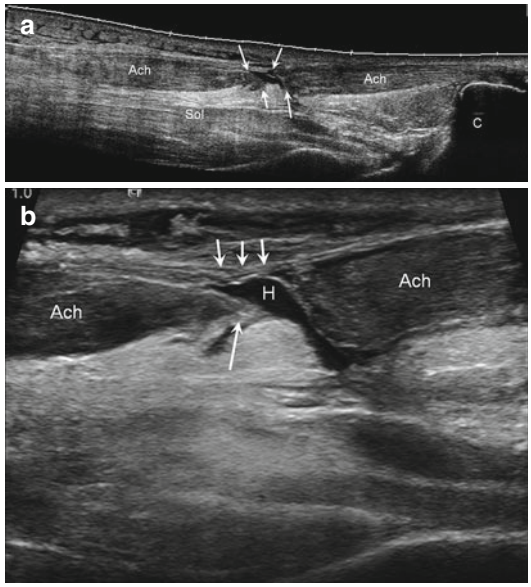

Fig. 5.98 Achilles tendon complete tear. (**a**) Long-axis ultrasound image of the Achilles tendon (*Ach*) shows a complete, minimally retracted tear (*arrows*); soleus (*Sol*), calcaneus (*C*). (**b**) Coned-down image of the tear (*long arrow*) of the Achilles tendon (*Ach*) shows herniation of the overlying tissues (*short arrows*) into the tear and intervening fluid/hemorrhage (*H*)

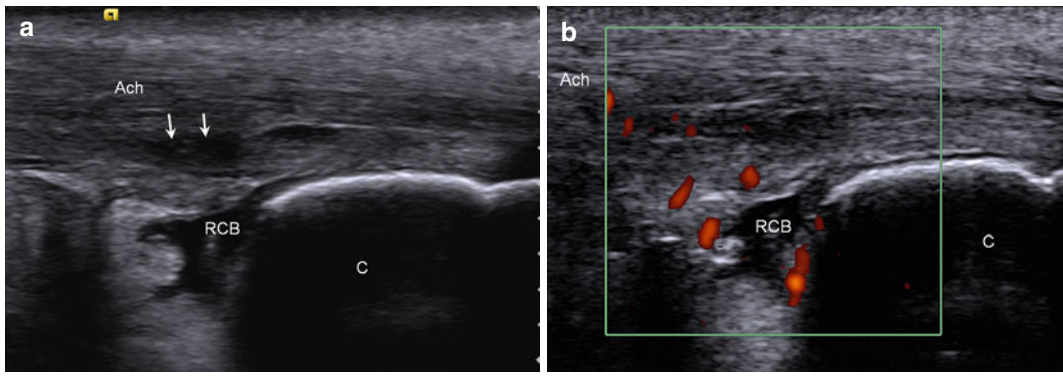

Fig. 5.99 Retrocalcaneal bursitis. Longitudinal ultrasound images of the Achilles tendon (*Ach*) insertion (**a**) without and (**b**) with power Doppler interrogation demonstrate Achilles tendinosis with a low-grade intrasubstance tear (*short arrows*), retrocalcaneal bursitis (*RCB*), and hyperemia in image (**b**); calcaneus (*C*)

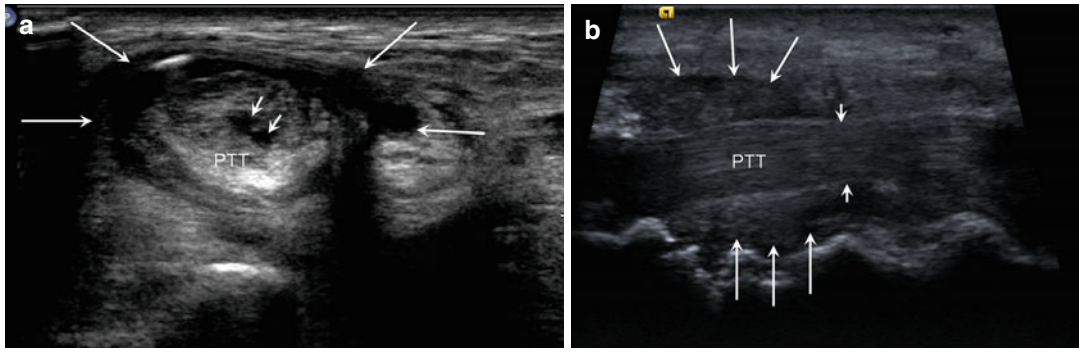

Fig. 5.100 Posterior tibialis tendon pathology. (**a**) Short-axis ultrasound image of the posterior tibialis tendon (*PTT*) demonstrates thickening of the tendon with surrounding fluid (*long arrows*) reflecting tenosynovitis and an intrasubstance split tear of the tendon (*short arrows*). (**b**) Long-axis ultrasound image in a different patient with stenosing tenosynovitis shows thickened synovium (*long arrows*) surrounding the posterior tibial tendon (*PTT*) with focal narrowing (*short arrows*) reflecting the "stenosing" component

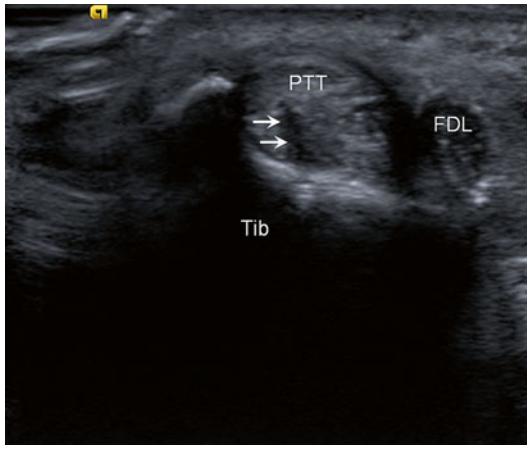

Fig. 5.101 Posterior tibialis tendon split tear. Short-axis ultrasound image of the medial ankle shows an intrasubstance split tear (*arrows*) of the posterior tibialis tendon (*PTT*); flexor digitorum longus tendon (*FDL*), tibia (*Tib*)

entire width of the tendon with retraction of the torn edges and interposed fluid and/or hemorrhage (Miller et al. 1996).

Dynamic sonographic imaging is useful in assessing for posterior tibial tendon subluxation or dislocation that may occur following prior injury to the flexor retinaculum. Because the abnormal motion may be present only following certain ankle motions, this pathology may be missed on static MRI (Prato et al. 2004).

The flexor digitorum longus and flexor hallucis longus tendons are less frequently injured; however, they should be routinely evaluated during a medial ankle examination in an athlete. Flexor hallucis longus (FHL) injuries have been reported in both elite ballet dancers and other athletes involved in running, climbing, or other activities that involve abrupt changes in direction during activity (Sammarco and Cooper 1998). While tears of the tendon may display sonographic appearances similar to other tendon tears, FHL pathology more frequently manifests as tendinosis and tenosynovitis. FHL pathology may also be seen in the setting of posterior impingement due to the presence of a large accessory ossicle posterior to the talus, the os trigonum (Fig. 5.102). This occurs with repetitive, extreme plantar flexion of the ankle (Michelson and Dunn 2005; Sammarco and Cooper 1998). Dynamic evaluation of the FHL may demonstrate impingement. Impingement may also be seen with synovitis in the posterior recess of the tibiotalar joint.

5.9.3 Peroneal Tendons

The pathology of the peroneal tendons is similar to that seen in the medial ankle tendons. This most frequently occurs at the level of the lateral malleolus due to friction of the tendons against the adjacent bone. Tendinosis appears as hypoechoic enlargement of the affected tendon

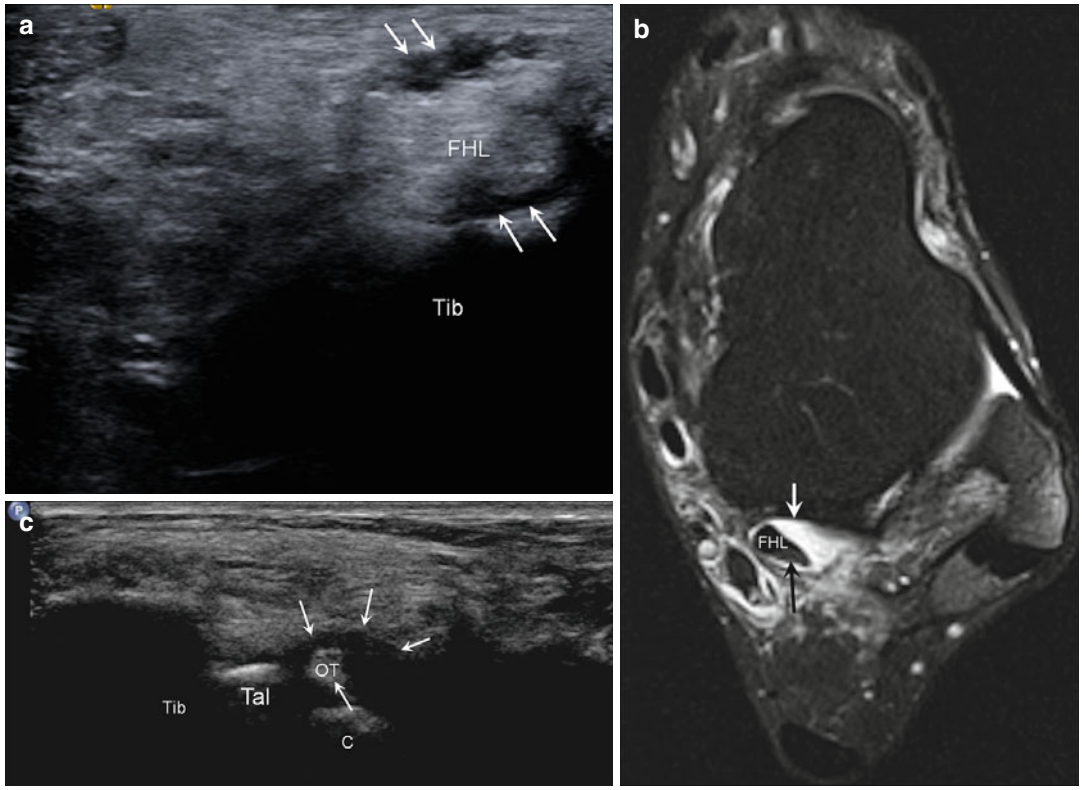

Fig. 5.102 Posterior impingement. (**a**) Short-axis ultrasound image of the posterior ankle shows thickening of the flexor hallucis longus (*FHL*) with tenosynovitis (*arrows*); tibia (*Tib*). (**b**) Corresponding axial fluid-sensitive MRI of the ankle shows the FHL with mild increased intrasubstance high signal (*black arrow*) and surrounding fluid (*white arrow*). (**c**) Long-axis ultrasound image shows an os trigonum (*OT*) surrounded by fluid (*arrows*) in this patient with posterior impingement; tibia (*Tib*), talus (*T*), calcaneus (*C*)

without fiber disruption (Grant et al. 2005). Partial tearing results in hypoechoic or anechoic regions involving a portion of the tendon, while complete tearing involves the entire width of the tendon. Longitudinal split tears may also affect either of the peroneal tendons; however, the peroneus brevis is more frequently affected due to its interposition between the peroneus longus tendon and the fibula (Fig. 5.103) (Grant et al. 2005). While tears of the peroneal tendons more frequently occur at the level of the lateral malleolus, the peroneus longus tendon may tear more distally in association with a fracture of an os peroneum, an intratendinous ossicle normally found within the tendon (Brigido et al. 2005). Separation of the fragments of the ossicle of greater than 6 mm indicates fracture rather than a bipartite os peroneum, which is a normal anatomic variant. The former also indicates full-thickness tearing of the peroneus longus (Brigido et al. 2005).

Tenosynovitis may also involve the peroneal tendons, appearing as distension of the tendon sheath with fluid of varied echogenicity based on the composition and the presence of synovial hypertrophy that results in a more echogenic appearance than simple fluid (Bianchi et al. 2010a). The presence of peritendinous hyperemia indicates the presence of synovial tissue rather than fluid (Breidahl et al. 1998).

Dynamic imaging of the peroneal tendons is important, particularly in the setting of a prior superior peroneal retinaculum injury that can occur following lateral ankle sprain. Injury to the retinaculum may result in subluxation or frank dislocation of the peroneal tendons anterolaterally that may only be demonstrated during dynamic evaluation in dorsiflexion and ankle

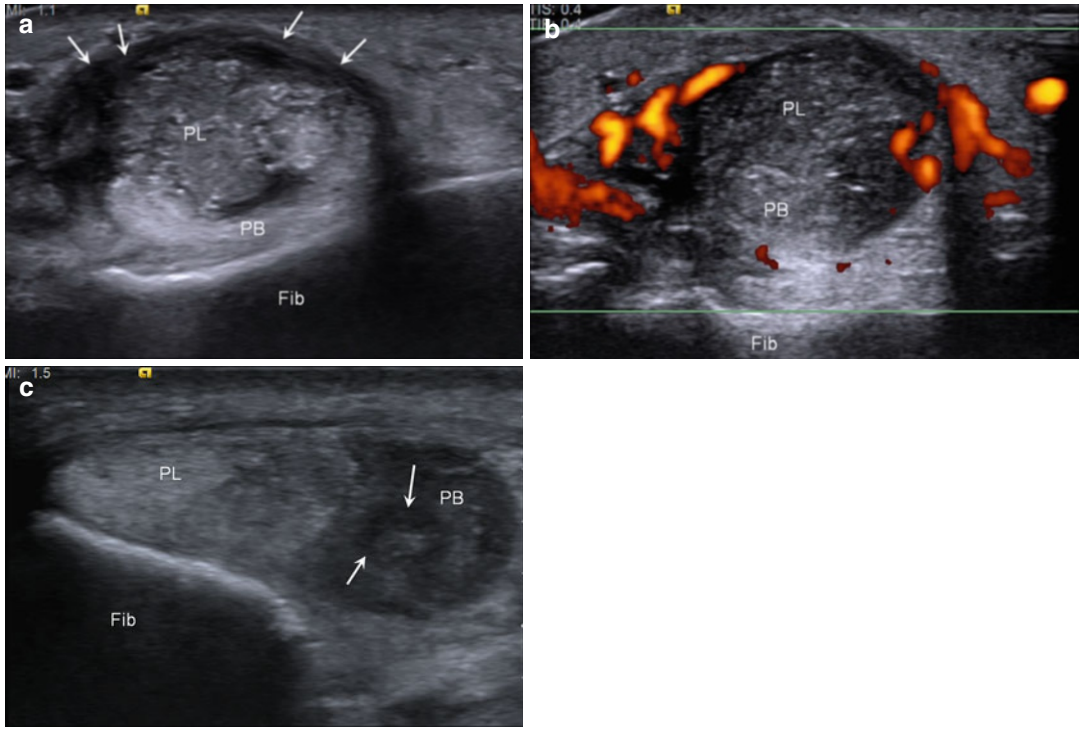

Fig. 5.103 Peroneal tendinosis. (**a**) Short-axis ultrasound image of the lateral ankle demonstrates marked thickening of the peroneus longus tendon (*PL*) with mass effect on the subjacent peroneus brevis (*PB*) and surrounding fluid (*arrows*). (**b**) Short-axis ultrasound image of the peroneus longus (*PL*) and peroneus brevis (*PB*) in a different patient shows tendons that are thickened and demonstrate hyperemia with power Doppler interrogation. (**c**) Transverse ultrasound image of the peroneal tendons in a third patient shows thickening of and hypoechogenicity within the peroneus longus (*PL*) and peroneus brevis tendons (*PB*) with an intrasubstance split tear (*arrows*) in the peroneus brevis; fibula (*Fib*)

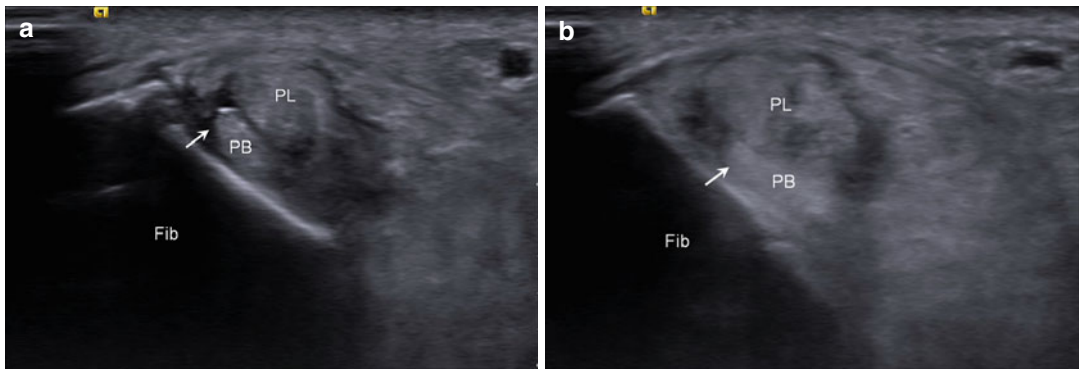

Fig. 5.104 Peroneus brevis intrasheath subluxation. Transverse ultrasound images of the lateral ankle in (**a**) inversion and (**b**) eversion demonstrate subluxation of the peroneus brevis tendon (*PB*) with respect to the peroneus longus (*PL*). *Short arrow* shows movement of anterior edge of the peroneus brevis tendon with respect to the peroneus longus; fibula (*Fib*)

eversion (Diaz et al. 1998; Neustadter et al. 2004). Another variant of subluxation is termed intrasheath subluxation where the tendons demonstrate abnormal motion with respect to each other but remain located along the posterior margin of the fibula (Fig. 5.104). This is frequently associated with tendinosis and tendon tearing (Thomas et al. 2009).

5.9.4 Anterior Extensor Tendons

The anterior extensor tendons of the ankle are the less frequently injured than both the medial flexor and peroneal tendons. Nevertheless, when abnormal, the imaging characteristics are similar to the other ankle tendons described previously. This pathology includes tendinosis, tenosynovitis, partial tearing, and full-thickness tearing.

Of the extensor tendons, the anterior tibialis (AT) tendon is more frequently injured than the extensor hallucis longus and extensor digitorum tendons. Although chronic pathology of the AT tendon has more frequently been reported in overweight, middle-aged women between the ages of 50 and 70 years, it has also been seen in young athletes involved in uphill or downhill running due to overuse (Mengiardi et al. 2005; Ng et al. 2013). Acute, spontaneous rupture has been seen in other athletes including fencing and cross-country skiing (Ng et al. 2013). Clinically, patients present with a palpable mass related to the retracted tendon and a palpable defect in the tendon (Ng et al. 2013). Penetrating trauma may result in injury of the tendon, possibly due to laceration from a ski boot or hockey skate blade (Ebrahimi et al. 2010). Rupture of the AT tendon most commonly occurs between 5 and 30 mm from the insertion (Fig. 5.105) (Dooley et al. 1980; Geppert et al. 1993; Ouzounian and Anderson 1995). At ultrasound, the torn tendon presents with a gap between the torn edges with thickening of and decreased echogenicity within the tendon stumps. The retracted end may display a refractive shadow.

Because of their superficial location, extensor digitorum longus (EDL) and extensor hallucis longus (EHL) are more frequently injured in the setting of penetrating trauma (Al-Qattan 2007). Sports-related injuries have been reported during ultramarathon running and tae kwon do (Kobayashi et al. 2007; Lee et al. 2009).

Other pathology involving the anterior compartment of the ankle includes muscle hernias, most commonly involving the anterior tibialis muscle. Sonographically, muscle hernias appear as hypoechoic muscle tissue that bows the overlying hyperechoic fascia or extends through a defect in the fascia. A perforating vessel may accompany the hernia. This is frequently due to the sequela of prior trauma. Patients frequently present with a palpable mass that is accentuated with muscle contraction. Dynamic imaging may be necessary to elicit the pathology (Fig. 5.106) (Beggs 2003).

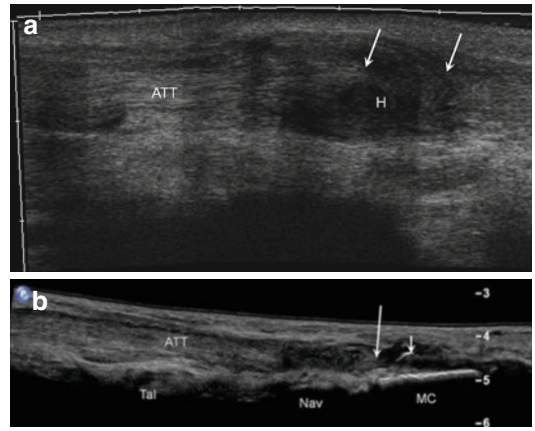

Fig. 5.105 Anterior tibialis tendon pathology. (**a**) Longitudinal ultrasound image of the anterior tibialis tendon (*ATT*) shows a high-grade partial deep surface tear (*arrows*) with intervening fluid/hemorrhage (*H*). (**b**) Long-axis ultrasound image of the anterior tibialis tendon (*ATT*) in a different patient shows complete rupture of the tendon (*long arrow*) with a small osseous avulsion fracture (*short arrow*); talus (*Tal*), navicular (*Nav*), medial cuneiform (*MC*)

5.9.5 Ligaments of the Ankle

The lateral ligaments of the ankle, specifically the anterior talofibular (ATFL) and calcaneofibular ligaments (CFL), are more frequently injured than the medial ligaments, specifically the deltoid ligament. At imaging, the normally hyperechoic band-like ligaments may appear enlarged and hypoechoic in the setting of acute sprain. Partial tearing manifests as a focal hypoechoic or anechoic cleft within the ligament, with some fibers remaining intact. Full-thickness tears are characterized by complete disruption of the ligament fibers with intervening fluid or hemorrhage (Fig. 5.107) (Peetrons et al. 2004). In the setting of an osseous avulsion, a hyperechoic, linear

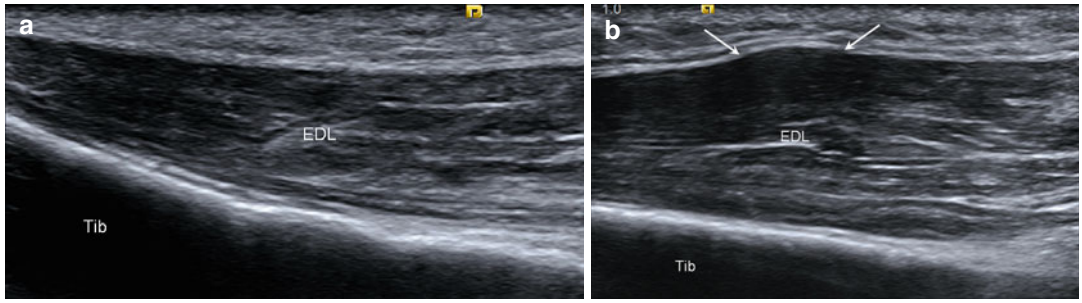

Fig. 5.106 Extensor digitorum longus muscle hernia. Longitudinal ultrasound images of the extensor digitorum longus (*EDL*) muscle (**a**) without and (**b**) with muscle flexion show a focal herniation of the muscle (*arrows*) with bulging of the overlying tissues; tibia (*Tib*)

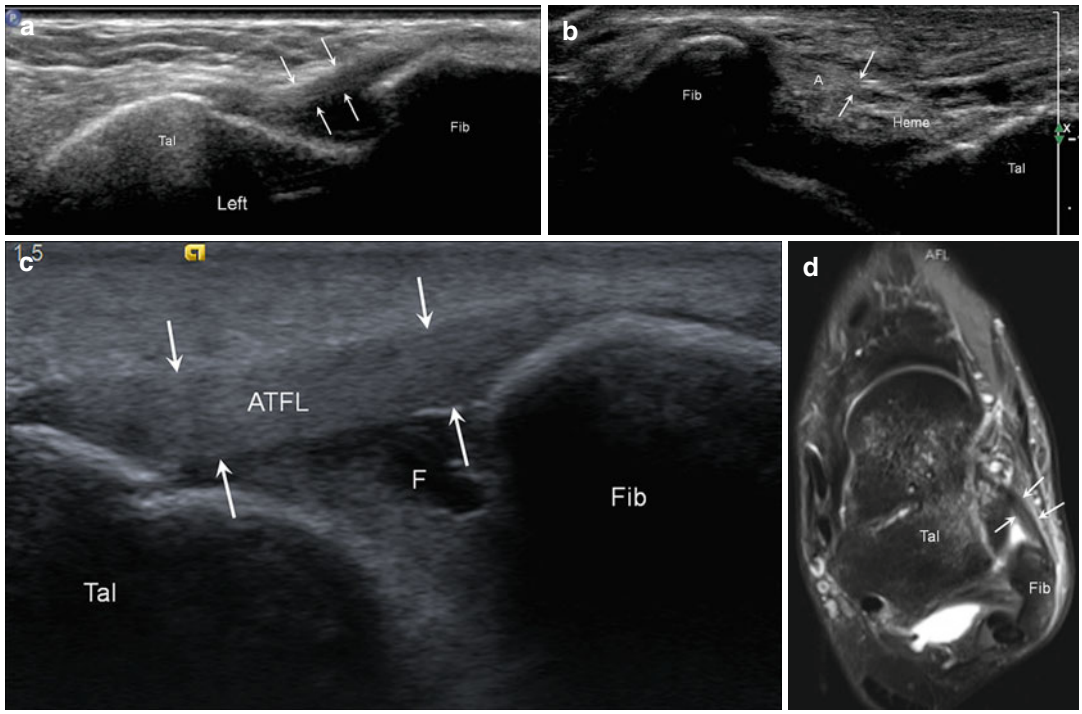

Fig. 5.107 Anterior talofibular ligament pathology. (**a**) Longitudinal ultrasound image of a normal, band-like anterior talofibular ligament (*arrows*). (**b**) Long-axis ultrasound image in a patient with a tear (*arrows*) of the anterior talofibular ligament (*A*) from the talus (*Tal*) with hemorrhage (*Heme*) filling the gap. (**c**) Long-axis ultrasound image in a different patient with a ligament sprain with thickening (*arrows*) of the ligament (*ATFL*) and adjacent fluid (*F*). (**d**) Corresponding axial fluid-sensitive MRI of the ankle shows the thickened, hyperintense ligament (*arrows*); fibula (*Fib*)

bone fragment remains attached to the torn ligament fibers. Remote ligament injuries may appear as thickening or attenuation of the affected ligament, with possible heterotopic ossification (Hsu et al. 2006; Peetrons et al. 2004).

The ATFL and CFL are readily evaluated sonographically; however, the posterior talofibular ligament (PTFL) is not well assessed, as it is partially obscured by the lateral malleolus (Peetrons et al. 2004).

The major medial ankle ligament, the deltoid ligament, is more difficult to image sonographically because it is composed of multiple ligaments that form the superficial and deep components. Everting and dorsiflexing the ankle allow for an improved acoustic window to evaluate the ligament. Injuries to the ligament appear similar sonographically to lateral ligament injuries (Fig. 5.108) (Adler et al. 2004; Peetrons et al. 2004).

Injuries to the syndesmotic ligaments may also be imaged sonographically, in particular the anterior tibiofibular ligament. The appearance of the injured anterior tibiofibular ligament is similar to that of the ATFL, CFL, and deltoid ligaments with fiber disruption in the setting of a tear and hypoechoic thickening in the setting of an acute sprain (Peetrons et al. 2004). Dynamic imaging with the ankle in dorsiflexion and eversion may produce widening of the interspace between the distal tibia and fibula (Peetrons et al. 2004). This injury has been termed a "high ankle sprain," and if undiagnosed, it may result in persistent anterolateral ankle pain (Peetrons et al. 2004).

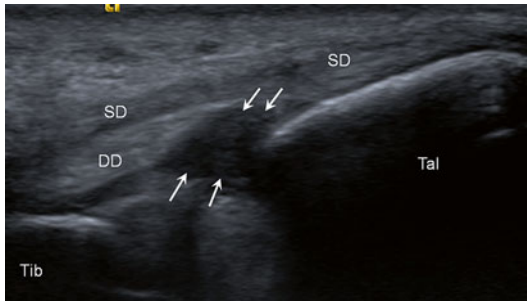

Fig. 5.108 Deltoid ligament tear. Longitudinal ultrasound image of the medial ankle demonstrates tearing (*arrows*) of the deltoid fibers of the deltoid ligament (*DD*) at the insertion on the talus (*Tal*). The superficial fibers of the deltoid (*SD*) remain intact; tibia (*Tib*)

5.9.6 Plantar Fascia

The normal plantar fascia appears as a hyperechoic, fibrillar structure similar to normal tendons. The fascia attaches to the plantar surface of the calcaneus and normally measures 3–4 mm (Rawool and Nazarian 2000). In the setting of plantar fasciitis, the fascia is thickened greater than 4 mm and is hypoechoic. Tears may be present manifesting as hypoechoic or anechoic clefts involving some or all of the fascia fibers (Fig. 5.109) (Cardinal et al. 1996; Rawool and Nazarian 2000).

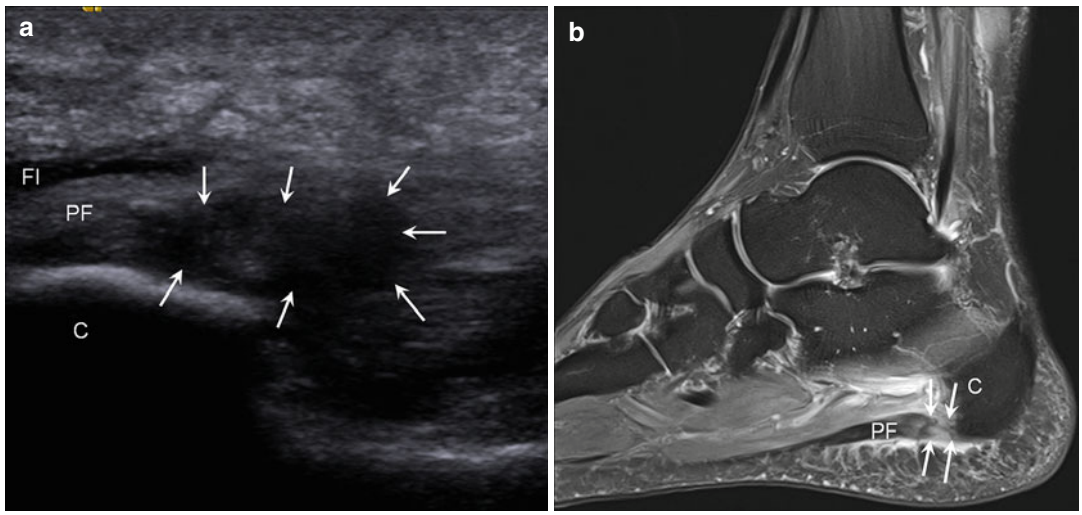

Fig. 5.109 Plantar fasciitis. (**a**) Long-axis ultrasound image of the plantar fascia (*PF*) demonstrates thickening of the fascia with a high-grade partial deep surface tear (*arrows*) near the origin from the calcaneus (*C*) with perifascial fluid (*Fl*). (**b**) Corresponding sagittal fluid-sensitive MRI shows thickening of and abnormal signal within the plantar fascia (*PF*) with tearing (*arrows*); calcaneus (*C*)

5.9.7 Plantar Plate and Turf Toe

The plantar plates of the great toe and lesser toes may be assessed sonographically. The normal sonographic appearance of the plantar plate is a hyperechoic band of tissue extending from the head of the metatarsal to the base of the proximal phalanx in the lesser toes (Fig. 5.110) (Klein et al. 2012). In the great toe, the anatomy is more complex and includes the intersesamoidal ligaments, the metatarsosesamoid ligaments, the plantar plate, and the sesamoid–phalangeal ligaments (Stoller 2007b). Like ligaments elsewhere in the body, these ligaments appear as echogenic, band-like structures (Jacobson 2002). When abnormal, the plantar plate may appear inhomogeneous and hypoechoic with hypoechoic or anechoic focal clefts or defects reflecting tears. The tears in the lesser toes most frequently occur at the distal insertion at the base of the proximal phalanx (Fig. 5.111) (Klein et al. 2012). Tears may be accentuated with dynamic imaging of the toe in dorsiflexion (Klein et al. 2012). Tears of the plantar plate complex in the great toe more frequently occur at the metatarsal neck (Stoller 2007b).

5.9.8 Stress Fractures

As stated above, MRI is the modality of choice for the diagnosis of stress injuries due to its greater sensitivity and specificity in all stages of stress injury, particularly when plain radiographs are normal (Khy et al. 2012). Nevertheless, ultrasound has been shown to be beneficial in the diagnosis of stress fractures in the metatarsal bones. Sonographically, stress fractures demonstrate hypoechoic periosteal thickening with a small adjacent hypoechoic fluid collection and soft tissue edema (Fig. 5.112). Hyperemia with color or power Doppler interrogation is also present. Occasionally, a focal disruption of the hyperechoic cortex is present (Fig. 5.113). As the healing process progresses, hyperechoic callous formation develops at the fracture site (Fig. 5.112) (Bodner et al. 2005; Khy et al. 2012). Patients will report point tenderness with transducer pressure.

5.9.9 Ganglia of the Foot and Ankle

The most frequently encountered mass in the foot and ankle is a ganglion cyst. Like in the hand and wrist, these cysts are usually anechoic with posterior acoustic enhancement (Fig. 5.114). Sometimes, particularly after trauma, the cyst may appear more complex, multiloculated, and hypoechoic. Cysts may communicate with joints or tendon sheaths in the foot and ankle. No internal flow should be present with power or color Doppler interrogation (Ortega et al. 2002). As in the hand and wrist, ganglia may be safely aspirated percutaneously with ultrasound guidance.

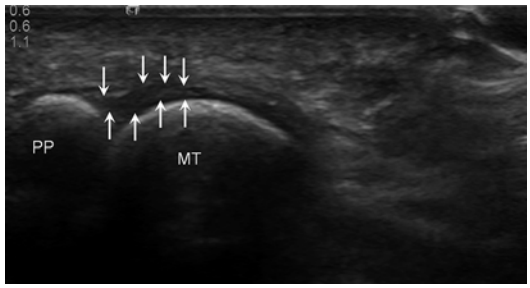

Fig. 5.110 Normal plantar plate. Longitudinal ultrasound image along the plantar aspect of the second metatarsophalangeal joint shows the normal, band-like echogenic appearance of the plantar plate (*arrows*) extending from the metatarsal head (*MT*) to the base of the proximal phalanx (*PP*)

Fig. 5.111 Plantar plate tear. Longitudinal ultrasound image along the plantar aspect of the second metatarsophalangeal joint shows a tear (*arrows*) at the insertion of the plantar plate (*PL*) on the base of the proximal phalanx (*PP*); metatarsal head (*MT*), flexor digitorum tendon (*FD*)

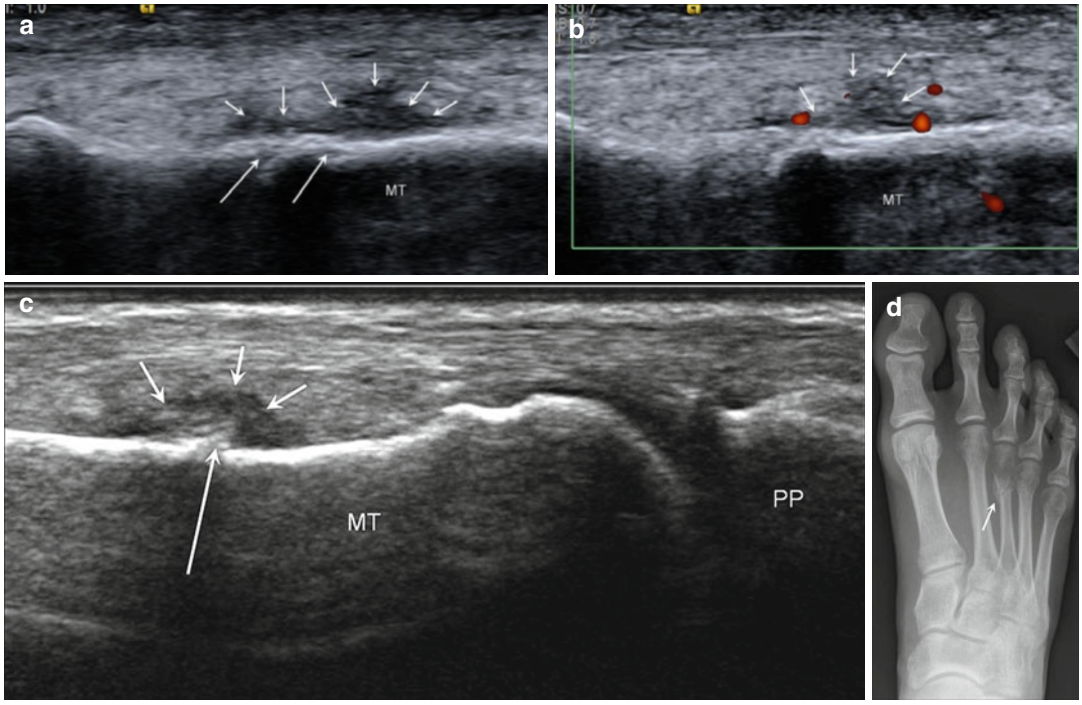

Fig. 5.112 Foot stress fracture. Longitudinal ultrasound image of the second metatarsal (*MT*) in (**a**) without and in (**b**) with power Doppler interrogation shows periosteal reaction (*short arrows*) with hyperemia in (**b**). There is focal cortical buckling at the site of the fracture (*long arrows*) in (**a**). (**c**) Long-axis ultrasound image in a different patient shows a healing fracture of the third metatarsal (*MT*) with callous (*long arrow*) and periosteal reaction (*short arrows*); proximal phalanx (*PP*). (**d**) Corresponding anteroposterior radiograph shows the healing fracture of the third metatarsal neck (*arrow*)

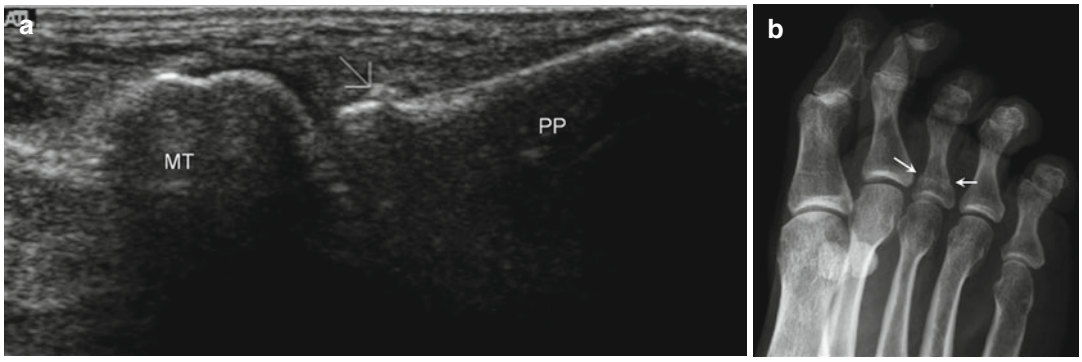

Fig. 5.113 Fracture with cortical disruption. (**a**) Long-axis ultrasound image of the toe in a patient referred for a presumed neuroma showing focal cortical disruption (*arrow*) at the base of the proximal phalanx (*PP*) at the site of an unsuspected fracture; metatarsal (*MT*). Subsequent radiograph (**b**) confirms the fracture (*arrows*)

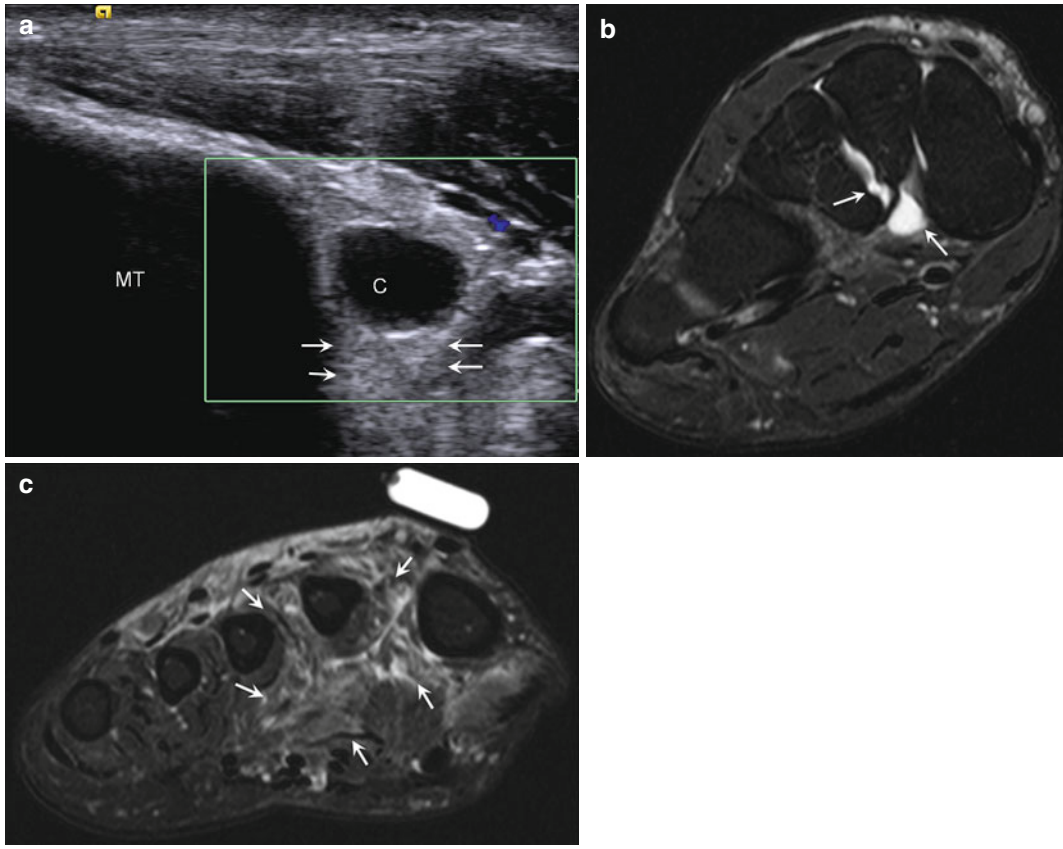

Fig. 5.114 Foot ganglion cyst. (**a**) Long-axis ultrasound image along the plantar aspect of the foot shows a ganglion cyst (*C*) with posterior acoustic enhancement (*arrows*) arising between the metatarsal (*MT*) bases. Coronal fluid-sensitive MRIs show in (**b**) the cyst (*arrows*) and in (**c**) denervation edema in the foot musculature more distally (*arrows*) due to nerve compression by the cyst

5.10 Percutaneous Ultrasound-Guided Interventions in Sports Medicine

A full discussion of musculoskeletal ultrasound-guided interventional procedures and techniques is beyond the scope of this chapter. Nevertheless, a number of interventional procedures that are useful in the treatment of athletes deserve mention.

The real-time nature of ultrasound makes it ideally suited to provide guidance for a variety of musculoskeletal interventions (Adler and Sofka 2003; Brophy et al. 1995; Cardinal et al. 1998; Christensen et al. 1988; Cunnane et al. 1996; Davidson and Jayaraman 2011; Grassi et al. 2001; Koski 2000; Sofka et al. 2001). Continuous observation of the needle ensures accurate needle placement and appropriate distribution of the injected and/or aspirated material (Fig. 5.115). Needles can be positioned close to neurovascular bundles without damaging nerves or vessels (Fig. 5.116).

The current generation of high-frequency small parts transducers allows excellent depiction of soft tissue details and articular surfaces, particularly in the hand, wrist, foot, and ankle (Ahmed and Nazarian 2010), facilitating exact needle insertion into nondistended structures, such as joints, tendon sheaths, or bursae. Injected fluid produces a contrast effect, which improves delineation of adjacent structures (e.g., labral morphology) and shows the distribution of the injected material (Koski et al. 2005; Luchs et al.

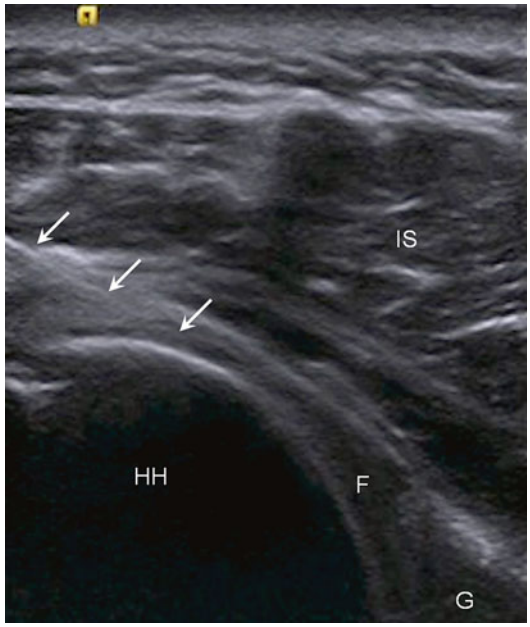

Fig. 5.115 Shoulder injection. Longitudinal ultrasound image of the posterior aspect of the shoulder shows intra-articular positioning of the needle (*arrows*) in the joint with distension of the posterior recess with fluid (*F*); humeral head (*HH*), glenoid (*G*), infraspinatus muscle (*IS*)

2007). The advent of newer technology that permits image registration to other modalities, such as computed tomography or MRI, is expected to enhance further the role of ultrasound in performing a broad variety of interventions (Krücker et al. 2011). Ultrasound guidance to target sites of maximal tendon and/or muscle pathology has been used to administer growth factors using platelet-rich plasma (PRP) or autologous blood (Connell et al. 2006; de Vos et al. 2010; James et al. 2007; Mishra and Pavelko 2006; Peerbooms et al. 2010). Ultrasound guidance does not involve ionizing radiation, and this is an advantage in the pediatric and adolescent population.

5.10.1 Ultrasound-Guided Therapeutic Injections/ Aspirations into Joints and Tendon Sheaths

The most common clinical indication for ultrasound-guided injections generally relates to pain that has failed to respond to conservative measures, regardless of the anatomic site. The pain may be the result of a chronic repetitive or an acute sports-related injury. These injections may be performed within or around joints (Fig. 5.115) or surrounding tendons (Fig. 5.117). Bursae and ganglia may also be aspirated and injected. Ultrasound guidance is effective in ensuring that the needle tip is correctly placed prior to injection of the therapeutic mixture.

Most injections use long-acting corticosteroid in combination with local anesthetic in relatively small volumes. A detailed review of these agents is beyond the scope of this chapter. Examples of the corticosteroids utilized are triamcinolone, methylprednisolone, betamethasone, and dexamethasone.

The most commonly used anesthetics are lidocaine and bupivacaine (i.e., Marcaine) (Cox et al. 2003; Kamath et al. 2008; MacMahon et al. 2009). They are both local injectable anesthetics but differ in the onset and duration of action. Lidocaine has rapid onset (seconds) and short duration (1–2 h). Bupivacaine becomes effective in 5–10 min and generally lasts 4–6 h.

A test injection with 1 % lidocaine (Fig. 5.118) shows bright echoes filling the joint or tendon sheath demonstrating appropriate location of the needle tip. This will prevent injection of the therapeutic mixture directly into a tendon during peritendinous injections (Fig. 5.117). Intratendinous injections have been associated with tendon rupture as has been reported with blind injections of the plantar fascia. Blind injections into the heel have been associated with rupture of the plantar fascia and failure of the longitudinal arch (Kim et al. 2010). Occasionally, abnormalities such as tendon tears, following intrasheath injections, or intra-articular pathology, such as labral tears, after joint injections may become more visible following distension with the injected material, similar to MR arthrography (Fig. 5.119).

5.10.2 Bursal and Ganglion Cyst Injections

Distended bursae provide anatomic targets for therapeutic injections. Injections are often

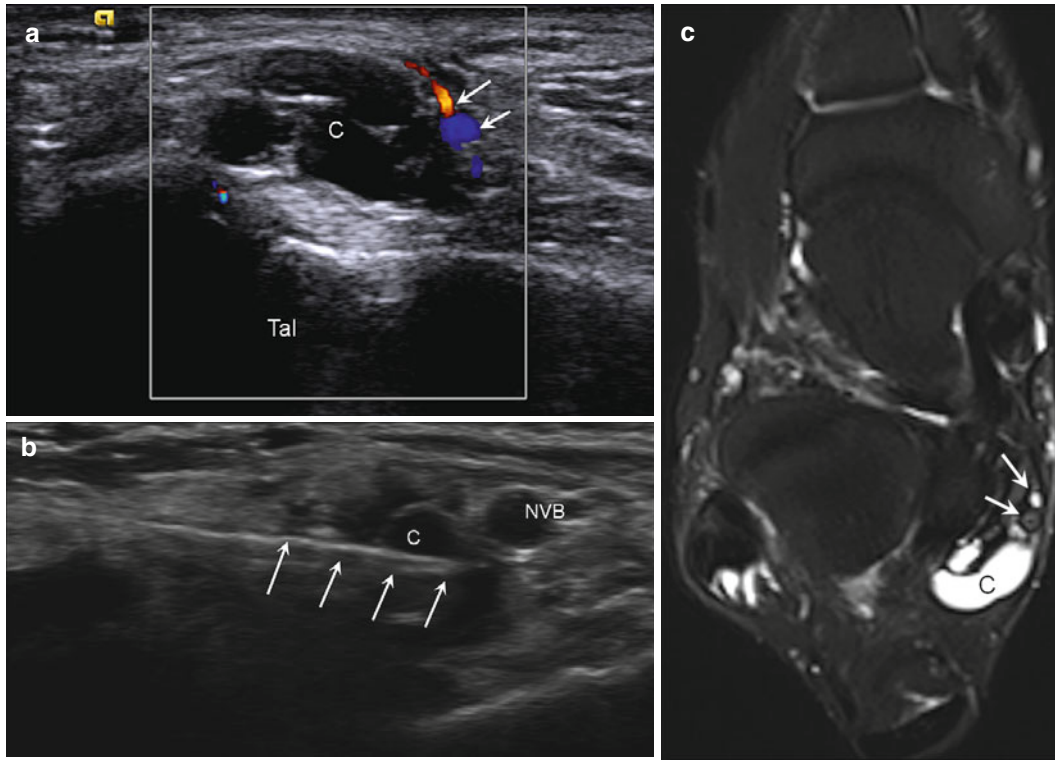

Fig. 5.116 Needle position adjacent to neurovascular bundle. (**a**) Long-axis ultrasound image of the medial ankle with color Doppler shows a multiloculated ganglion cyst (*C*) adjacent to the neurovascular bundle (*arrows*) in the tarsal tunnel; talus (*Tal*). (**b**) Long-axis ultrasound image shows direct visualization of the needle (*arrows*) within the cyst (*C*) during aspiration. The neurovascular bundle (*NVB*) is observed in real-time throughout the procedure and can be avoided. (**c**) Axial fluid-sensitive MRI shows the cyst (*C*) adjacent to the neurovascular bundle (*arrows*)

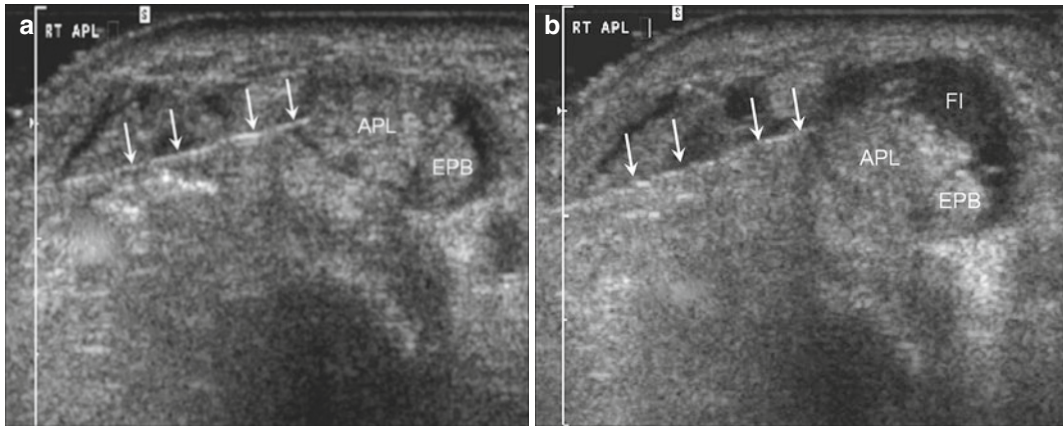

Fig. 5.117 Tendon sheath injection. Short-axis ultrasound images of the first extensor compartment of the wrist (**a**) before and (**b**) after injection of steroid mixture (*Fl*) show the needle tip (*arrows*) adjacent to and not within the abductor pollicis longus tendon (*APL*) illustrating how the injection may be performed safely even if the sheath is collapsed; extensor pollicis brevis (*EPB*). A test injection of lidocaine is performed first to confirm the needle is not intratendinous prior to steroid injection

requested for localized bursitis with or without tendon abnormality. Alternatively, bursitis or a distended synovial cyst or ganglion cyst may cause mechanical impingement of adjacent tendons and/or neurovascular structures as seen in the setting of paralabral cysts in the shoulder. Cyst decompression and administration of a therapeutic agent may alleviate symptoms. Ultrasound guidance avoids intratendinous injections and adjacent neurovascular structures (Figs. 5.120 and 5.121), and the needle may be redirected as necessary in a multiloculated cyst (Aina et al. 2001; Farin et al. 1996).

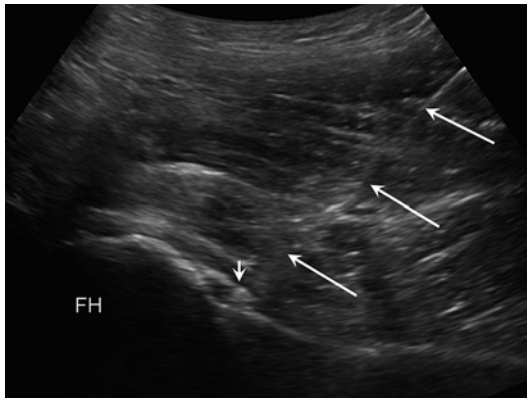

Fig. 5.118 Test injection. Long-axis ultrasound image of the anterior hip shows a small amount of lidocaine (*short arrow*) injected to confirm the intra-articular location of the needle (*long arrows*); femoral head (*FH*)

5.10.3 Calcific Tendonitis

Symptomatic intra- or peritendinous deposition of calcium hydroxyapatite often appears as a nodular echogenic mass within or adjacent to the tendon and may or may not display posterior acoustic shadowing. Calcific tendonitis most often occurs in the shoulder but may occur elsewhere in the musculoskeletal system as described above. Ultrasound-guided fragmentation and lavage have been described (Jensen et al. 2008; Lin et al. 2007; Rabago et al. 2009) with excellent results reported.

Injection of small aliquots (1–2 cc) of saline into the calcification results in distension, followed by the release of pressure and subsequent decompression back into the syringe, releasing

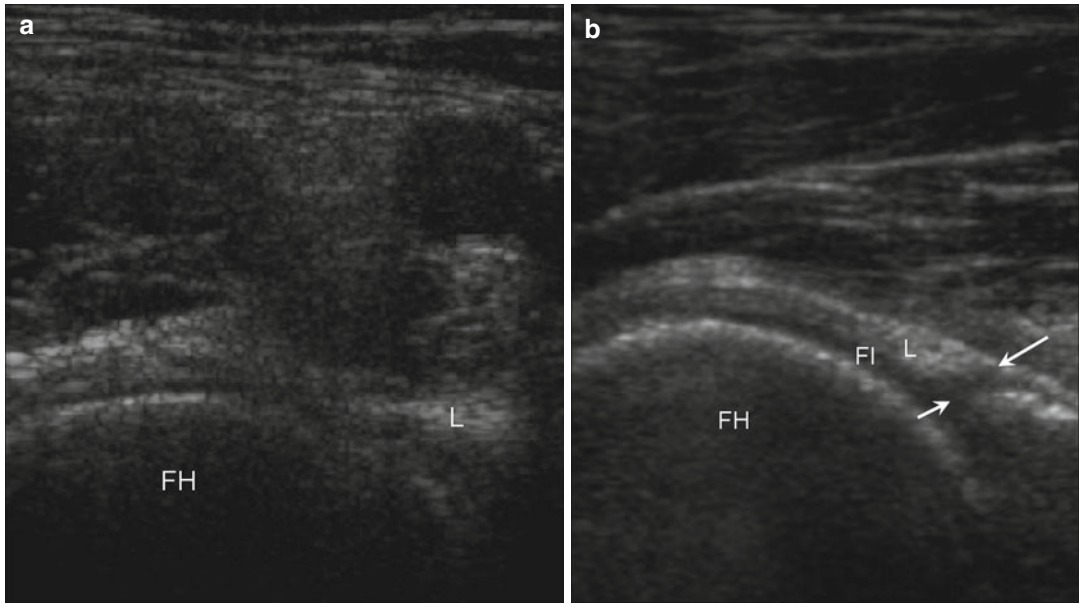

Fig. 5.119 Arthrogram effect. Long-axis ultrasound images of the anterior hip (**a**) before and (**b**) after intra-articular therapeutic injection reveal a tear (*arrows*) at the base of the anterosuperior labrum (*L*) after the joint is distended by fluid (*Fl*) in image (**b**); femoral head (*FH*)

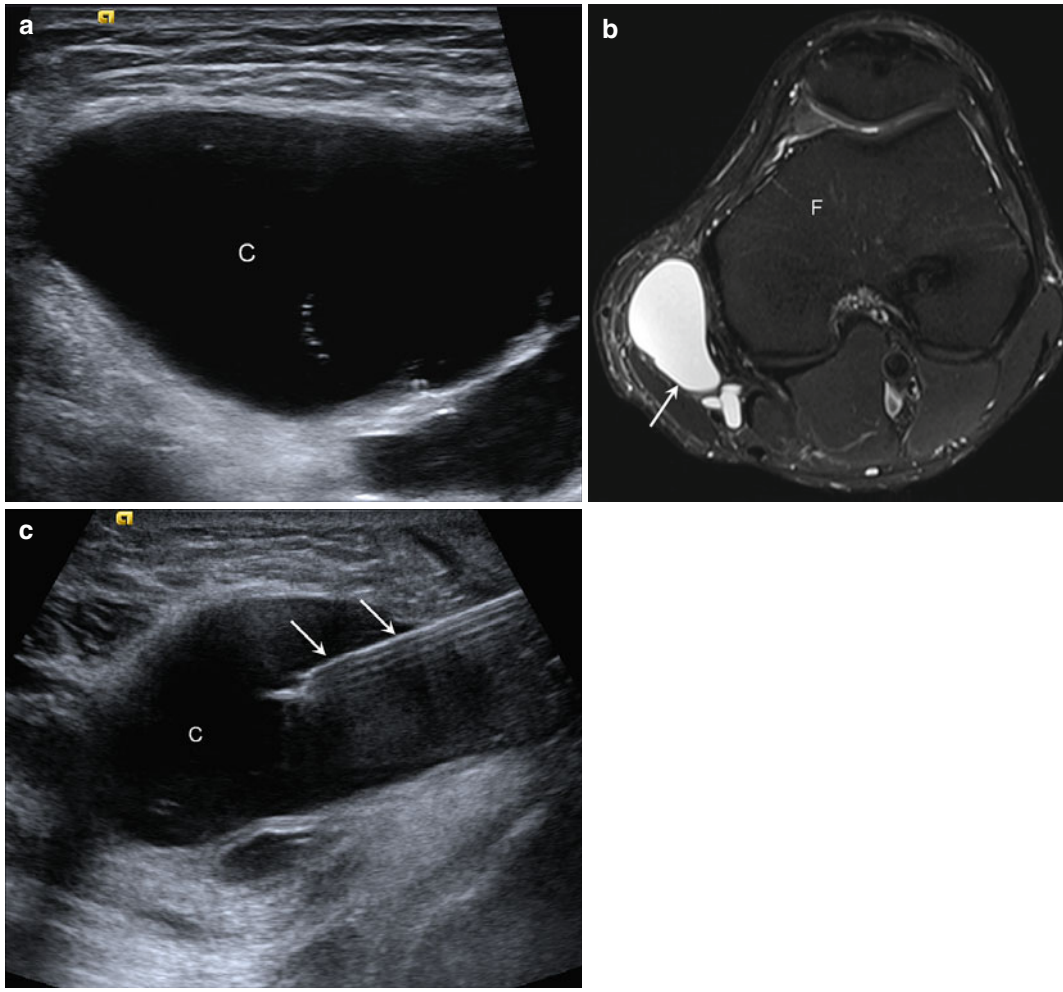

Fig. 5.120 Ganglion cyst aspiration. (**a**) Long-axis ultrasound image along the medial aspect of the knee shows a large ganglion cyst (*C*). (**b**) Corresponding axial fluid-sensitive MRI shows the cyst (*arrow*); femur (*F*). (**c**) Long-axis ultrasound image shows direct visualization of the needle (*arrows*) during aspiration of the cyst (*C*) that is decreasing in size

calcium from the deposit. The returning fluid often has the appearance of a "puff of smoke," as it contains progressive amounts of calcific debris (Fig. 5.122).

The needle is then used to fenestrate the pseudocapsule and to inject anesthetic and steroid mixture into the subdeltoid bursa. If the calcification is too small or too fragmented to allow lavage and decompression, an effective technique is to fenestrate the calcium deposit and perform a peritendinous therapeutic injection (Rabago et al. 2009).

5.10.4 Intratendinous Injections/ Percutaneous Dry Needling Techniques

Intratendinous injection therapies are thought to promote a direct healing response. These techniques date back to as early as the 1930s in the case of prolotherapy and to the 1970s in the case of autologous blood/PRP injections (Mehdizade and Adler 2007). Ultrasound imaging is believed to ensure optimal deposition of injected material

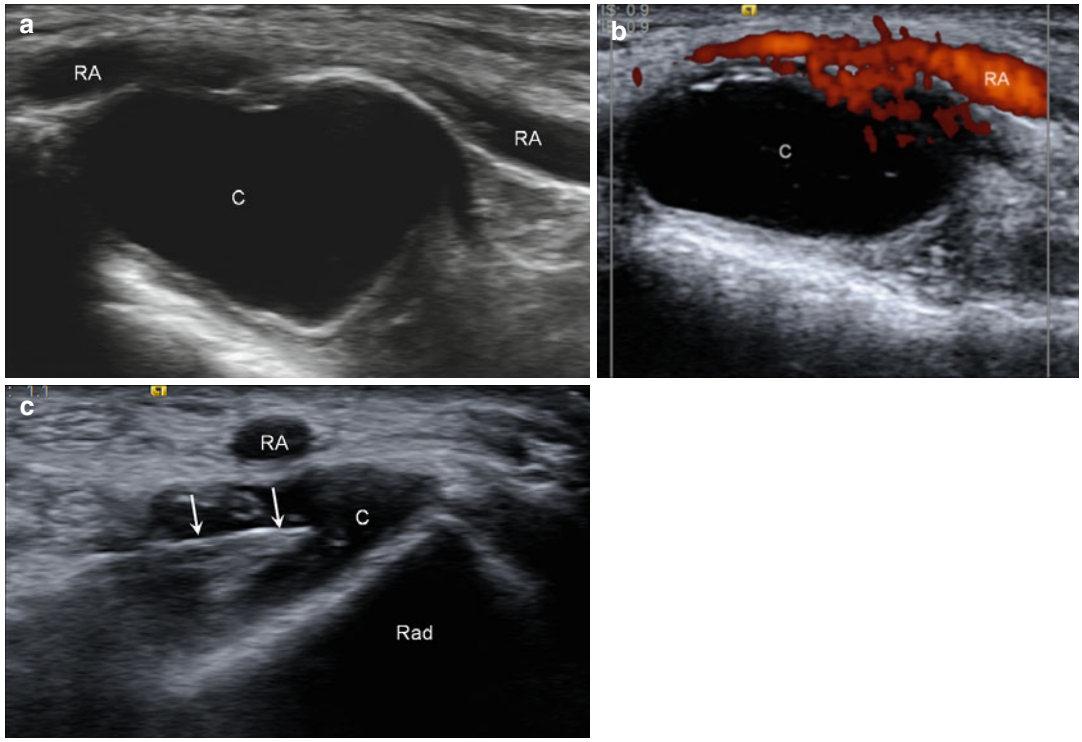

Fig. 5.121 Ganglion cyst aspiration adjacent to radial artery. Long-axis ultrasound images of the volar wrist (**a**) without and (**b**) with power Doppler interrogation show a large ganglion cyst (*C*) immediately subjacent to the radial artery (*RA*). (**c**) Short-axis ultrasound image shows direct visualization of the needle (*arrows*) during cyst (*C*) aspiration that can be done safely despite the close proximity to the radial artery (*RA*) because the structures are observed in real time; radius (*Rad*)

and can be used to assess the distribution of injected material and the response to therapy (Fig. 5.123).

Dry needling (i.e., multiple needle perforations of the tendon without injection of therapeutic material) can promote a healing response, which has been postulated to relate to the presence of microhemorrhage with the release of platelets (de Mos et al. 2008).

Autologous blood or platelet concentrates derived from autologous blood take advantage of a variety of growth factors contained within platelets that promote vascular and cellular proliferation. Platelet-rich plasma, in particular, allows for the delivery of high concentrations of these growth factors to the area of injury (Foster et al. 2009; Klauser et al. 2010). Theoretically, PRP has the potential to improve tendon healing. It contains a more concentrated amount of platelets than whole blood and includes many reparative growth factors such as platelet-derived growth factor, transforming growth factor-beta, epidermal growth factor, and vascular endothelial growth factor. Clinical studies have suggested that autologous blood or PRP significantly improves healing in refractory tendinosis, although definitive studies showing the efficacy of either technique are still lacking (Connell et al. 2006; James et al. 2007; Klauser et al. 2010; Mishra and Pavelko 2006; Peerbooms et al. 2010). Dry needling techniques have been employed successfully in patients with lateral epicondylitis refractory to other conservative measures (de Mos et al. 2008). Autologous blood and PRP injections have been successfully used in the elbow and knee (Connell et al. 2006; James et al. 2007). The advantage of performing these procedures under ultrasound guidance becomes evident when injecting tendons close to neurovascular structures, such as the hamstring tendon origin.

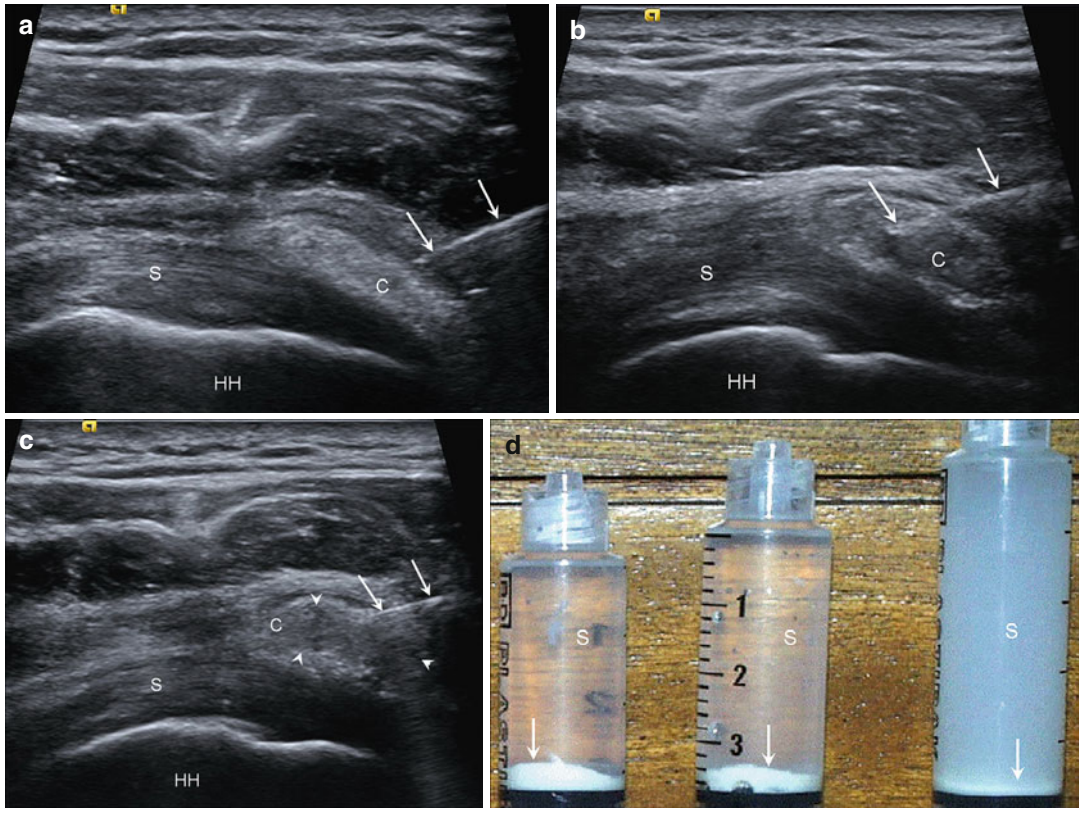

Fig. 5.122 Calcific tendinitis/bursitis lavage. (**a**) Long-axis ultrasound image of the shoulder shows a bursal calcific deposit (*C*) overlying the supraspinatus tendon (*S*) just prior to insertion of the needle (*arrows*). Long-axis ultrasound images show the needle (*arrows*) within the calcific deposit (*C*) in image (**b**) before and in image (**c**) after distension with saline (*arrowheads*) during lavage; humeral head (*HH*). (**d**) Photograph of the syringes post-procedure showing saline (*S*) with calcific sediment (*arrows*) layering dependently

5.10.5 Perineural Injections

Ultrasound has shown promise in evaluating and treating patients with painful lesions of peripheral nerves due to compressive neuropathies (Speed 2007; Tagliafico et al. 2010a, 2012). Injections include nerve blocks with long-acting anesthetic, therapeutic injections (Fig. 5.124) using an injectable steroid, or neurolytic therapy with an agent that promotes cellular death such as absolute ethanol (Chua et al. 2011; Ramamurthy et al. 1989; Sabharwal et al. 2009; Tagliafico et al. 2010b). A thorough knowledge of the normal sonographic appearances of nerves and their anatomic course is a prerequisite (Martinoli 2010). In the case of small sensory nerves, which can be difficult to visualize, knowledge of the anatomic relationships of the nerves to adjacent anatomic compartments is of value. As previously described, nerves are best visualized in short axis as clusters of hypoechoic fascicles with echogenic septations (endoneurium), which have a surrounding echogenic epineurial sleeve. An enlarged hypoechoic nerve may indicate neuritis.

5.10.6 Percutaneous Tenotomy

A promising new technique is percutaneous tenotomy with ultrasound guidance termed "fasciotomy and surgical tenotomy" (FAST) (Koh et al. 2013). This technique has been described in the treatment of chronic elbow tendinopathy (lateral epicondylitis). A detailed

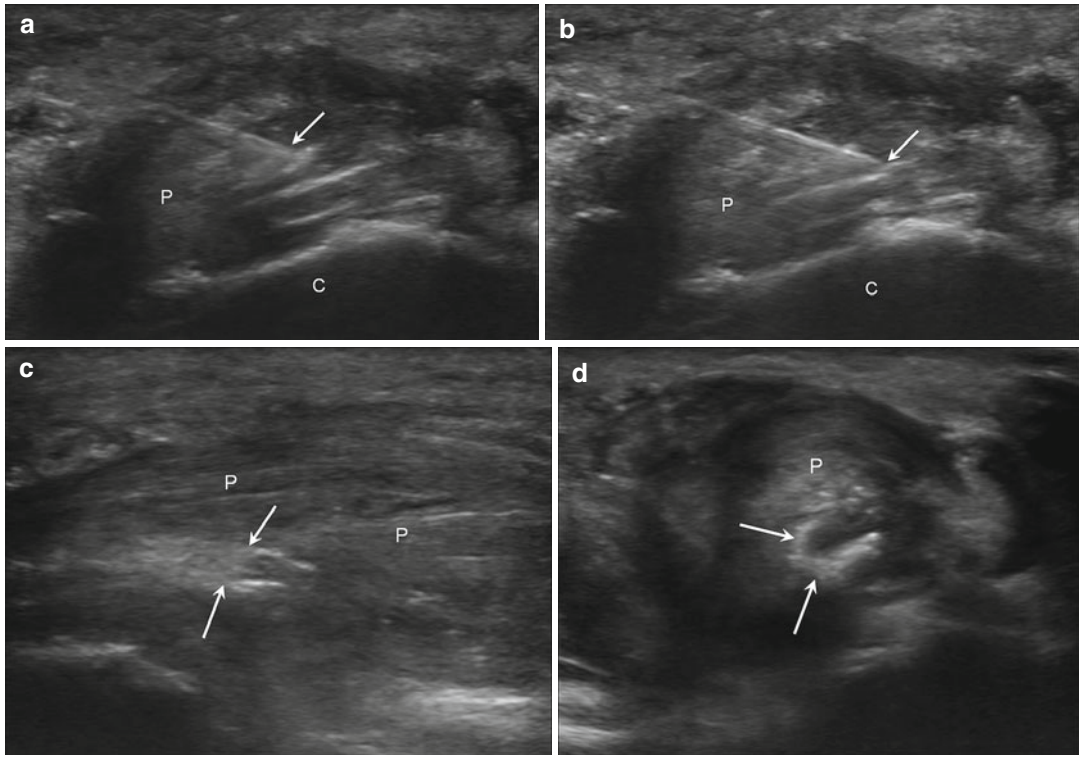

Fig. 5.123 Platelet-rich plasma injection. Long-axis ultrasound images of the abnormal peroneal tendons (*P*) at the level of the calcaneus (*C*) prior to PRP injection demonstrate fenestration of the tendons with advancement of the needle tip (*arrow*) deeper into the tendon between images (**a**) and (**b**). (**c**) Long- and (**d**) short-axis ultrasound images following PRP injection show the echogenic material (*arrows*) within the peroneal tendons (*P*)

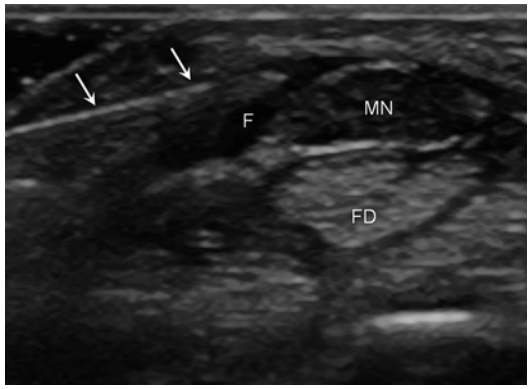

Fig. 5.124 Carpal tunnel perineural injection. Short-axis ultrasound image of the carpal tunnel shows a perineural injection surrounding the enlarged, hypoechoic median nerve (*MN*) with the needle tip (*arrows*) located adjacent to the nerve and with the injected material (*F*); flexor digitorum tendons (*FD*)

discussion of the technique is beyond the scope of this chapter; however, the procedure involves placement of a small device through a skin incision under ultrasound guidance into an area of tendinopathy to debride and remove the diseased tissue (Fig. 5.125) (Barnes 2011; Koh et al. 2013). The use of ultrasound allows for targeting and removal of the pathologic tissue without damage to the surrounding normal tissue (Koh et al. 2013). Recent studies have shown similar efficacy and results to arthroscopic tenotomy with few complications (Koh et al. 2013). Candidates for the FAST procedure are those who have failed conservative therapy (Koh et al. 2013). FAST is now being used to treat recalcitrant tendinopathy elsewhere in the body (Koh et al. 2013).

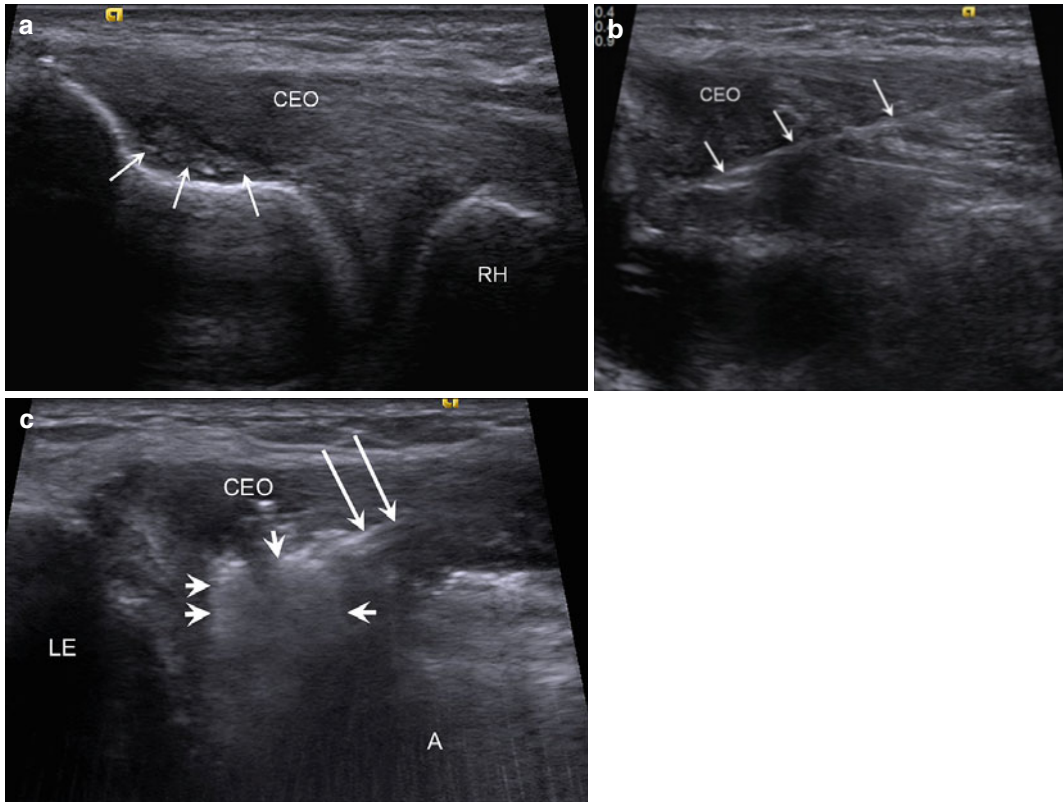

Fig. 5.125 Lateral epicondylitis percutaneous tenotomy (FAST). (**a**) Long-axis ultrasound image of the lateral elbow prior to the procedure shows a thickened and hypoechoic common extensor origin (*CEO*) with deep surface tearing (*arrows*); lateral epicondyle (*LE*), radial head (*RH*). (**b**) Long-axis ultrasound image shows placement of the tenotomy device (*arrows*) within the tendon origin (*CEO*). (**c**) Long-axis ultrasound image during the procedure demonstrates the needle tip (*long arrows*) within the tendon (*CEO*) with echogenic material (*short arrows*) representing normal saline that cools the device tip and assists in aspiration of the debrided tissue. Linear artifact (*A*) results from the vibration of the device and the motion of the saline during continuous irrigation

5.10.7 Summary

Ultrasound provides several distinct advantages as a guidance method for therapeutic injections. Observing and adjusting the needle position in real time ensures that therapeutic injections are delivered accurately and other structures such as neurovascular bundles are avoided. As clinical examples have shown, the current generation of ultrasound scanners provides excellent depiction of the relevant anatomy. The needle has a unique sonographic appearance and can be monitored in real time, as can the steroid–anesthetic injection. The same principles apply to ultrasound-guided aspirations and biopsies. Given these advantages, ultrasound guidance should be the method of choice to perform a large variety of guided musculoskeletal interventions.

Conclusion

In summary, ultrasound is an extremely useful tool in the evaluation of sports-related injuries due to its wide availability as well as the ability to perform dynamic imaging while interacting with the patient and correlating symptoms with findings at imaging. A wide

spectrum of structures in the musculoskeletal system is amenable to detailed evaluation, including tendons, ligaments, muscles, nerves, joints, cartilage, and bursae. In addition, the lack of radiation makes ultrasound a desirable modality to use in the young, athletic population for both diagnosis and guidance of therapeutic interventions. The real-time nature of ultrasound and the ability to identify soft tissue structures sonographically allow for a greater flexibility in treating a wide range of musculoskeletal disorders percutaneously. With continued advances in technology, image quality and the diagnostic capabilities of ultrasound will continue to expand.

References

Abate M, Salini V, Rimondi E et al (2011) Post traumatic myositis ossificans: sonographic findings. J Clin Ultrasound 39:135–140

Adler RS, Finzel K (2005) The complementary roles of MR imaging and ultrasound of tendons. Radiol Clin North Am 43:771–807

Adler RS, Garofalo G (2009) Ultrasound in the evaluation of the inflammatory myopathies. Curr Rheumatol Rep 11:302–308

Adler RS, Sofka CM (2003) Percutaneous ultrasound-guided injections in the musculoskeletal system. Ultrasound Q 19:3–12

Adler R, Sofka CM, Positano RG (2004) Atlas of foot and ankle sonography. Lippincott Williams & Wilkins, Philadelphia

Ahmed R, Nazarian LN (2010) Overview of musculoskeletal sonography. Ultrasound Q 26:27–35

Aina R, Cardinal E, Bureau NJ et al (2001) Calcific shoulder tendinitis: treatment with modified US-guided fine-needle technique. Radiology 221:455–461

Alfredson H (2011) Midportion Achilles tendinosis and the plantaris tendon. Br J Sports Med 45:1023–1025

Al-Qattan MM (2007) Surgical treatment and results in 17 cases of open lacerations of the extensor hallucis longus tendon. J Plast Reconstr Aesthet Surg 60:360–367

Aström M, Gentz CF, Nilsson P et al (1996) Imaging in chronic Achilles tendinopathy: a comparison of ultrasonography, magnetic resonance imaging and surgical findings in 27 histologically verified cases. Skeletal Radiol 25:615–620

Azzoni R, Cabitza P (2002) Is there a role for sonography in the diagnosis of tears of the knee menisci? J Clin Ultrasound 30:472–476

Barbarie JE, Wong AD, Cooperberg PL et al (1998) Extended field-of-view sonography in musculoskeletal disorders. AJR Am J Roentgenol 171:751–757

Barnes DE (2011) Ultrasound energy in tendon treatment. Oper Tech Orthop 23:78–83

Beggs I (2003) Sonography of muscle hernias. AJR Am J Roentgenol 180:395–399

Bianchi S (2008) Ultrasound of the peripheral nerves. Joint Bone Spine 75:643–649

Bianchi S, Martinoli C (2007) Shoulder. In: Bianchi S, Martinoli C (eds) Ultrasound of the musculoskeletal system. Springer, Berlin, pp 190–331

Bianchi S, Adelwahab IF, Zwass A et al (1994a) Ultrasonographic evaluation of wrist ganglia. Skeletal Radiol 23:201–203

Bianchi S, Zwass A, Abdelwahab IF et al (1994b) Diagnosis of tears of the quadriceps tendon of the knee: value of sonography. AJR Am J Roentgenol 162:1137–1140

Bianchi S, Martinoli C, Abdelwahab IF et al (1998) Sonographic evaluation of tears of the gastrocnemius medial head ("tennis leg"). J Ultrasound Med 17: 157–162

Bianchi S, Poletti PA, Martinoli C et al (2006) Ultrasound appearance of tendon tears. Part 2: lower extremity and myotendinous tears. Skeletal Radiol 35:63–77

Bianchi S, Delmi M, Molini L (2010a) Ultrasound of peroneal tendons. Semin Musculoskelet Radiol 14: 292–306

Bianchi S, Martinoli C, Waser NP et al (2010b) Central aponeurosis tears of the rectus femoris: sonographic findings. Skeletal Radiol 14:131–161

Bianchi S, Sailly M, Molini L (2011) Isolated tear of the plantaris tendon: ultrasound and MRI appearance. Skeletal Radiol 40:891–895

Blankenbaker DG, Tuite MJ (2010) Temporal changes of muscle injury. Semin Musculoskelet Radiol 14:176–193

Bleakney RR, White LM, Maffulli N (2007) Imaging of the Achilles tendon. In: Maffulli N, Almekinders LC (eds) The Achilles tendon. Springer, London, pp 25–39

Bodner G, Stöckl B, Fierlinger A et al (2005) Sonographic findings in stress fracture of the lower limb: preliminary findings. Eur Radiol 15:356–359

Bonaldi VM, Chhem RK, Drolet R et al (1998) Iliotibial band friction syndrome: sonographic findings. J Ultrasound Med 17:257–260

Bosworth BM (1941) Calcium deposits in the shoulder and subacromial bursitis: a survey of 12,122 shoulders. JAMA 116:2477–2482

Bouffard JA, Eyler WR, Introcaso JH et al (1993) Sonography of tendons. Ultrasound Q 11:259–286

Boutry N, Titécat M, Demondion X et al (2005) High-frequency ultrasonographic examination of the finger pulley system. J Ultrasound Med 24:1333–1339

Breidahl WH, Adler RS (1996) Ultrasound-guided injection of ganglia with corticosteroids. Skeletal Radiol 25:635–638

Breidahl WH, Stafford Johnson DB, Newman JS et al (1998) Power Doppler sonography in tenosynovitis: significance of the peritendinous hypoechoic rim. J Ultrasound Med 17:103–107

Brigido MK, Fessell DP, Jacobson JA et al (2005) Radiography and US of os peroneum fractures and

associated peroneal tendon injuries: initial experience. Radiology 237:235–241
Brophy DP, Cunnane G, Fitzgerald O et al (1995) Technical report: ultrasound guidance for injection of soft tissue lesions around the heel in chronic inflammatory arthritis. Clin Radiol 50:120–122
Bryant L, Shnier R, Bryant C et al (2002) A comparison of clinical estimation, ultrasonography, magnetic resonance imaging, and arthroscopy in determining the size of rotator cuff tears. J Shoulder Elbow Surg 11:219–224
Buck FM, Hodler J, Zanetti M et al (2011) Ultrasound for the evaluation of femoroacetabular impingement of the cam type: diagnostic performance of qualitative criteria and alpha angle measurements. Eur Radiol 21:167–175
Calleja M, Connell DA (2010) The Achilles tendon. Semin Musculoskelet Radiol 14:307–322
Campbell R (2013) Ultrasound of the athletic groin. Semin Musculoskelet Radiol 17:34–42
Cardinal E, Buckwalter KA, Braunstein EM et al (1994) Occult dorsal carpal ganglion: comparison of US and MR imaging. Radiology 193:259–262
Cardinal E, Chhem RK, Beauregard CG et al (1996) Plantar fasciitis: sonographic evaluation. Radiology 201:257–259
Cardinal E, Chhem RK, Beauregard CG (1998) Ultrasound-guided interventional procedures in the musculoskeletal system. Radiol Clin North Am 36:597–604
Chang CY, Wang SF, Chiou HJ et al (2002) Comparison of shoulder ultrasound and MR imaging in diagnosing full-thickness rotator cuff tears. Clin Imaging 26:50–54
Chen YJ, Liang SC (1997) Diagnostic efficacy of ultrasonography in stage I posterior tibial tendon dysfunction: sonographic-surgical correlation. J Ultrasound Med 16:417–423
Chen P, Maklad N, Redwine M et al (1997) Dynamic high-resolution sonography of the carpal tunnel. AJR Am J Roentgenol 168:533–537
Chew ML, Giuffrè BM (2005) Disorders of the distal biceps brachii tendon. Radiographics 25:1227–1237
Chiou HJ, Chang CY, Chou YH et al (1998) Triangular fibrocartilage of wrist: presentation on high resolution ultrasonography. J Ultrasound Med 17:41–48
Chiou HJ, Chou YH, Wu JJ et al (2002) Evaluation of calcific tendonitis of the rotator cuff: role of color Doppler ultrasonography. J Ultrasound Med 21:289–295
Cho KH, Park BH, Yeon KM (2000) Ultrasound of the adult hip. Semin Ultrasound CT MR 21:214–223
Choi YS, Lee SM, Song BY et al (2002) Dynamic sonography of external snapping hip syndrome. J Ultrasound Med 21:753–758
Christensen RA, Van Sonnenberg E, Casola G et al (1988) Interventional ultrasound in the musculoskeletal system. Radiol Clin North Am 26:145–156
Chua NH, Vissers KC, Sluijter ME (2011) Pulsed radiofrequency treatment in interventional pain management: mechanisms and potential indications-a review. Acta Neurochir (Wien) 153:763–771
Clavero JA, Golanó P, Fariñas O et al (2003) Extensor mechanism of the fingers: MR imaging-anatomic correlation. Radiographics 23:593–611
Connell DA, Potter HG, Sherman MF et al (1999) Injuries of the pectoralis major muscle: evaluation with MR imaging. Radiology 210:785–791
Connell D, Burke F, Coombes P et al (2000) Sonographic examination of lateral epicondylitis. AJR Am J Roentgenol 176:777–782
Connell DA, Ali KE, Ahmad M et al (2006) Ultrasound-guided autologous blood injection for tennis elbow. Skeletal Radiol 35:371–377
Cox B, Durieux ME, Marcus MA (2003) Toxicity of local anesthetics. Best Pract Res Clin Anaesthesiol 17: 111–136
Crag JG, Jacobson JA, Moed BR (1999) Ultrasound of fracture and bone healing. Radiol Clin North Am 37(737–751):ix
Crass JR, van de Vegte GL, Harkavy LA et al (1988) Tendon echogenicity: ex vivo study. Radiology 167:499–501
Cunnane G, Brophy DP, Gibney RG et al (1996) Diagnosis and treatment of heel pain in chronic inflammatory arthritis using ultrasound. Semin Arthritis Rheum 25: 383–389
Daenen B, Houben G, Bauduin E et al (2004) Sonography in wrist tendon pathology. J Clin Ultrasound 28:779–786
Davidson J, Jayaraman S (2011) Guided interventions in musculoskeletal ultrasound: what's the evidence? Clin Radiol 66:140–152
Davies SG, Baudouin CJ, King JB et al (1991) Ultrasound, computed tomography and magnetic resonance imaging in patellar tendonitis. Clin Radiol 43:52–56
De Maeseneer M, Vanderdood K, Marcelis S et al (2002) Sonography of the medial and lateral tendons and ligaments of the knee: the use of bony landmarks as an easy method for identification. AJR Am J Roentgenol 178:1437–1444
de Mos M, van der Windt AE, Jahr H et al (2008) Can platelet-rich plasma enhance tendon repair? A cell culture study. Am J Sports Med 36:1171–1178
De Smet AA, Winter TC, Best TM et al (2002) Dynamic sonography with valgus stress to assess elbow ulnar collateral ligament injury in baseball pitchers. Skeletal Radiol 31:671–676
de Vos RJ, Weir A, Van Schie HT et al (2010) Platelet-rich plasma injection for chronic Achilles tendinopathy: a randomized controlled trial. JAMA 303:144–149
Deslandes M, Guillin R, Cardinal E et al (2008) The snapping iliopsoas tendon: new mechanisms using dynamic sonography. AJR Am J Roentgenol 190:576–581
Diaz GC, van Holsbeeck M, Jacobson JA (1998) Longitudinal split of the peroneus longus and peroneus brevis tendons with disruption of the superior peroneal retinaculum. J Ultrasound Med 17:525–529
Dooley BJ, Kudelka P, Menelaus MB (1980) Subcutaneous rupture of the tendon of tibialis anterior. J Bone Joint Surg Br 62-B:471–472
Douis H, Gilett M, James SL (2011) Imaging in the diagnosis, prognostication, and management of lower limb muscle injury. Semin Musculoskelet Radiol 15:27–41
Downey R, Jacobson JA, Fessell DP et al (2011) Sonography of partial-thickness tears of the distal triceps brachii tendon. J Ultrasound Med 30:1351–1356

Drakonaki EE, Garbi A (2010) Metatarsal stress fracture diagnosed with high-resolution sonography. J Ultrasound Med 29:473–476

Drapé JL, Dubert T, Silbermann O et al (1994) Acute trauma of the extensor hood of the metacarpophalangeal joint: MR imaging evaluation. Radiology 192:469–476

Duncan I, Sullivan P, Lomas F (1999) Sonography in the diagnosis of carpal tunnel syndrome. AJR Am J Roentgenol 173:681–684

Ebrahim FS, De Maeseneer M, Jager T et al (2006) US diagnosis of UCL tears of the thumb and Stener lesions: technique, pattern-based approach, and differential diagnosis. Radiographics 26:1007–1020

Ebrahimi FV, Tofighi M, Khatibi H (2010) Closed tibial fracture associated with laceration of tibialis anterior tendon. J Foot Ankle Surg 49:86.e19–86.e22

Erickson SJ (1997) High-resolution imaging of the musculoskeletal system. Radiology 205:593–618

Farin PU, Jaroma H (1995) Sonographic findings of rotator cuff calcifications. J Ultrasound Med 14:7–14

Farin P, Jaroma H (1996) Sonographic detection of tears of the anterior portion of the rotator cuff (subscapularis tendon tears). J Ultrasound Med 15:221–225

Farin PU, Jaroma H, Harju A (1990) Shoulder impingement syndrome: sonographic evaluation. Radiology 176:845–849

Farin PU, Jaroma H, Harju A et al (1995a) Medial displacement of the biceps brachii tendon: evaluation with dynamic sonography during maximal external shoulder rotation. Radiology 195:845–848

Farin PU, Jaroma H, Soimakallio S (1995b) Rotator cuff calcifications: treatment with ultrasound-guided technique. Radiology 195:841–843

Farin PU, Rasanen H, Jaroma H et al (1996) Rotator cuff calcifications: treatment with ultrasound-guided percutaneous needle aspiration and lavage. Skeletal Radiol 25:551–554

Fehrman DA, Orwin JF, Jennings RM (1995) Suprascapular nerve entrapment by ganglion cysts: a report of six cases with arthroscopic findings and review of the literature. Arthroscopy 11:727–734

Fleckenstein JL, Shellock FG (1991) Exertional muscle injuries: magnetic resonance imaging evaluation. Top Magn Reson Imaging 3:50–70

Foster TE, Puskas BL, Mandelbaum BR et al (2009) Platelet-rich plasma: from basic science to clinical applications. Am J Sports Med 37:2259–2272

Friedman L, Finlay K, Jurriaans E (2001) Ultrasound of the knee. Skeletal Radiol 30:361–377

Friedman L, Finlay K, Popovich T et al (2003) Sonographic findings in patients with anterior knee pain. J Clin Ultrasound 31:85–97

Gaary EA, Potter HG, Altchek DW (1997) Medial elbow pain in the throwing athlete: MR imaging evaluation. AJR Am J Roentgenol 168:795–800

Ganz R, Parvizi J, Beck M et al (2003) Femoroacetabular impingement: a cause for osteoarthritis of the hip. Clin Orthop Relat Res 417:112–120

Ganz R, Leunig M, Leunig-Ganz K et al (2008) The etiology of osteoarthritis of the hip: an integrated mechanical concept. Clin Orthop Relat Res 466:264–272

Garrett WE (1996) Muscle strain injuries. Am J Sports Med 24:S2–S8

Geppert MJ, Sobel M, Hannafin JA (1993) Microvasculature of the tibialis anterior tendon. Foot Ankle 14:261–264

Grant TH, Kelikian AS, Jereb SE et al (2005) Ultrasound diagnosis of peroneal tendon tears: a surgical correlation. J Bone Joint Surg Am 87:1788–1794

Grassi W, Farina A, Filippucci E et al (2001) Sonographically guided procedures in rheumatology. Semin Arthritis Rheum 30:347–353

Grobbelaar N, Bouffard JA (2000) Sonography of the knee, a pictorial review. Semin Ultrasound CT MR 21:231–274

Hartgerink P, Fessell DP, Jacobson JA et al (2001) Full- versus partial-thickness Achilles tendon tears: sonographic accuracy and characterization in 26 cases with surgical correlation. Radiology 220:406–412

Hashimoto BE, Hayes AS, Ager JD (1994) Sonographic diagnosis and treatment of ganglion cysts causing suprascapular nerve entrapment. J Ultrasound Med 13:671–674

Hayter CL, Adler RS (2012) Injuries of the elbow and current treatment of tendon disease. AJR Am J Roentgenol 199:1–11

Hergan K, Mittler C, Oser W (1995) Ulnar collateral ligament: differentiation of displaced and nondisplaced tears with US and MR imaging. Radiology 194:65–71

Herneth LM, Siegmeth A, Bader TR et al (2001) Scaphoid fractures: evaluation with high-spatial-resolution ultrasound: initial results. Radiology 220:231–235

Hoksrud A, Ohberg L, Alfredson H et al (2008) Color Doppler ultrasound findings in patellar tendinopathy (jumper's knee). Am J Sports Med 36:1813–1820

Howard CB, Vinzberg A, Nyska M et al (1993) Aspiration of acute calcareous trochanteric bursitis using ultrasound guidance. J Clin Ultrasound 21:45–47

Hsu CC, Tsai WC, Chen CP et al (2006) Ultrasonographic examination for inversion ankle sprains associated with osseous injuries. Am J Phys Med Rehabil 85:785–792

Husarik DB, Saupe N, Pfirrmann CW et al (2009) Elbow nerves: MR findings in 60 asymptomatic subjects—normal anatomy, variants, and pitfalls. Radiology 252: 148–156

Jacobson JA, Fessell DP, Lobo Lda G et al (2010) Entrapment neuropathies I: upper limb (carpal tunnel excluded). Semin Musculoskelet Radiol 14:473–486

Jacobson JA (1999) Musculoskeletal sonography and MR imaging: a role for both imaging methods. Radiol Clin North Am 37:713–735

Jacobson JA (2002) Ultrasound in sports medicine. Radiol Clin North Am 40:363–386

Jacobson JA (2013a) Shoulder ultrasound. In: Fundamentals of musculoskeletal ultrasound, 2nd edn. Elsevier, Philadelphia, pp 3–71

Jacobson JA (2013b) Elbow ultrasound. In: Fundamentals of musculoskeletal ultrasound, 2nd edn. Elsevier, Philadelphia, pp 72–109

Jacobson JA (2013c) Wrist and hand ultrasound. In: Fundamentals of musculoskeletal ultrasound, 2nd edn. Elsevier, Philadelphia, pp 110–161

Jacobson JA, Oh E, Propeck T et al (2002) Sonography of the scapholunate ligament in four cadaveric wrists: correlation with MR arthrography and anatomy. AJR Am J Roentgenol 179:523–527

Jacobson JA, Propeck T, Jamadar DA et al (2003) US of the anterior bundle of the ulnar collateral ligament: findings in five cadaver elbows with MR arthrographic and anatomic comparison—initial observations. Radiology 227:561–566

Jacobson JA, Lancaster S, Prasad A et al (2004) Full-thickness and partial-thickness supraspinatus tendon tears: value of US signs in diagnosis. Radiology 230: 234–242

Jacobson JA, Miller BS, Morag Y (2005) Golf and racquet sport injuries. Semin Musculoskelet Radiol 9:346–359

Jamadar DA, Jacobson JA, Theisen SE et al (2002) Sonography of the painful calf: differential considerations. AJR Am J Roentgenol 179:709–716

James SL, Ali K, Pocock C et al (2007) Ultrasound guided dry needling and autologous blood injection for patellar tendinosis. Br J Sports Med 41:518–521

Jensen KT, Rabago DP, Best TM et al (2008) Early inflammatory response of knee ligaments to prolotherapy in a rat model. J Orthop Res 26:816–823

Jobe FW, Nuber G (1986) Throwing injuries of the elbow. Clin Sports Med 5:621–636

Kainberger FM, Engel A, Barton P et al (1990) Injury to the Achilles tendon: diagnosis with sonography. AJR Am J Roentgenol 155:1031–1036

Kalume BM, De Maeseneer M, Jacobson JA et al (2009) Improved visualization of the radial insertion of the biceps tendon at ultrasound with a lateral approach. Eur Radiol 29:1817–1821

Kamath R, Strichartz G, Rosenthal D (2008) Cartilage toxicity from local anesthetics. Skeletal Radiol 37: 871–873

Kaplan LJ, Potter HG (2004) MR imaging of ligament injuries to the elbow. Magn Reson Imaging Clin N Am 12:221–232

Kazam JK, Nazarian LN, Miller TT et al (2011) Sonographic evaluation of femoral trochlear cartilage in patients with knee pain. J Ultrasound Med 30:797–802

Keogh CF, Wong AD, Wells NJ et al (2004) High-resolution sonography of the triangular fibrocartilage: initial experience and correlation with MRI and arthroscopic findings. AJR Am J Roentgenol 182:333–336

Kermarrec E, Desmondion X, Khalil C et al (2010) Ultrasound and magnetic resonance imaging of the peripheral nerves: current techniques, promising directions and open issues. Semin Musculoskelet Radiol 14:463–472

Khan KM, Bonar F, Desmond PM et al (1996) Patellar tendinosis (jumper's knee): findings at histopathologic examination. US and MR imaging. Victorian Institute of Sport Tendon Study Group. Radiology 200:821–827

Khy V, Wyssa B, Bianchi S (2012) Bilateral stress fractures of the tibia diagnosed by ultrasound. A case report. J Ultrasound 15:130–134

Kichouh M, De Maeseneer M, Jager T et al (2011) Ultrasound findings in injuries of dorsal extensor hood: correlation with MR and follow-up findings. Eur J Radiol 77:249–253

Kijowski R, De Smet AA (2005) Magnetic resonance imaging findings in patients with medial epicondylitis. Skeletal Radiol 34:196–202

Kijowski R, Tuite M, Sanford M (2005) Magnetic resonance imaging of the elbow. Part II: abnormalities of the ligaments, tendons, and nerves. Skeletal Radiol 34:1–18

Kim C, Cashdollar MR, Mendicino RW et al (2010) Incidence of plantar fascia ruptures following corticosteroid injection. Foot Ankle Spec 3:335–337

Klauser AS, Halpern EJ, DeZoro T et al (2009) Carpal tunnel syndrome assessment with US: value of additional cross-sectional area measurements of the median nerve in patients versus health volunteers. Radiology 250:171–177

Klauser AS, Faschingbauer R, Bauer T et al (2010) Entrapment neuropathies II: carpal tunnel syndrome. Semin Musculoskelet Radiol 14:487–500

Klausner A, Frauscher F, Bodner G et al (2002) Finger pulley injuries in extreme rock climbers: depiction with dynamic US. Radiology 222:755–761

Klausner AS, Martinoli C, Tagliafico A et al (2013) Greater trochanteric pain syndrome. Semin Musculoskelet Radiol 17:43–48

Klein EE, Weil L Jr, Weil LS Sr et al (2012) Magnetic resonance imaging versus musculoskeletal ultrasound for identification and localization of plantar plate tears. Foot Ankle Spec 5:359–365

Kobayashi H, Sakurai M, Kobayashi T (2007) Extensor digitorum longus tenosynovitis caused by talar head impingement in an ultramarathon runner: a case report. J Orthop Surg (Hong Kong) 15:245–247

Koh JS, Mohan PC, Howe TS et al (2013) Fasciotomy and surgical tenotomy for recalcitrant lateral elbow tendinopathy: early clinical experience with a novel device for minimally invasive percutaneous microresection. Am J Sports Med 41:636–644

Kong A, Van Der Vliet A (2008) Imaging of tibialis posterior dysfunction. Br J Radiol 81:826–836

Kong A, Van der Vliet A, Zadow S (2007) MRI and US of gluteal tendinopathy in greater trochanteric pain syndrome. Eur Radiol 17:1772–1783

Koski JM (2000) Ultrasound guided injections in rheumatology. J Rheumatol 27:2131–2138

Koski JM, Saarakkala SJ, Heikkinen JO et al (2005) Use of air-steroid-saline mixture as contrast medium in greyscale ultrasound imaging: experimental study and practical applications in rheumatology. Clin Exp Rheumatol 23:373–378

Koulouris G, Connell D (2005) Hamstring muscle complex: an imaging review. Radiographics 25:571–586

Krücker J, Xu S, Venkatesan A et al (2011) Clinical utility of real-time fusion guidance for biopsy and ablation. J Vasc Interv Radiol 22:515–524

Kwak HS, Han YM, Lee SY et al (2006) Diagnosis and follow-up US evaluation of ruptures of the medial head of the gastrocnemius ("tennis leg"). Korean J Radiol 7:193–198

La S, Fessell DP, Femino JE et al (2003) Sonography of partial-thickness quadriceps tendon tears with surgical correlation. J Ultrasound Med 22:1323–1329; quiz 30–31

Lee D, Bouffard JA (2001) Ultrasound of the knee. Eur J Ultrasound 14:57–71
Lee JC, Healy J (2004) Sonography of lower limb muscle injury. AJR Am J Roentgenol 182:341–351
Lee JI, Song IS, Jung YB et al (1996) Medial collateral ligament injuries of the knee: ultrasonographic findings. J Ultrasound Med 15:621–625
Lee J, Brookenthal KR, Ramsey ML et al (2000) MR imaging assessment of the pectoralis major myotendinous unit: an MR imaging-anatomic correlative study with surgical correlation. AJR Am J Roentgenol 174:1371–1375
Lee KT, Choi YS, Lee YK et al (2009) Extensor hallucis longus tendon injury in taekwondo athletes. Phys Ther Sport 10:101–104
Levin D, Nazarian LN, Miller TT et al (2005) Lateral epicondylitis of the elbow: US findings. Radiology 237: 230–234
Lin J, Adler RS, Bracilovic A (2007) Clinical outcomes of ultrasound-guided aspiration and lavage in calcific tendonitis of the shoulder. HSS J 3:99–105
Linklater JM, Hamilton B, Carmichael J et al (2010) Hamstring injuries: anatomy, imaging, and intervention. Semin Musculoskelet Radiol 14:131–161
Luchs JS, Sofka CM, Adler RS (2007) Contrast effect of combined steroid and anesthetic injections: in vitro analysis. J Ultrasound Med 26:227–231
MacMahon PJ, Eustace SJ, Kavanagh EC (2009) Injectable corticosteroid and local anesthetic preparations: a review for radiologists. Radiology 252:647–661
Martin CE, Schweitzer ME (1998) MR imaging of epicondylitis. Skeletal Radiol 27:133–138
Martinoli C (2010) Imaging of the peripheral nerves. Semin Musculoskelet Radiol 14:461–462
Martinoli C, Derchi LE, Pastorino C et al (1993) Analysis of echotexture of tendons with US. Radiology 186:839–843
Martinoli C, Bianchi S, Nebiolo M et al (2000) Sonographic evaluation of digital annular pulley tears. Skeletal Radiol 29:387–391
Mehdizade A, Adler RS (2007) Sonographically guided flexor hallucis longus tendon sheath injection. J Ultrasound Med 26:233–237
Mellado JM, Bencardino JT (2005) Morel-Lavallée lesion: review with emphasis on MR imaging. Magn Reson Imaging Clin N Am 13:775–782
Mengiardi B, Pfirrmann CW, Vienne P et al (2005) Anterior tibial tendon abnormalities: MR imaging findings. Radiology 235:977–984
Michelson J, Dunn L (2005) Tenosynovitis of the flexor hallucis longus: a clinical study of the spectrum of presentation and treatment. Foot Ankle Int 26:291–303
Miller MD (2003) Treatment of pectoralis major rupture. In: Miller MD, Howard RF, Plancer KD (eds) Surgical atlas of sports medicine. Saunders, Philadelphia, p 341
Miller TT (2013) The patellar tendon. Semin Musculoskelet Radiol 17:56–59
Miller TT, Adler RS (2000) Sonography of tears of the distal biceps tendon. AJR Am J Roentgenol 175:1081–1086
Miller SD, Van Holsbeeck M, Boruta PM et al (1996) Ultrasound in the diagnosis of posterior tibial tendon pathology. Foot Ankle Int 17:555–558
Miller TT, Shapiro MA, Schultz E et al (2002) Comparison of sonography and MRI for diagnosing epicondylitis. J Clin Ultrasound 30:193–202
Miller TT, Adler RS, Friedman L (2004) Sonography of injury of the ulnar collateral ligament of the elbow-initial experience. Skeletal Radiol 33:386–391
Mishra A, Pavelko T (2006) Treatment of chronic elbow tendinosis with buffered platelet-rich plasma. Am J Sports Med 34:1774–1778
Mole D, Gonzalvez M, Roche O et al (1997) Introduction to calcifying tendinitis. In: Gazielly DF, Gleyze P, Thomas T (eds) The cuff. Elsevier, Paris, pp 141–143
Morag Y, Jamadar DA, Miller B et al (2011) The subscapularis: anatomy, injury and imaging. Skeletal Radiol 40:255–269
Morrey BF, An KN (1983) Articular and ligamentous contributions to the stability of the elbow joint. Am J Sports Med 11:315–319
Moschilla G, Breidahl W (2002) Sonography of the finger. AJR Am J Roentgenol 178:1451–1457
Muhle C, Ahn JM, Yeh L et al (1999) Iliotibial band friction syndrome: MR imaging findings in 16 patients and MR arthrographic study of six cadaveric knees. Radiology 212:103–110
Mukherjee K, Perrin SM, Hughes PM (2007) Morel-Lavallee lesion in an adolescent with ultrasound and MRI correlation. Skeletal Radiol 36:S43–S45
Nazarian LN, McShane JM, Ciccotti MG et al (2003) Dynamic US of the anterior band of the ulnar collateral ligament of the elbow in asymptomatic major league baseball pitchers. Radiology 227:149–154
Neal C, Jacobson JA, Brandon C et al (2008) Sonography of Morel-Lavallee lesions. J Ultrasound Med 27:1077–1081
Nestor BJ, O'Driscoll SW, Morrey BF (1992) Ligamentous reconstruction for posterolateral rotatory instability of the elbow. J Bone Joint Surg Am 74:1235–1241
Neustadter J, Raikin SM, Nazarian LN (2004) Dynamic sonographic evaluation of peroneal tendon subluxation. AJR Am J Roentgenol 183:985–988
Ng JM, Rosenberg ZS, Bencardino JT et al (2013) US and MR Imaging of the extensor compartment of the ankle. Radiographics 33:2047–2064
Nirschl RP, Pettrone FA (1979) Tennis elbow: the surgical treatment of lateral epicondylitis. J Bone Joint Surg Am 61:832–839
O'Callaghan BI, Kohut G, Hoogewoud HM (1994) Gamekeeper thumb: identification of the Stener lesion with US. Radiology 192:477–480
O'Driscoll SW, Horii E, Carmichael SW et al (1991) The cubital tunnel and ulnar neuropathy. J Bone Joint Surg Br 73:613–617
O'Driscoll SW, Morrey BF, Korinek S et al (1992) Elbow subluxation and dislocation. A spectrum of instability. Clin Orthop Relat Res 280:186–197
Okamoto M, Abe M, Shirai H et al (2000) Diagnostic ultrasonography of the ulnar nerve in cubital tunnel syndrome. J Hand Surg Br 25:499–502
Olsen BS, Vaesel MT, Sojbjerg JO et al (1996) Lateral collateral ligament of the elbow joint: anatomy and kinematics. J Shoulder Elbow Surg 5:103–112

Ortega R, Fessell DP, Jacobson JA et al (2002) Sonography of ankle ganglia with pathologic correlation in 10 pediatric and adult patients. AJR Am J Roentgenol 178:1445–1449

Ouzounian TJ, Anderson R (1995) Anterior tibial tendon rupture. Foot Ankle Int 16:406–410

Palmer WE, Kuong SJ, Elmadbouh HM (1999) MR imaging of myotendinous strain. AJR Am J Roentgenol 173:703–709

Parra JA, Fernandez MA, Encinas B (1997) Morel-Lavallée effusions in the thigh. Skeletal Radiol 26: 239–241

Patten RM, Mack LA, Wang KY et al (1992) Nondisplaced fractures of the greater tuberosity of the humerus: sonographic detection. Radiology 182:201–204

Peerbooms JC, Sluimer J, Bruijn DJ et al (2010) Positive effect of an autologous platelet concentrate in lateral epicondylitis in a double-blind randomized controlled trial. Platelet-rich plasma versus corticosteroid injection with a 1-year follow-up. Am J Sports Med 38:255–262

Peetrons P (2002) Ultrasound of muscles. Eur Radiol 12:35–43

Peetrons P, Creteur V, Bacq C (2004) Sonography of ankle ligaments. J Clin Ultrasound 32:491–499

Pelsser V, Cardinal E, Hobden R (2001) Extraarticular snapping hip: sonographic findings. AJR Am J Roentgenol 176:67–73

Pfirrmann CW, Jost B, Pirkl C et al (2008) Quadriceps tendinosis and patellar tendinosis in professional beach volleyball players: sonographic findings in correlation with clinical symptoms. Eur Radiol 18:1703–1709

Potter HG, Hannafin JA, Morwessel RM et al (1995) Lateral epicondylitis: correlation of MR imaging, surgical and histopathologic findings. Radiology 196:43–46

Prato N, Abello E, Martinoli C et al (2004) Sonography of posterior tibialis tendon dislocation. J Ultrasound Med 23:701–705

Premkumar A, Perry MB, Dwyer AJ et al (2002) Sonography and MR imaging of posterior tibial tendinopathy. AJR Am J Roentgenol 178:223–232

Rabago D, Best TM, Zgierska AE et al (2009) A systematic review of four injection therapies for lateral epicondylosis: prolotherapy, polidocanol, whole blood and platelet-rich plasma. Br J Sports Med 43:471–478

Ramamurthy S, Walsh NE, Schoenfeld LS et al (1989) Evaluation of neurolytic blocks using phenol and cryogenic block in the management of chronic pain. J Pain Symptom Manage 4:72–75

Rawool NM, Nazarian LN (2000) Ultrasound of the foot and ankle. Semin Ultrasound CT MRI 21:275–284

Rehman A, Robinson P (2005) Sonographic evaluation of injuries to the pectoralis muscles. AJR Am J Roentgenol 184:1205–1211

Renoux J, Zeitoun-Eiss D, Brasseur JL (2009) Ultrasonographic study of wrist ligaments: review and new perspectives. Semin Musculoskelet Radiol 13: 55–65

Richards PJ, Win T, Jones PW (2005) The distribution of microvascular response in Achilles tendonopathy assessed by colour and power Doppler. Skeletal Radiol 34:336–342

Robinson P, Bhat V, English B (2011) Imaging in the assessment and management of athletic pubalgia. Semin Musculoskelet Radiol 15:14–26

Sabharwal T, Katsanos K, Buy X et al (2009) Image-guided ablation therapy of bone tumors. Semin Ultrasound CT MR 30:78–90

Sammarco GJ, Cooper PS (1998) Flexor hallucis longus tendon injury in dancers and nondancers. Foot Ankle Int 19:356–362

Schaberg JE, Harper MC, Allen WC (1984) The snapping hip syndrome. Am J Sports Med 5:361–365

Schaeffeler C, Mueller D, Kirchhoff C et al (2011) Tears at the rotator cuff footprint: prevalence and imaging characteristics in 305 MR arthrograms of the shoulder. Eur Radiol 21:1477–1484

Scott SC (2000) Closed injuries to the extension mechanism of the digits. Hand Clin 16:367–373

Seiler JG 3rd, Parker LM, Chamberland PD et al (1995) The distal biceps tendon: two potential mechanisms involved in its rupture: arterial supply and mechanical impingement. J Shoulder Elbow Surg 4:149–156

Sekiya JK, Swaringen JC, Wojtys EM et al (2010) Diagnostic ultrasound evaluation of posterolateral corner knee injuries. Arthroscopy 26:494–499

Sell S, Schulz R, Balentsiefen M et al (1996) Lesions of the Achilles tendon. A sonographic, biochemical and histological study. Arch Orthop Trauma Surg 115:28–32

Sernik RA, Abicalaf CA, Pimentel BF et al (2008) Ultrasound features of carpal tunnel syndrome: a prospective case-control study. Skeletal Radiol 37:49–53

Seymour R, Lloyd DC (1998) Sonographic appearances of meniscal cysts. J Clin Ultrasound 26:15–20

Shortt CP, Zoga AC, Kavanagh EC et al (2008) Anatomy, pathology, and MRI findings in the sports hernia. Semin Musculoskelet Radiol 12:54–61

Silvestri E, Martinoli C, Derchi LE et al (1995) Echotexture of peripheral nerves: correlation between US & histologic findings. Radiology 197:291–296

Sofka CM, Adler RS (2004) Sonography of cubital bursitis. AJR Am J Roentgenol 183:51–53

Sofka CM, Collins AJ, Adler RS (2001) Use of ultrasonographic guidance in interventional musculoskeletal procedures: a review from a single institution. J Ultrasound Med 20:21–26

Speed CA (2007) Injection therapies for soft tissue lesions. Best Pract Res Clin Rheumatol 21:333–347

Speer KP, Lohnes J, Garrett WE Jr (1993) Radiographic imaging of muscle strain injury. Am J Sports Med 21:89–95

Stoller DW (2007a) The hip. In: Magnetic resonance imaging in orthopaedics and sports medicine, 3rd edn. Lippincott, Williams & Wilkins, Philadelphia, pp 41–304

Stoller DW (2007b) The ankle and foot. In: Magnetic resonance imaging in orthopaedics and sports medicine, 3rd edn. Lippincott, Williams & Wilkins, Philadelphia, pp 733–1050

Tagliafico A, Altafini L, Garello I et al (2010a) Traumatic neuropathies: spectrum of imaging findings and post-

operative assessment. Semin Musculoskelet Radiol 14:512–522
Tagliafico A, Bodner G, Rosenberg I et al (2010b) Peripheral nerves: ultrasound-guided interventional procedures. Semin Musculoskelet Radiol 14:559–566
Tagliafico A, Cadoni A, Fisci E et al (2012) Nerves of the hand beyond the carpal tunnel. Semin Musculoskelet Radiol 16:129–136
Talijanovic MS, Carlson KL, Kuhn JE et al (2000) Sonography of the glenoid labrum: a cadaveric study with arthroscopic correlation. AJR Am J Roentgenol 174:1717–1722
Taljanovic MS, Goldberg MR, Sheppard JE et al (2011) US of the intrinsic and extrinsic wrist ligaments and triangular fibrocartilage complex: normal anatomy and imaging technique. Radiographics 31, e44
Teefey SA, Hasan SA, Middleton WD et al (2000a) Ultrasonography of the rotator cuff. A comparison of ultrasonographic and arthroscopic findings in one hundred consecutive cases. J Bone Joint Surg Am 82:498–504
Teefey SA, Middleton WD, Bauer GS et al (2000b) Sonographic differences in the appearance of acute and chronic full-thickness rotator cuff tears. J Ultrasound Med 19:377–381
Teefey SA, Middleton WD, Boyer MI (2000c) Sonography of the hand and wrist. Semin Ultrasound CT MR 21:192–204
Teefey SA, Rubin DA, Middleton WD et al (2004) Detection and quantification of rotator cuff tears. Comparison of ultrasonographic, magnetic resonance imaging and arthroscopic findings in seventy-one consecutive cases. J Bone Joint Surg Am 86:708–716
Thain LM, Adler RS (1999) Sonography of the rotator cuff and biceps tendon: technique, normal anatomy and pathology. J Clin Ultrasound 27:446–458
Thoirs K, Williams MA, Phillips M (2008) Ultrasonographic measurements of the ulnar nerve at the elbow: role of confounders. J Ultrasound Med 27:737–743
Thomas JL, Lopez-Ben R, Maddox J (2009) A preliminary report on intra-sheath peroneal tendon subluxation: a prospective review of 7 patients with ultrasound verification. J Foot Ankle Surg 48:323–329
Tirman PF, Feller JF, Janzen DL et al (1994) Association of glenoid labral cysts with labral tears and glenohumeral instability: radiologic findings and clinical significance. Radiology 190:653–658
Tran N, Chow K (2007) Ultrasonography of the elbow. Semin Musculoskelet Radiol 11:105–116
Troelsen A, Jacobsen S, Bolvig L et al (2007) Ultrasound versus magnetic resonance arthrography in acetabular labral tear diagnostics: a prospective comparison in 20 dysplastic hips. Acta Radiol 48:1004–1010
Troelsen A, Mechlenburg I, Gelineck J et al (2009) What is the role of clinical tests and ultrasound in acetabular labral tear diagnostics? Acta Orthop 80:314–318
Tuite MJ, Turnbull JR, Orwin JF (1998) Anterior versus posterior, and rim-rent rotator cuff tears: prevalence and MR sensitivity. Skeletal Radiol 27:237–243
Tung GA, Entzian D, Stern JB et al (2000) MR imaging and MR arthrography of paraglenoid labral cysts. AJR Am J Roentgenol 174:1707–1715
Tyler P, Saifuddin A (2010) The imaging of myositis ossificans. Semin Musculoskelet Radiol 14:201–216
Uhthoff HK, Sarkar K (1989) Calcifying tendonitis. Baillieres Clin Rheumatol 3:567–581
van Holsbeeck MT, Introcaso JH (2001) Sonography of muscle. In: Musculoskeletal ultrasound, 2nd edn. Mosby, St. Louis, pp 23–75
van Holsbeeck MT, Kolowich PA, Eyler WR et al (1995) US depiction of partial-thickness tears of the rotator cuff. Radiology 197:443–446
Vardakas DG, Musgrave DS, Varitimidis SE et al (2001) Partial rupture of the distal biceps tendon. J Shoulder Elbow Surg 10:377–379
Vinson EN, Helms CA, Higgins LD (2007) Rim-rent tear of the rotator cuff: a common and easily overlooked partial tear. AJR Am J Roentgenol 189:943–946
Walz DM, Newman JS, Konin GP et al (2010) Epicondylitis: pathogenesis, imaging, and treatment. Radiographics 30:167–184
Ward SI, Teefey SA, Paletta GA Jr et al (2003) Sonography of the medial collateral ligament of the elbow: a study of cadavers and healthy adult male volunteers. AJR Am J Roentgenol 180:389–394
Wareluk P, Szopinski K (2012) Value of modern sonography in the assessment of meniscal lesions. Eur J Radiol 81:2366–2369
Weaver JS, Jacobson JA, Jamadar DA et al (2005) Sonographic findings of pectoralis major tears with surgical, clinical, and magnetic resonance imaging correlation in 6 patients. J Ultrasound Med 24:25–31
Westacott DJ, Minns JI, Foguet P (2011) The diagnostic accuracy of magnetic resonance imaging and ultrasonography in gluteal tendon tears-a systematic review. Hip Int 21:637–645
Wiener SN, Seitz WH Jr (1993) Sonography of the shoulder in patients with tears of the rotator cuff: accuracy and value for selecting surgical options. AJR Am J Roentgenol 160:103–107
Wilson FD, Andrews JR, Blackburn TA et al (1983) Valgus extension overload in the pitching elbow. Am J Sports Med 11:83–88
Wohlwend JR, van Holsbeeck M, Craig J et al (1998) The association between irregular greater tuberosities and rotator cuff tears: a sonographic study. AJR Am J Roentgenol 171:229–233
Young CM, Rayan GM (2000) The sagittal band: anatomic and biomechanical study. J Hand Surg Am 25:1107–1113
Zoga AC, Kavanagh EC, Omar IM et al (2008) Athletic pubalgia and the "sports hernia": MR imaging findings. Radiology 247:797–807
Zubler V, Mamisch-Saupe N, Pfirrmann CW et al (2011) Detection and quantification of glenohumeral joint effusion: reliability of ultrasound. Eur Radiol 21: 1858–1864